UNIVERSITY OF SOUTHAMPTON

Integrated Design for an Optically Driven Micromachined Silicon Pressure Transducer

David Robert Vincent

Doctor of Philosophy

Department of Electronics and Computer Science

March 1993

Abstract

A new pressure and temperature sensing technique based on fibre optics and micromachined silicon for immunity to electromagnetic interference and improved accuracy has been developed. The work described here applies this technique in the construction of a benchtop prototype with pressure and temperature sensitivities of +6kHz/bar and -0.3kHz/°C respectively. Also an original technique for all-optical operation of the sensor is applied and characterised in this prototype. This greatly reduces the cost of the system and an original method of temperature compensation is devised to improve the accuracy further. The sensors displayed considerable systematic variation in their frequency and amplitude of oscillation during the first few months of the project. The cause of the drift was identified as the aluminium metallisation layer. This aspect has not previously been reported. A comprehensive design approach is established and new optimum parameters for the dimensions of the micromachined silicon are derived, which will enable the transducer to meet specified performance figures for a wide range of applications in avionic and industrial markets.

Acknowledgements

I would like to thank my wife for her perserverance during the course of this work, Professor John Brignell, my supervisor, for his help and Dr J N Ross for many useful discussions. I would also like to thank my employers, Penny and Giles Ltd., for their support during difficult times.

To my Wife, Leonor

Table of Contents

Figures

Physical Constants

(The symbol used in the text is included in brackets).

Thermal Conductivity(C)[1]:

Aluminium=201 $W.m^{-1}$

Silicon=157 $W.m^{-1}$

Chromium=69.1 $W.m^{-1}.°C$

Electronic diffusion constants (silicon)[2]=$0.3x10^{-4}$ to $3x10^{-4}m^2s^{-1}$

Lattice Contraction Coefficient for Boron[3]=$2.3x10^{-30}m^3$

Refractive Index of Silicon[3]=3.4

Poisson's Ratio for Silicon[3]=0.27

Density(ρ)[1]:

Aluminium=2710$kg.m^{-3}$

Silicon=2330$kg.m^{-3}$

Young's Modulus(E):

Aluminium[1]=$71x10^9$ $N.m^{-2}$

Silicon[2]=$190x10^9$ $N.m^{-2}$

Silicon Carbide[2]=$700x10^9$ $N.m^{-2}$

Coefficient of Thermal Expansion (at room temperature)(α):

Aluminium[1]=$25x10^{-6}$

Silicon[2]=$2.33x10^{-6}$

Silicon Carbide[2]=$4.5x10^{-6}$

Specific Heat Capacity(S):

Aluminium[1]=913 J $kg^{-1}K^{-1}$

Silicon[3]=712 J kg-1 K^{-1}

Planck's Constant(h)[1]=6.626×10^{-34} Js

Charge on the electron (e)[1]=1.6×10^{-19}C

Symbols

ρ = Density

E = Young's Modulus

α = coefficient of thermal expansion

D_{El} = Electronic Diffusion Constant

ω = Angular Frequency

ν= Poisson's ratio

f = frequency

f_n= frequency of the nth mode

β_n = a constant for the nth mode of oscillation

F= Force

l= length of the beam

b= breadth of the beam

t= thickness of the beam

T= Tension

P= Pressure across the diaphragm

r= radius of the diaphragm

h= thickness of the diaphragm

Abbreviations

SCS = Single Crystal Silicon

VCO = Voltage Controlled Oscillator

PSD = Phase Sensitive Detector

Chapter 1: Introduction

1.0 Project Aim

The aim of this project is to design and build an optically powered high accuracy pressure transducer based on microcomachined silicon resonator technology. This technology is intrinsically safe, immune to transmission noise and several sensors could be multiplexed onto a single fibre. The novelty in this work does not come from the basic sensor concept but from the design approach to integrating it with a system and optimising the sensor design to make a complete, working pressure transducer suitable for industrial and avionic applications. The design areas of the technology that were addressed were the cost, signal processing and packaging. The main cost centre was identified as the optical system and a method for substantially reducing the optical content was devised and implemented. A potential packaging technology and manufacturer for the sensor were identified and a proposed design is included at the end of this thesis. Signal processing is still required for stable closed loop operation of the transducer.

1.1 Transducer Design

Figure 1.1 General Transducer System

A transducer is defined as a device that converts one form of signal energy into another [5] and the term could be used to define anything from thermocouples to LED's. When making measurements, a transducer is used to convert information about some quantity (the measurand) into a format which is compatible with our ability to absorb and use information to control our environment or some other physical process. To understand their operation, transducers may be broken down into standard parts which fulfil distinct roles within this function[6]. This is illustrated in figure 1.1, where the term 'transducer' is used in its more general definition for the input and output stages. In order to illustrate the approach taken in this work as well as the more usual format for a transducer, it is more informative to break

this concept down to more realistic components. In figure 1.2, the input transducer is called the sensor. The term is used here to indicate a device which modulates some input energy (power) with information about the target measurand before retransmission of that energy (information). Energy is transmitted to and from the sensor, via the transmission medium, from the interface to some standard power source (usually electrical) and information carrier (for example a digital bus, 4-20mA, 0-5V or direct display).

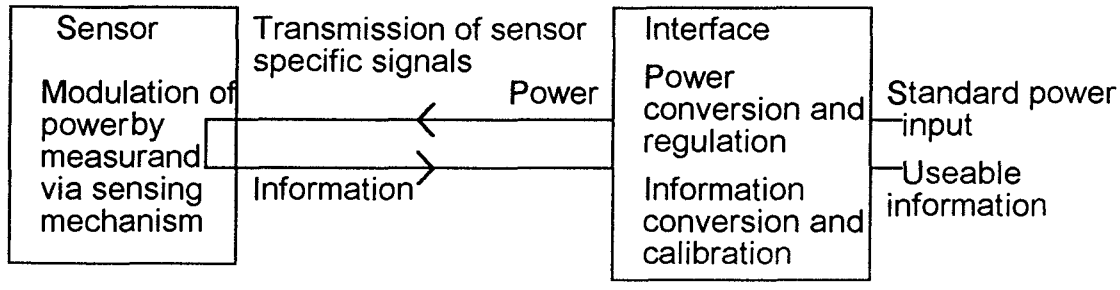

Figure 1.2 More Realistic Transducer System

The science of good transducer design is in:-

1) Isolating the measurand from the effect of other parameters (temperature, chemical composition, phase) in the target medium.

2) Maintaining a constant transfer function over time which is independent of input power and other environmental factors.

3) Suitable specification of its dynamic and its steady state performance.

Information generated at the output of a transducer must represent the state of the target measurand accurately enough for the system requirements, responding quickly enough to changes in the input measurand and, (for a stable input) represent that value accurately. This third point (the performance of the transducer), is used to define the requirements of each component in the transducer. The most important aspect of total transducer performance is the second point, the repeatability. This is the primary measure of transducer performance, even if its output is not linear with respect to the measurand. If the transducer performance is repeatable for all environmental conditions, then some sensitivity to secondary parameters may be acceptable and removed at some later stage in the

system. Figure 1.3 illustrates the factors that degradate transducer performance, with particular reference to pressure measurement. The sensor accuracy may be affected by secondary environmental factors such as thermal stress in the sensor housing, transmission of the signal from the sensor can suffer from electromagnetic noise in wires or vibration and stress in fibre-optic cables, and the electronic signal processing may contain resistors or frequency references that are required for sensor calibration and these may be sensitive to temperature.

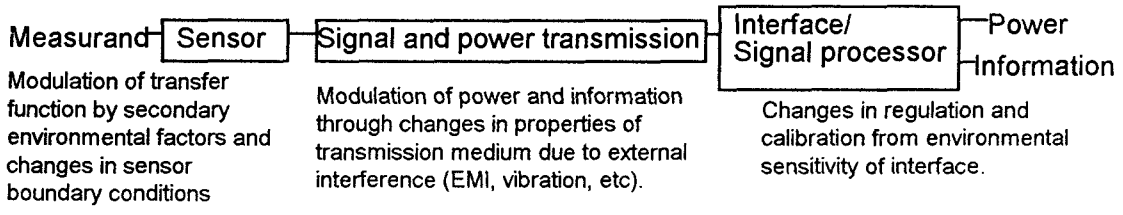

Figure 1.3 Causes of Inaccuracy In Transducers

1.2 Pressure Measurement

The most common, low cost method for pressure measurement in industrial processes is to measure the strain in a diaphragm which separates the volume of interest and some reference pressure. Pressure sensors of this type have been improved by finding more accurate methods for measuring the strain and by improving the physical properties of the diaphragm (reducing hysteresis and creep are two major objectives). Recent sensor designs use silicon for mechanical stability and piezo-resistive strain gauges for linearity and low temperature sensitivity[7].

An alternative method for pressure measurement is to measure the resonant frequency of a structure that is put under stress by the pressure. A vibrating cylinder is frequently used[8], and this technology is frequently found in situations where high accuracy is required. This is because the materials that are used (for example quartz)[9] are highly stable, and it is possible to measure the frequency output of these devices very accurately using a digital technique.

Pressure measurement technology is chosen by the size, cost, accuracy and robustness that is required to fulfil the application. In

industrial processes, the small size and low cost of diaphragm based transducers makes them appropriate, while frequency-out transducers are used in avionic and calibration applications where the additional cost is justified by the higher accuracy that is required.

1.3. History

The drive for improved sensor technology comes from the need of the process industry for more process information of higher accuracy, from more demanding (for example corrosive media or explosive atmospheres) environments. The use of more information about a process can enable more accurate process control, leading to improved yields and lower

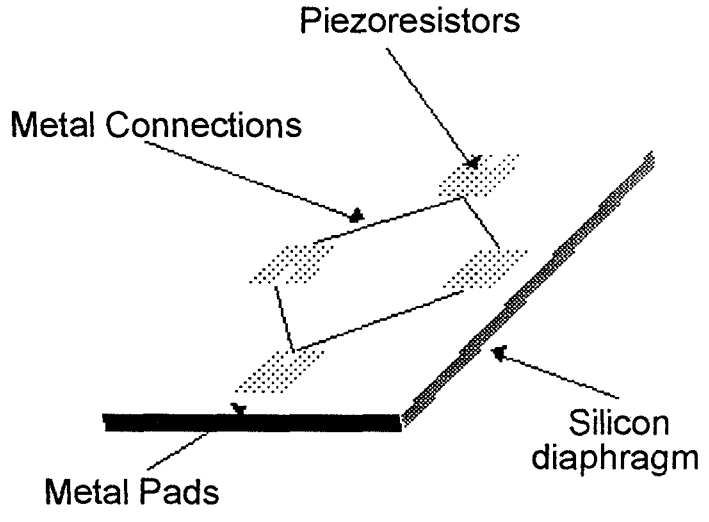

Figure 1.4 Conventional Piezoresistive Pressure Sensor

product cost.

Silicon sensors have been developed since the early 1950's and the advantage of the technology was soon recognised and developed to meet the need of the American space programme for small robust and accurate pressure sensors [10]. Single Crystal Silicon (SCS) was chosen as the best material due to its high physical strength and stability, and because the technology to micromachine single crystal structures had already been developed by the microelectronics industry[2]. These are batch fabrication techniques and are therefore ideal for manufacture of large numbers of very high quality, low cost sensors[7,11,12].

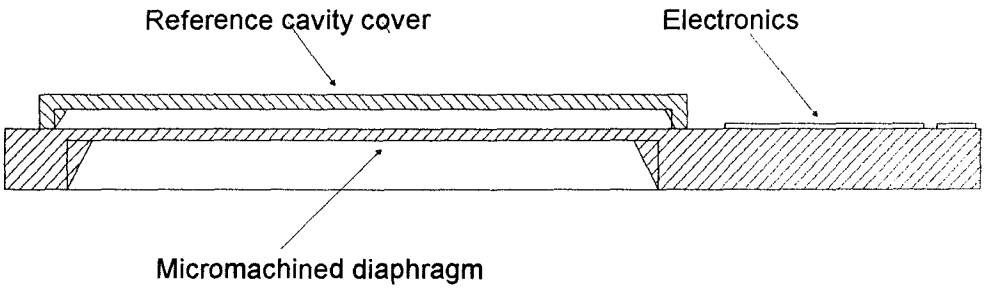

Figure 1.5 Capacitive Pressure Sensor

Neither gallium arsenide nor germanium possess such useful chemical or physical properties as silicon[2,7]. Gallium arsenide is toxic and difficult to etch, its attraction to the electronics industry is its electronic properties. Germanium and SCS are processed using similar techniques, but germanium lacks the same mechanical strength.

The earliest silicon pressure or strain sensors were based on the piezoresistive effect. Small piezoresistors are diffused in a Wheatstone bridge configuration into the surface of a thin silicon diaphragm. Figure 1.4 shows a schematic of a simple piezoresistive pressure sensor. The differential bridge current is a measure of the strain in the diaphragm due to the pressure difference across it. This technology produces devices of far lower cost than the traditional electro-mechanical pressure transducers and is now becoming the standard for general purpose industrial pressure sensors of up to 0.1% accuracy (see section 2.1)

Capacitive sensors have the potential to improve upon piezoresistive technology with improved sensitivity, drift and temperature characteristics[7]. In capacitive technology movement of a diaphragm (see Figure 1.5) is detected by measuring the capacitance between it and a conducting plate on the other side of a small evacuated cavity. A major advantage of using silicon in this case is that the complete sensor and measurement circuitry can be fabricated on to the same substrate using conventional manufacturing processes, thus reducing cost and minimising stray capacitances. This does, however place restrictions on the operating environment of the sensor due to the need to protect the circuitry against temperature extremes (typically

over 120°C). This technology originally met problems due to thermal effects in measurement circuitry being far larger than capacitance changes due to the measurand and but some new devices are now becoming available to fulfill their promise of better intrinsic linearity and accuracy than piezoresistive sensors [7,11,12].

A further development in pressure sensors is to couple a vibrating structure to pressure (see Figure 1.6). The resonator may be actuated electromagnetically, electrothermally, opto-electromagnetically or optically [13-31]. The resonator can vary in size and material from large quartz or magnetic tubes oscillating between 5-30kHz to micromachined silicon resonators oscillating at 1MHz or more. Sensors that produce a frequency output directly have the advantage of greater immunity to transmission noise and compatibility with digital signal processing.

Recent developments in the use of integrated circuits with silicon sensor systems have led to the concept of a 'smart' sensor. These sensors can compensate digitally for secondary sensitivities (mainly temperature) and communicate their calibrated values through a digital interface to a central controller. This local, distributed processing power gives the host more freedom to deal with a greater number of sensors providing more accurate information, thus potentially leading to more accurate process control [32-39].

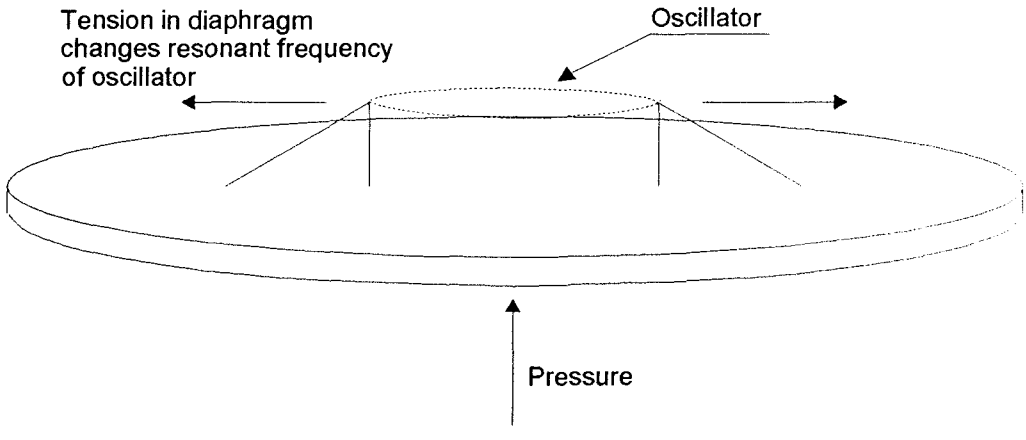

Figure 1.6 Oscillator Coupled to Pressure via a Diaphragm

As many processes occur in hazardous environments, with potentially explosive gases present and/or the presence of a great deal of electromagnetic noise, the use of optical fibre becomes increasingly attractive. Although it is possible to use a sealed electromechanical sensor which communicates via optic fibre [40-43] the use of a purely optical system is potentially much more cost and energy efficient [13-20].

Recent studies have shown that it is possible to ignite a flammable atmosphere with optically heated dust particles. Although initial studies suggested an optical power density maximum of $5mW.mm^{-2}$ there is a minimum particle size which is effective in ignition, such that for optical fibre systems the highest optical power is nearer 50mW, irrespective of the smallest focal point of the system (i.e., independent of the maximum optical power density)[44], and this is an order of magnitude greater than the power requirements of most optical sensors. This means that as long as the input power is limited, safety of an optic fibre system is easier to assure than an electrical system of comparable function.

The advantages of using fibre optic technology in sensing which are relevant to this project are:-

- Small size and weight
- Intrinsic Safety
- Sensor multiplexing onto a single fibre
- Immune to Electromagnetic Interference (EMI)
- Rugged and reliable
- Potential for high temperature capability

From an industrial standpoint, sensor distribution, EMI immunity and reliability are seen as the most important aspects which make optical technology desirable.

Once the potential for a new method of measurement has been seen and it has been demonstrated to be of sufficient accuracy, it must be packaged suitably for the harsh environments to be encountered in the application of the new technology. The first stage in this process is to mount the sensor element in such a way as to minimise (in the case of a pressure transducer) the sensitivity to temperature and any

instability in the packaging to the bonding of the diaphragm. This is done by choosing a material with suitable strength and temperature coefficient which can form a stable bond with silicon.

There are many techniques that may be used to form strong, reliable bonds with silicon[45-50] but the two techniques that offer the strongest solution and are easy to implement are used to bond silicon glasses to silicon and silicon to silicon. In each case the bond strength is at least as strong as the parent materials. These techniques are:-

1) Anodic Bonding[46-48].
The glass and silicon are pressed together and heated until the glass becomes conductive. A voltage (500V) ia applied and a small current flows, with alkali metal ions moving away from the silicon into the body of the glass. These ions leave spare oxygen bonds behind which join to the silicon. The silicon and glass are also pressed together by the strong electric field across the interface although this residual field is not necessarily desirable. On cooling, the bond strength is generally found to be higher than either the silicon or the glass parts. This technique has the advantage of allowing optical alignment of the compoents before bonding.

2) Silicon to Silicon Fusion Bonding[49].
As a result of the normal wafer RCA cleaning process a hydrophillic layer of silane (SiOH) is left on the surface of a silicon wafer. If this is placed in contact with another silicon surface in the same condition a strong hydrogen bond forms. When the silicon is heated to around 300°C the hydrogen moves away from the bond area to leave a permanent SiOSi layer which is stable. The oxygen may be removed by heating to around 1100°C but this may not be compatible with the rest of the structure at that stage of manufacture. In a similar technique, the silicon is coated with a thin layer of silicon nitride or thermal oxide. The joining technique is the same but water is liberated which migrates to the silicon-silion oxide/nitride boudary.

Both bonding techniques form strong, stable bonds which can be used to form a hermetically sealed vacuum cavity. The aim of these packaging techniques is to maximise stability, even at the expense of

temperature performance, since non-repeatability is the sensor parameter that can not be compensated for elsewhere in the system.

The above developments in technology, integrated into a coherent system, will lead to a transducer which is compact, robust, accurate and temperature compensated. It would be immune to electromagnetic noise and safe to use in a potentially hazardous environment.

1.4 Proposed Transducer

The basic strain measurement principle of this sensor is to measure the resonant frequency of vibration of an encastré beam (both ends clamped) attached to the centre of the diaphragm. When a pressure difference is applied the change in the fundamental resonant frequency of the encastré beam (which is coupled to the tension in the surface of the diaphragm) is proportional to the pressure difference (see figures 1.6 and 1.7).

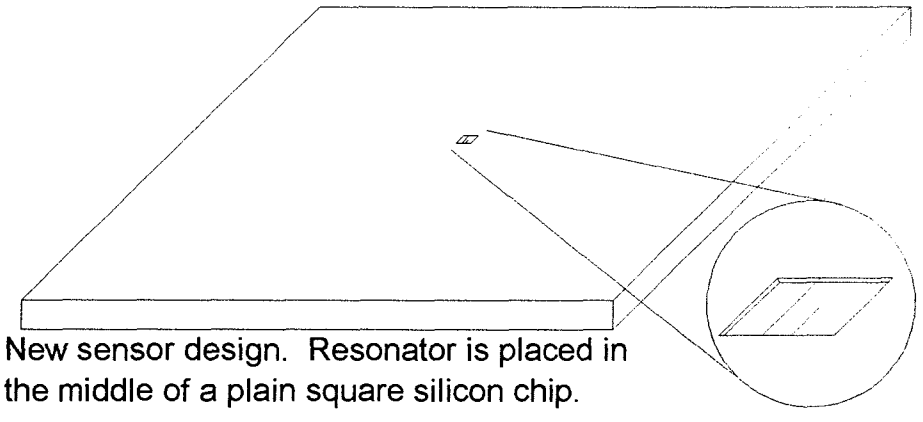

Figure 1.7 Proposed Silicon Design

The vibration of the bridge is actuated and detected optically, so that the electronics may be kept away from the active part, and the sensor head construction may be optimised towards maximum stability and a low temperature sensitivity.

Since the frequency is transmitted as an amplitude modulation of a low power optical signal the information transmission is immune to electromagnetic interference, changes in the transmission

characteristics of the fibre and is (due to the small cross section of the fibre and the low powers involved) intrinsically safe [44].

The frequency information is detected interferometrically and fed into signal processing electronics. By feeding this frequency back (phase shifted) as the modulation frequency for the actuating laser, the system as a whole will act as a pressure in, frequency out transducer, with the frequency tracking the input automatically, and providing a clear signal for measurement.

In order to communicate the information the frequency is measured digitally and can then be transmitted in either analogue or digital format. Digital output is obviously preferable for high accuracy to avoid the problems associated with accurate voltage measurement. The digital frequency measurement circuitry may also calibrate the output for the required range and measurand.

The central design target of this project is a novel pressure transducer. The above description outlines its basic format, and the aim of this work is to realise the full potential of this technology. The aims of the novel design steps that are taken in this work are:-

1) Temperature Calibration
By placing a cantilever and an encastré beam on the diaphragm, cantilever resonance may be used as a measure of the change in material properties of the pressure sensitive encastré beam with temperature.

2) Operation Over a Wide Range of Temperatures
Since there is a highly accurate method for measuring sensor temperature for active calibration, the packaging may be optimised for maximum stability, slightly compromising temperature cross-sensitivity.

3) Producing a Useable Transducer Output
The target transducer design has a frequency output which automatically tracks the pressure change (closed loop operation) to provide an easy interface to the outside world. This could also be a digital communication from the controlling microprocessor. The

acquisition time for each new pressure for a given accuracy of measurement must also be as short as possible for meaningful results.

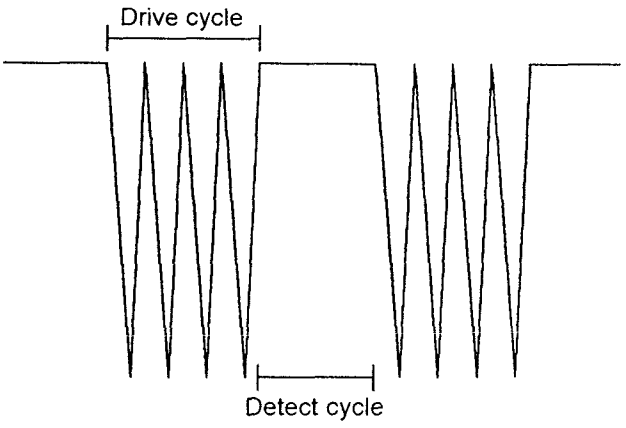

Figure 1.8 Optical Drive Waveform

4) Reducing Cost

The optical system is simplified by using only a single light source for actuation and detection of vibrations. This is achieved by actuating vibrations with a tone burst (drive mode for the optical system) and detecting oscillations with a steady light output (vibrometer mode for the optical system). Figure 1.8 is a schematic of this waveform. The other methods of single fibre operation for this type of sensor use direct feedback by forming an optical cavity between the sensor and optical reference, and single pulse actuation.

5) System Integration

This work attempts to integrate all the aspects of this particular sensor technology to predict total transducer response, accuracy, cost and feasibility as well as investigating the system experimentally. Other work has generally concentrated on aspects of the sensor technology, such as the temperature characteristics of the sensor without particular regard for specific packaging or electronics.

The intention of this thesis is to place a new transducer within the context of its competing technologies, develop a model of its technology to a stage where predictions may be made about its operation, and then use that model to design a transducer with the required performance. An experimental prototype is described that demonstrates the fundamental principles, while allowing certain basic practical techniques to be developed and some measurement of system performance to be made. The results are presented, and the overall work discussed. The conclusions follow together with suggestions for further work on packaging and signal processing.

Chapter 2: Previous Work

2.0 Introduction

The two parameters which are to be measured by the new sensor technology are pressure and temperature. In this chapter the existing temperature and pressure measurement technologies are briefly described and their comparative advantages assessed. More recent work on other resonant silicon and optical sensors is also discussed, thus placing the new sensor in the context of its contemporary technologies. Temperature is included because compensation of the new device is so important, not because temperature measurement is a primary objective of this project.

2.1 Temperature

Current industrial thermometry relies on three techniques, according to the temperature range to be measured [51]. Up to 600°C the best accuracy is available from a platinum resistance thermometer such as the PT100 (which needs some linearising circuitry). Between 600° and 1300°C a thermocouple will be used which is less accurate than a resistance thermometer at lower temperatures but can withstand higher temperatures. A great many different types of thermocouple are available according to the temperature range, cost and accuracy required[52]. The third type is the pyrometer which measures blackbody radiation given off at high temperatures. Since the silicon sensor will not be expected to perform above a few hundred degrees Celsius the only effective competing technology is the platinum resistance thermometer. This can give an accuracy of 0.01°C and has excellent stability but is not optical and would therefore not be suitable in some of the specialised applications of an optical sensor. A possible alternative technique to the above is to use a silicon junction diode as an absolute temperature sensor. This is already commonly used for temperature compensation in commercial pressure transducers[8].

Low temperature optical sensors are available. Early examples of these rely on the phosphorescent properties of certain crystals and require some reference signal to compensate for transmission line

variability. More recently, time-dependent techniques have been developed which measure the decay of temperature dependent fluorescence. Electrical or mechanical systems may be used which use optical power transmission coupled to a transformer to excite a temperature probe[51,53].

Distributed optical temperature sensing is also possible. The most successful technique of this type uses time domain reflectometry to measure temperature-dependent back scattering of laser light down specially designed fibres. Systems have been developed by YORK VSOP and the CEGB, with applications in monitoring of building temperatures for environment control and other ares where high-speeed response is not required but information over a large area or number of points[51,54]. Improved performance has been achieved by using a repetitive pseudo-random bit sequence to increase the amount of light and a phase sensitive detector to locate points along the fibre.

2.2 Pressure.

2.2.0 Introduction

There are currently two dominant low-cost pressure sensor technologies in the marketplace. They are both based on silicon and use manufacturing techniques developed by the integrated circuit industry. In applications where greater stability and resolution are required resonant structures dominate, for example the magnetically actuated Solartron transducer[8]. Although there is a lot of current research being undertaken in the area of optical pressure sensors, until recently the only product available was a pressure switch used for safety and proximity applications. A new product has recently been announced using an optically driven micromachined silicon resonator[55,56] in an oil and gas borehole application where the high temperature performance and reliability of the device has encouraged application of this technology.

2.2.1 Piezoresistive Pressure Sensors[7].

These sensors use piezoresistors implanted, diffused or deposited into a diaphragm to measure the strain produced by a pressure across the diaphragm and a schematic of the layout of the strain gauges is given

in figure 1.4. They can be configured as either absolute or differential sensors and are the most dominant technology in the marketplace today. The response of these sensors is linear and has a temperature sensitivity which is sufficiently linear to be compensated for over a temperature change of 100- 120°C, although the maximum operating temperature is around 200°C.

Diaphragms are usually made from single crystal silicon, and the piezoresistors from specially treated polysilicon, which is deposited on the surface. Insulation between the diaphragm and resistors is achieved by a reverse bias pn junction between them. The operating temperature is limited by an increase in the reverse current flowing in this junction. To minimise the temperature coefficient of the device piezoresistors are placed on the diaphragm in a Wheatstone bridge configuration, and metal foil or hybrid resistors are placed on the substrate next to the diaphragm which can be trimmed for temperature compensation. Ideally, the temperature coefficient could be reduced to zero by these means but an additional external resistor network is generally required to compensate for variations in silicon processing and this is added automatically as part of the normal sensor characterisation and testing. The operating temperature may be extended to 300°C by use of an insulating layer of SiO_2 between the SCS and polysilicon, or by making the diaphragm entirely of Si_3N_4 or Sapphire[7,46] to prevent pn junction breakdown.

2.2.2 Capacitive Pressure Sensors[7,12]

Capacitive sensors have yet to make an impact on the market place due to the difficulties in measuring small changes in capacitances of only a few picofarads (up to 30pF for a large device). The principle is based on measurement of the capacitance between a diaphragm and the substrate, separated by an evacuated cavity as illustrated in Figure 1.5. The diaphragm may be made from polysilicon [12] or anodically bonded high dielectric constant glass (such as 7070 or 1729). Although the technology promises to be more sensitive and operates at up to 300°C problems of drift are caused by out-gassing of the glass into the reference cavity. Temperature affects the output by changing the dielectric constant of the diaphragm, thermal mismatch between the

glass and silicon and by additional thermally sensitive parasitic capacitances.

Although the output of a capacitive sensor is not linear with pressure this can be dealt with by microelectronics and will not be a problem. Ideally, to minimise stray capacitances the processing circuit should share the substrate with the sensor. The two production processes are compatible, but again, thermally changed capacitances in the circuit can swamp the signal.

Capacitive pressure sensor technology has a lot of promise and although many sensors have been built, commercial devices are still relatively rare. An early example of this technology was the device manufactured by Fulmer Research which displayed excellent long term stability (at ambient temperature over a period of years)[57].

2.2.3 High Accuracy Pressure Sensors

Although silicon technology dominates the low cost industrial pressure metrology applications, there are other cases where higher accuracy and stability is required, such as calibration of other pressure transducers[8,58,59] and in aircraft. For these applications, a resonant cylinder technology may be used. Solartron developed a magnetically actuated resonant cylinder which forms a closed loop oscillator. One side of the cylinder is evacuated as a reference, and the resonant frequency of the oscillator depends on the air pressure on the other side. This sensor has a large temperature coefficient, and a pn junction diode is used as an absolute thermometer for temperature calibration. Each unit is calibrated to a fourth order polynomial (temperature and frequency coefficients) which is unique for each sensor, thus a significant amount of processing by a microprocessor is required in order to achieve a result which is an order of magnitude better than other technologies. Non-magnetic quartz resonators are used in less rugged transducers, working on a piezo-electric principle[59]. Typical frequencies are from 5kHz to 30kHz(higher order resonance) for the magnetic oscillator, with a typical Q of 2000. Quartz resonators have higher Q's (around 30000 or more) which gives them a higher accuracy.

There is also considerable interest in non-optically coupled resonating silicon and quartz microstructures. These may be actuated thermally,piezoelectrically and electromagnetically. Although they will not have the advantages of optical technology, the all-electronic operation is likely to prove more amenable to mass production and is receiving a great deal of interest [20-28]. A successful microcomachined silicon pressure sensor has been produced, which uses electrostatic actuation of the resonator. The sensor is non-linear but stable, and has a temperature sensitivity of 10-50ppm/°C, as expected for a bare silicon resonator[22,23]. The disadvantage of the device with respect to this work is that the complexity of manufacturing the resonator makes the technology inaccessible. Projects that have the aim of emulating this work must use devices that are simpler to make, even though they may not be as effective mechanically.

2.3 Optical Sensors[35-38,56-58]

Whilst experimental optical sensors have been in existence for several years, there are still very few commercial devices available. These include an optical safety device used as a pressure switch (through microbending of the fibre) and optical temperature gauges using blackbody and fluorescent radiation. In general, optic fibre sensors are classified as extrinsic (the fibre acts as a communications medium only) and intrinsic (the light is modulated by changing some transmission property of the fibre by the measurand directly). Within the class of extrinsic sensors, hybrid transducers convert optical to electrical power at the transducer and may use conventional sensing techniques tomake a measurement before retransmitting the information optically, and all-optical extrinsic sensors modulate the light directly in the sensor without conversion to some other form of power. The trouble with intrinsic fibre sensors is the high sensitivity of optic fibre to a large number of variable parameters. The hybrid approach maintains the safety and noise immunity advantages of optic fibre transmission without having to develop a new measurement technique as well and many new transducers have been developed which use this approach. Whilst the final sensor might be more bulky and complicated than an entirely new solution, this may be an important step to market acceptance of an all-optical sensor. A typical example

of using optic fibre in this way is a quartz resonator sensor. This uses a transformer to step up the voltage from a photodiode(PD) which requires pulsed light from an optic fibre. The output of the transformer is used to vibrate a quartz resonator. This vibration is detected and the frequency is transmitted by a LED back down the fibre. If the quartz resonator is coupled to pressure and the loop is closed, the system becomes a frequency out, hybrid electro-optical pressure transducer[9,27,28,40-43,53]. As with other resonators, the frequency is only 5-10 kHz, which is not much of an improvement on existing oscillating measurement systems (higher frequencies are preferred for more accurate frequency measurement). An alternative approach has been taken by concentrating on developing a low power processing and energising system, using (again) a transformer to increase the voltage available (from a amplitude modulated light source)and storing the energy in a capacitor. The capacitor can then be discharged, producing an energy pulse sufficient to actuate a standard piezoelectric pressure transducer up to ten times a second. This solution may well be attractive to users suspicious of new sensor technologies. Information can be transmitted as pulse encoded information down the fibreoptic, the light being generated by a LED [53].

A frequent disadvantage of hybrid sensors which convert optical to electrical energy at the sensor head is the relatively high cost and complexity of the devices produced.

2.4 Optical Micromachined Resonant Sensors

The earliest report of an optically actuated and interrogated micromachined resonator was in 1985[18]. This was a gold coated silica beam on a silicon substrate . It served to demonstrate the feasibility of the technique and although it was not coupled to pressure, made a high accuracy temperature sensor with a millisecond response due to its small size and high frequency. The silicon and gold structure produced a deflection of 17nm and a Q of about 30 in air. The optical system consisted of a laser diode drive with a separate HeNe heterodyne interferometer for interrogation, that was, at this stage of development, implemented in bulk optics. This device was manufactured by growing an oxide layer on the silicon substrate,

patterning with photoresist, then etching the device out and sputtering with gold, thus implementing the device using simple silicon processing techniques. A similar device was reported that was actuated using very low power levels, of the order of a few microwatts.

The next device to be optically actuated was a micromachined silicon resonator that was originally designed for electrostatic operation[13,22,23]. It was manufactured by defining the structure in highly boron doped silicon and etching round it with Ethylene Diamine Pyrocatechol (EDP, a known carcinogen) and water. This is an anisotropic etchant which does not etch the highly doped silicon and leaves clean sides to the etchpit, defined by the crystalline planes[2]. More recent devices use potassium hydroxide solutions, which is less anisotropic but is not carcinogenic[72]. This device was originally designed as a pressure sensor and was incorporated into a test rig that allowed operation under vacuum (no oscillations were observed in air due to the size of the device and inefficiency of actuation). In this case, a simple single mode fibreoptic detection system using a HeNe laser and fibre coupler was used, with a separate laser diode driven system for actuation. The resonator was mechanically complex, and it was possible to excite several different modes, with deflections up to 5nm and a Q of between 4000 and 18000. The unusually high Q is partly due to the resonator not having metallisation, and partly due to its being a pair of coupled resonators. The couple will only resonate at a frequency where the responses of the individual resonators overlap.

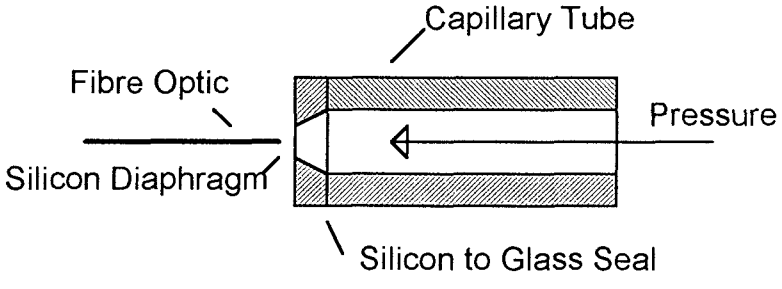

Figure 2.1 Resonating Diaphragm

The first resonant micromachined silicon device that was specifically designed as a pressure sensor was a simple diaphragm, bonded to the end of a capillary tube[17] as shown schematically in figure 2.1.

This had the disadvantage of the resonator being directly in contact with the medium being measured, although if pressure is not the measurand, then it may be possible to measure the change in mass of the diaphragm due to the adsorption of some chemical species into its surface in a similar way to some surface acoustic devices[62]. The silicon was coated with a thin layer of aluminium to eliminate electronic strain and improve thermal drive efficiency. A bulk optic system with laser diode drive and a heterodyne HeNe interferometer was used. The change of resonant frequency was measured and followed the expected curve for a clamped plate under stress. It was actuated with an average power of 1mW, generating a maximum deflection of 20nm with a Q of 40.

The next development in optically activated microresonators was to etch a silicon beam into the surface of a diaphragm, giving the dual advantages of a linear dependence of frequency with pressure, and isolation of the resonator from the outside world[14]. More recently, a simple beam mounted on two pillars on a micromachined diaphragm has been manufactured, giving increased sensitivity of 3.5% per bar to 31% per bar[21] and micromachined cantilevers have been manufactured which exhibit sufficient movement for modulation of the reflected intensity to be used for interrogation[64].

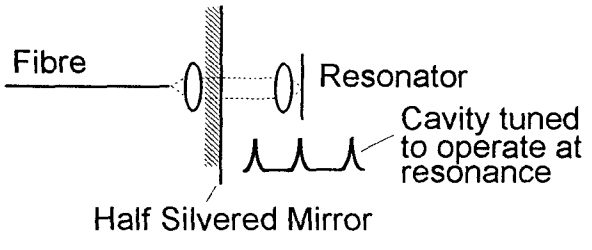

Figure 2.2 Self Resonant Sensor

After the initial work which investigated various types of resonator material and shape, attention turned to actuation and detection techniques, and investigation of the material characteristics[60-69]. Apart from the original bulk optic and dual optical source system, three techniques have been described in the literature for actuation and detection of vibrations with a single optical source. One of these used a single pulse to start vibrations and then measured the decaying oscillations with a steady optical output[28]. The resonant

frequency was measured using a spectrum analyzer and the resonator was longer and thinner than previous examples, with a resonant frequency of 89kHz. A more attractive system for single optical source drive of resonant sensors is illustrated in figure 2.2 and is the technique of self-oscillation[29,30]. A Fabry-Perot optical cavity is formed between the sensor and the fibre end. The length of the cavity is changed by opto-thermal distortion of the resonator. This changes the optical intensity which either relaxes or increases the movement of the beam. With suitable adjustment of the optical path in the cavity, these changes cause positive feedback which leads to sustained oscillation of the system. The frequency is measured by observing the intensity of the light in the same way as a normal vibrometer. This does require long term stability of the cavity and in the first report, oscillation was only maintained for a few minutes at a time. Stabilisation was later achieved by monitoring steady state, averaged intensity of light and adjusting the power (and therefore the wavelength) of the laser diode to maintain it. By closing the loop, reliable, long term sensor operation was achieved, with a signal to noise ratio of about 22dB. The third method is to use tone bursts, operating the system in a powered closed loop. A paper describing this method is included in Appendix C.

Figure 2.3 illustrates some other resonator designs used so far. a) and b) are typical examples of silicon or silica devices, where a) has a larger central section for increasing the amount of returning signal. c) has been used for examining material properties of micromachined silicon and d) is a larger device, 1.2mm long and 8μm thick that was originally actuated electrically[14,22,23].

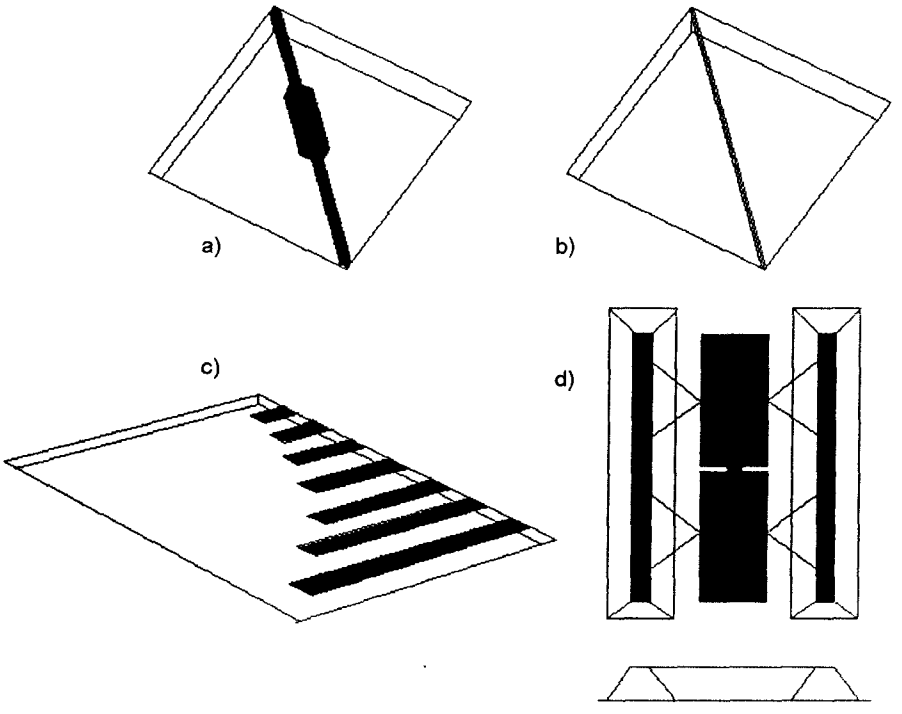

Figure 2.3 Different Microresonator Designs

Material characteristics that have been investigated,[63-66] are the effects of the high levels of boron doping used to manufacture the devices and the Young's modulus of the silicon and metallisation layers, and physical characteristics of the resonators are the effects of air damping and metallisation on the Q and actuation efficiency, comparisons between actuation of cantilevers and encastré beams, the effect of optical power on the resonant frequency and temperature characteristics of the different designs.

Measurements of Young's modulus for silicon and aluminium using resonant cantilevers and encastré beams have found values that are smaller than the standard for the bulk materials. This is because the aluminium is usually sputtered, and forms a solid layer by nucleation, leaving a large number of voids. The silicon contains a high percentage of boron doping which causes a much higher level of lattice defects than would be present in normal single crystal silicon. The Young's modulus for the silicon microresonators was found to be about 4% lower than the bulk silicon value, and others have measured similar differences, with some variation due to the different processing of each device.

In the study on the effect of metallisation on actuation efficiency and Q, it was found that actuation efficiency is improved by an order of magnitude, and the Q was significantly reduced by the damping effect of the metal. The effect of a range of thicknesses of Chromium on the silicon have been investigated on the coupled resonator[66]. It was found that there was a maximum response for a thickness of 200Å and above this the deflection reduced drastically[65]. These results are discussed further in Chapters 3 and 6. The variation in thermal sensitivity of the structure with construction and material condition showed that annealing bare silicon structures reduces thermal sensitivity slightly, a thin layer (75nm) of aluminium doubled thermal sensitivity, and a layer ten times as thick increased this value by a factor of fifty[64]. This increase was also apparent in the sensitivity of the device to the optical power, which affects the average temperature of the device and relaxes tension in the beam during oscillation (assuming actuation is due to the bi-metallic effect), lowering the resonant frequency. A thick layer of aluminium produced a significant sensitivity to optical power that would warrant some stabilisation for a heavily metallised structure. A 50μW change in optical power produced the equivalent change in frequency of 1mbar of pressure. Irrespective of the effects of metallisation, for high optical power levels, the deflection in the beam becomes significant with respect to its thickness and the frequency increases because of the increased tension in the beam caused by the large deflection. This is referred to as the 'Hard Spring' effect[71] and introduces both non-linearity and hysteresis into the response of the reonator. It places an upper limit on the power used to actuate the device.

A comparison between optically excited oscillations of cantilevers and encastré beams has demonstrated the increased ease of actuation of cantilevers, and their insensitivity to stress in the substrate. This means that they are far more robust with regard to manufacturing techniques and may be a more suitable candidate for a purely optical, commercial device. The theoretical work in the study assumes that the dominant actuation mechanism is differential expansion, and from the published experimental evidence[64] this is probably true.

The latest papers on the resonator characteristic rather than material properties have discussed actual packaged sensors[62,63,65]. One

paper describes an initial, mechanically complex sensor head, with all optical operation requiring two fibres. The temperature characteristic is described and, due to the mixture of materials used to mount the sensor, which uses a copper substrate to compensate for the extra temperature sensitivity caused by thick aluminium metallisation, is positive for temperatures below about 35°C and negative above. This means that some readings could be ambiguous, with the same temperature induced error at two different temperatures making digital or other compensation difficult.

A second, all optical pressure sensor[62,63] using the same resonator structure as [22,23] but mounted in a silicon tube has been developed for the harsh conditions experienced in oil and gas wells. The sensor has been characterised and a small production run quantity of 50 have been manufactured. Longer wavelength light for interrogation and actuation (1300nm and 1535nm respectively) was used, with a wave division multiplexer for separating the returning signal and drive light sources before detection. Both metallised and unmetallised structures are reported, the heavy doping in the silicon changing its absorption characteristics (due the high carrier density). The long wavelength of 1300nm for detection will help maintain fringe visibility as the cavity size changes with temperature (the distance between fringes being a function of wavelength). Also, technology for long wavelength operation of fibre-optic systems with laser diodes is well advanced for the communications industry, giving more stable operation and lower noise levels although these devices are more expensive. The signal to noise ratio was 30dB after 16dB of transmission loss.

Over the same period of development of the sensor technology from an electronically powered device to the first all-optical system and the subsequent pressure sensors, technology for interrogation of the resonators has also progressed. Some work discusses resonant sensor interrogation specifically[15,69], but the majority of the work is for vibrometers in general. At least two fundamentally different techniques have been used for sensor interrogation which are phase modulation and reflected amplitude modulation. Phase modulation (normal interferometry) is more sensitive, and where amplitude modulation has been used, it has been with cantilevers exhibiting a

large movement, or the reflection has been from an edge of the device where a small movement has a large effect on the amount of returning light.

The interferometric techniques that have been used are the complex, bulk optic heterodyne system[17], single mode, high coherence laser diode or HeNe systems, and multimode fibre systems with laser diodes and LED's[13,69]. Analysis of a simple multimode system[68] has investigated the dependence on fibre end to sensor separation of signal quality with respect to the properties of the fibre, the coherence length of the light source and the alignment of the fibre.

Micromachined resonant sensor technology has progressed to the state where commercial devices have become possible[54,55]. The published work discusses actuation mechanisms, detection and actuation techniques and packaging but there is still relatively little information on the expected accuracy of the technology or proposed complete systems. Piezoresistive and capacitive silicon sensors show excellent linearity, stability and accuracy over a wide range of temperatures and are of much lower cost than the optical sensors. This technology seems to be of greater interest in difficult environments[54,55] or as a distributed system[19].

Chapter 3: Theory

3.0 Introduction

This chapter describes the sensor operation, its basic physical principles and attempts a theoretical description of the parameters that will determine its overall performance. Sections 3.4.2 and 3.6.2 contain original theoretical work for calculation of the optimum beam dimensions and actuation efficiency respectively.

The overall transducer may be divided into three distinct sections:-

1) Modulation of sensor drive by the measurand via the sensor.

2) Transmission of signals to and from the sensor.

3) Generation of an appropriate drive signal and interpretation of the information coming back from the device.

The performance of each of these sections has a profound effect on the price/performance of the complete transducer, which will also be considered.

3.1 System Overview

The properties of each component that are important depend on its own function and on its interface with the rest of the system. To understand why particular properties are being described, some knowledge of the overall system is necessary, as discussed subsequently.

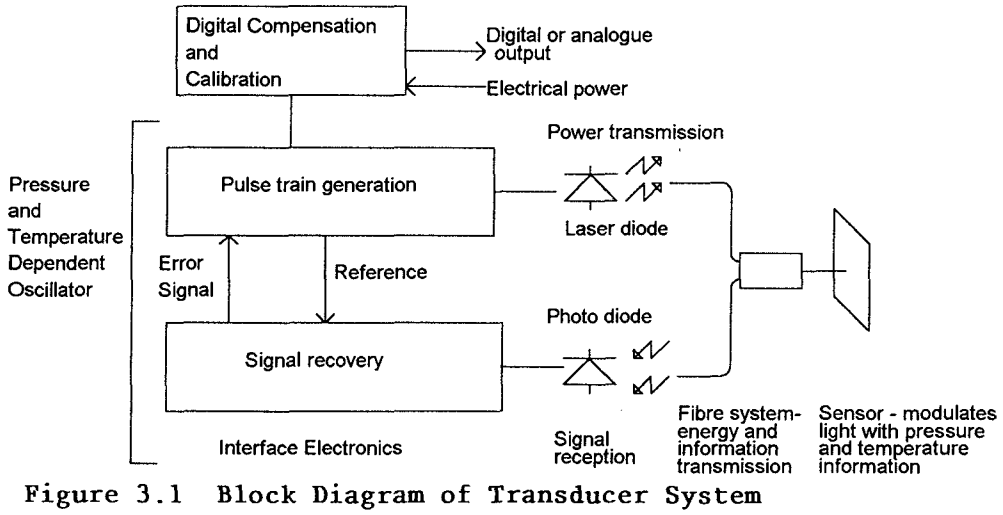

Figure 3.1 Block Diagram of Transducer System

3.2 Fundamental Sensor Mechanism

Figure 3.1 above illustrates the basic components of the measurand-to-frequency transducer. The main elements of this system are:-

1) The sensor. This has two resonators, one which is pressure and temperature dependent, the other which is temperature dependent. This provides a means of measuring the temperature and compensating for it very accurately.

Figure 3.2 illustrates the basic sensor concept of driving a microresonator into transverse oscillations by light from an optic fibre used in this type of transducer. The oscillations are detected by light from the same fibre. The resonant frequency of the bridge is changed by the tensile stress exerted on it by a differential pressure across the diaphragm. The change in frequency is proportional to the pressure difference across the diaphragm[14].

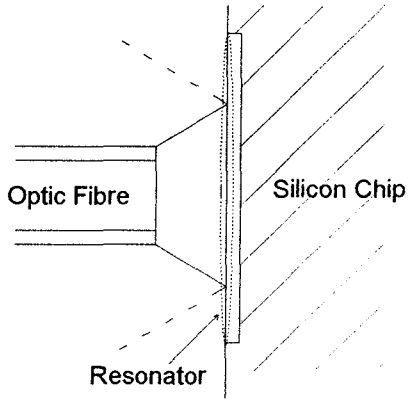

Figure 3.2 Optic Fibre to Silicon Resonator Configuration

2) Transmission of the optical excitation and detection energy via the optical fibre coupler, laser diode and photo diode. A major design feature of this system is the reduction of the optical system to a single light source and coupler whilst maintaining the advantage of driving the resonance, thus maximising optical drive signal modulation and enabling the use of a highly accurate method of frequency measurement and noise reduction.

3) Frequency measurement using a phase locked loop. This provides a suitable frequency output for digital measurement and integrates the components from micro bridge to electronics into a single pressure/temperature dependent oscillator.

3.3 Frequency Of Oscillation of a Silicon Bridge

The resonant frequency of the device can be calculated using standard equations for oscillating bars, with both fixed-fixed (encastré) and fixed-free(cantilever) boundary conditions. The general solution to the wave equation for a rectangular section bar is[71]:

$$y = A\cosh\beta x + B\sinh\beta x + C\cos\beta x + D\sin\beta x \qquad (1)$$

Where A,B,C,D are determined by the boundary conditions and may all be defined in terms of A, y is the transverse displacement of the beam a distance x from one end, and β is a constant defined by the mode of oscillation. Figure 3.3 illustrates solutions to this equation for the fundamental mode of an encastré beam and the first and second modes of a cantilever. The second mode of the cantilever is similar in form to the first mode of the encastré beam and should be suitable for single light source operation since the positions of maximum strain and maximum movement are both near the centre of the beam. The resonant frequency is given by:-

$$f_n = \frac{(\beta_n l)t}{2\pi l^2\sqrt{12}}\left(\frac{E}{\rho}\right)^{\frac{1}{2}} \qquad (2)$$

Where $\beta_n l$ is a constant for the nth mode of oscillation as given in the table below[71], and E, ρ, t, and l are the Young's modulus, density, thicknes and length of the beam respectively.

	$(\beta_1 l)$	$(\beta_2 l)$
Fixed-free	3.52	22.0
Fixed-fixed	22.4	61.7

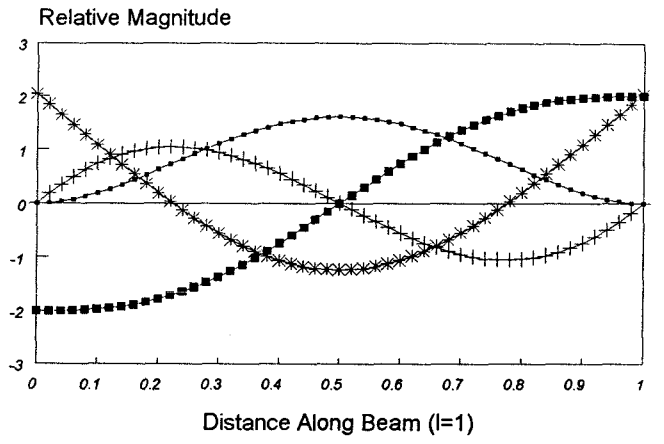

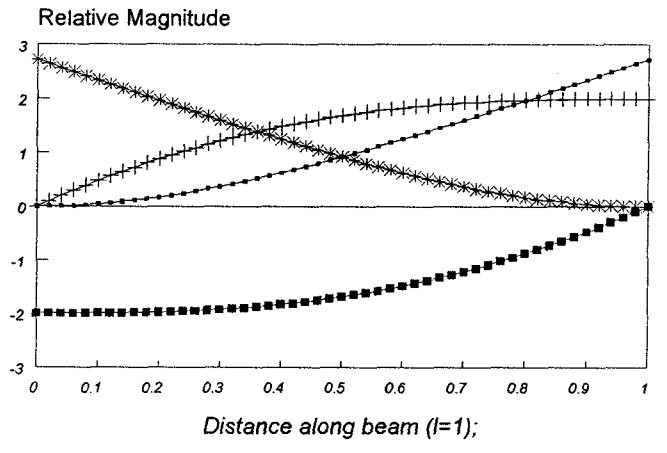

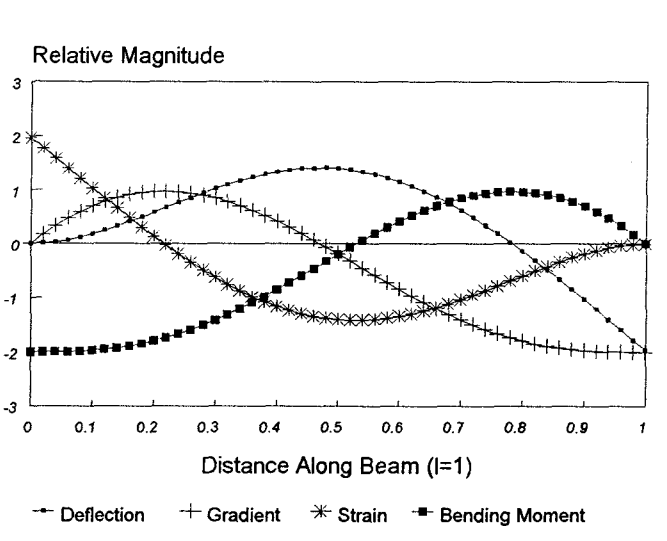

Figure 3.3 Solutions to the Wave Equation for a Rectangular Section Bar

The beam is stressed by a tension in the surface of the diaphragm caused by a differential pressure across its thickness. This tension, T, for an unclamped diaphragm is given by[73]:-

$$T = \frac{3(1+\nu)r^2}{8h^2}P \qquad (3)$$

Where r and h are the radius and thickness of the diaphragm, P is the pressure applied across the diaphragm and ν is Poisson's ratio.

By combining the wave equation for a string under tension with the solution above for a rectangular section beam (by resolving the wave vectors), and substituting the above expression for tension, the resonant frequency of a rectangular beam in a diaphragm is[14]:-

$$f = \frac{1.03}{t}\left(\frac{E}{\rho}\right)^{\frac{1}{2}}\left[\left(\frac{t}{l}\right)^2 + 0.055\frac{(1+\nu)r^2P}{Eh^2}\right] \qquad (4)$$

where the symbols are as defined above, to give a frequency dependence which is linear with pressure.

Differentiating this expression with respect to the pressure gives the rate of chamge of frequency with pressure. The fractional change in the output of a transducer for a given change in measurand is called the gauge factor. This is one of the central defining properties of the sensor:

$$\frac{df}{dP} = \frac{0.057(1+\nu)}{(E\rho)^{\frac{1}{2}}}\frac{r^2}{th^2} \qquad (5)$$

This should be divided by the frequency to find the normalised gauge factor. By inspection, it may be seen that it is independent of pressure (linear), and the length and width of the resonator (although the length affects the offset frequency) and proportional to the inverse of the thickness, so thin resonators are more sensitive. This suggests that a given resonator should be as thin as possible to increase sensitivity and as short as possible to increase the frequency (more accurate to measure in a given time) but it must be large enough for effective actuation using an economical, purely optical technique. These design parameters are discussed further in

Chapter 6 where they are used to assess the benefits of different actuation mechanisms for the types of microresonator structure.

If more general mechanical properties of the beam are being assessed, it is more useful to use a term for the total strain in the structure, ε which may contain thermal, electronic or material contributions to strain as well as pressure. A constant, k, can also be included which takes into account the composite nature of a metallised beam;

$$f = \frac{1}{t}\left(\frac{E_s}{\rho_s}\right)^{\frac{1}{2}}\left(1.04\left(\frac{t_s}{l}\right)^2 k + 0.31\varepsilon\right) \qquad (6)$$

k is defined by [61]:

$$k = \frac{4 + 6\left(\frac{t_m}{t_s}\right) + \left(\frac{E_s t_s}{E_m t_m}\right) + 4\left(\frac{t_m}{t_s}\right)^2 + \left(\frac{E_m}{E_s}\right)\left(\frac{t_m}{t_s}\right)^3}{\left[1 + \left(\frac{E_s t_s}{E_m t_m}\right)\right]\left[1 + \left(\frac{\rho_m t_m}{\rho_s t_s}\right)\right]} \qquad (7)$$

where E, ρ and t are as defined above, but with subscripts of s and m to denote silicon and metal respectively.

3.4 Optical Actuation of Vibrations

Sensor actuation is approached in two stages. First, the mechanism for generation of strain by light, and then the specific case of transverse waves in a micromachined silicon structure.

3.4.1 Photo-Generation of Strain in Silicon

There are two mechanisms for the generation of strain in silicon by light. The first is as a direct consequence of the absorption mechanism of light in silicon and is electronic strain[4]. Silicon absorbs light through ionisation of the lattice. Electrons that can gain sufficient energy from absorbing a photon move out of the 'valence' band (bound to one particular silicon atom) and into the 'conduction' band (free to move around the lattice) These electrons are called 'excess carriers'. Ionisation of the lattice causes a change in the binding energy and in silicon leads to an overall contraction which lasts for the excess carrier lifetime (i.e. the time before it decays to the valence band). There are two stages of

heat generation in this process. Any excess energy the electron gains through absorption of a photon is given out as heat as soon as it relaxes into the lowest available energy state in the conduction band which occurs immediately after ionisation. The second release of heat, which is the remainder of the energy of the photon, occurs when the electron decays back to the valence band. The lifetime of the state depends on the material and its conditions at the time (i.e. the temperature). The absorption length of light for silicon is of the order of a few microns, and increases with the wavelength of the light. If there is insufficient energy to promote a valence band electron into the conduction band, the photon will pass through the silicon and the silicon becomes transparent, at a wavelength of 1.1 microns.

The second mechanism for generation of strain by light in unmetallised silicon is thermal expansion[74-77]. This obviously requires a mechanism for conversion of light into heat and there are two ways. For bare silicon heat is generated by the decay of the electron into lower energy states (as above). The rate of conversion of the light into heat depends on the carrier lifetime and the wavelength of the light.

If the silicon is metallised (i.e. coated by a layer of metal which may be a few tens or hundreds of nanometres thick), light is converted directly into heat, carrier generation is prevented, and the shorter absorption length (a few nanometres) means that all the light is absorbed (or reflected). For thin unmetallised silicon, some light will pass through.

Each mechanism produces the same amount of heat from the light, but in unmetallised silicon the heat is generated over the lifetime of the carriers, which may be longer than the period of oscillation.

In their description of the effect of electronic strain on photoacoustic generation in silicon[4], Kino and Stearns give the following equations for signals from oxidised and metallised silicon to an acoustic transducer mounted on the sample:-

$$V_{Si} = \frac{K\pi a^2}{j\omega}\left(1-R_{Si}\right)\frac{I_o}{h\upsilon}\Delta^0\Big|_{r,x=0} \times \left[\frac{\alpha}{\rho S}\left(h\upsilon - E_g - 3kT\right) + \frac{1}{3}\frac{dE_g}{dP}\right] \qquad (8)$$

where V_{Si} is the voltage output of the acoustic transducer, K is some constant, a is the illuminated area, R_{Si} is the reflectivity of silicon, I_o is the incident light flux, ν is the frequency of the light, ω is the frequency of the acoustic waves, Δ^o is some normalising constant for the response of the transducer, E_g is the energy gap of the silicon, ρ is the density, S is the specific heat capacity, α is the thermal expansivity, k is Boltzmanns constant, T is the ambient temperature and dEg/dP is the change in the energy gap with pressure. The first half of the expression is the energy from the pulse of light and the second half is the response of the material to the light. The equivalent expression for the case of silicon metallised with Chromium is:-

$$V_{Cr} = \frac{K\pi a^2}{j\omega}\left(1-R_{Cr}\right)I_o\Delta^0\Big|_{r,x=0}\left[\frac{\alpha}{\rho S}\right] \qquad (9)$$

Where the V_{Cr} and R_{Cr} are voltage output of the transducer for the metallised silicon and reflectivity of chromium respectively. The bracketed expression in equation 8 has two terms (for the thermal and electronic contributions respectively). The first, unbracketed term is the effective flux density (this takes into to account the reflection of light). The thermal term (with thermal expansion, heat capacity and density) is for heat given off in the initial relaxation of photoelectrons to the lowest energy state. In the study of Kino and Stearns[4] it is assumed that excess carrier lifetime is long compared with the period of oscillation (less than a microsecond). The equivalent bracketed term in equation 9 only contains a thermal contribution.

For the specific experiment of Kino and Stearns where the wavelength of the light was 514nm, a 0.1μm thickness of Chromium was used and doping of the silicon was $3x10^{19}$P atoms.m^{-3}, measurements of the signal for the metallised and un-metallised silicon were made, experimental results showed that electronic strain (uncoated silicon) was -2.6 (a contraction) times thermal strain, which agreed with their theoretical results. The ratio would be higher for longer wavelength

light because the thermal contribution would be smaller. Kino and Stearns demonstrated the validity of the theory but used a sample that had a carrier lifetime far in excess of the acoustic period. Excess carrier recombination, with its resulting release of heat and relaxation of electronic strain was not taken into account. If the excess carrier lifetime is small compared with the period of oscillation, then electronic strain becomes unimportant. The short carrier lifetime may be a property of the type of silicon, or may be due to the injected carrier density reducing the lifetime because the probability of recombination increases. For the very highly (boron) doped silicon used for micromachined structures (manufacturing techniques are discussed in section 3.9), excess minority carrier (opposite type to the carriers produced by the dopant) lifetime will be short compared with excess majority carrier lifetime. Injection of excess carriers will disturb the minority equilibrium far more than the majority equilibrium and the minority carrier lifetime will be affected accordingly. To judge whether this is the case, the injected carrier density must be calculated for comparison with the carrier density due to boron doping. For an effective etch stop the boron doping could be $7 \times 10^{25}.m^{-3}$. For an illuminated area of 20μm×12μm, 4μm thick where 35% of the light is reflected[74], half of the light passes through the silicon (due to the long absorption length), and the optical power is 0.1mW, with a pulse length of 10^{-5} seconds (typical for this work), the excess carrier density is;

$$\text{Excess Carrier Density} = \frac{\text{Energy}}{\text{Energy of one photon} \times \text{Volume of silicon}} \qquad (10)$$

and gives a value of approximately 10^{24}, so the density of injected carriers is significant but not suffucient to disturb the equilibrium of majority carriers and reduce the lifetime. Typical values for excess carrier lifetimes [74] are around 10^{-5}seconds, although this value depends on the condition of the material. At these values of lifetime and carrier density, electronic strain will be significant and the injected carriers will not reduce the carrier lifetime significantly. Carrier lifetime in an unmetallised resonator could be used to increase or reduce electronic strain and improve actuation efficiency or, conversely, the period of oscillation could be chosen to match the measured lifetime of the silicon.

3.4.2 Opto-acoustic Wave Generation in Silicon Beam Resonators

In section 3.4.1 the mechanisms for the generation of stress through illumination of the silicon are discussed. This section discusses the application of this theory to the specific case of transverse vibrations in a thin micromachined resonator where the thickness of the material and the mode (transverse instead of longitudinal) of oscillation affects the way in which waves are generated. The type of wave being generated also changes the importance of the type of structure i.e., whether or not the silicon is metallised.

In each device, the amount of energy lost per cycle as a proportion of the total energy stored in the resonator is as important as the strain generation mechanism in determining the total deflection of the beam. This fraction is called the Q. If it indicates how many cycles it takes to dissipate the vibrational energy of the resonator, in one cycle of actuation, 1/Q of the resulting energy input will be lost in the next cycle. This means that it will take Q cycles to dissipate the energy equivalent to one cycle of actuation, therefore the total energy at resonance is Q times the energy for one cycle.

In bulk acoustic wave generation an area on the surface of some large block of material is illuminated periodically. Thermal expansion (or some other photogenerated strain) compresses the surrounding area and if the acoustic wavelength corresponding to the period of oscillation is longer than the thermal (or other) diffusion length for the same time, compression waves corresponding to the period of illumination propagate through the material. If this condition is not met, there is no stress field and therefore no wave is present. These bulk acoustic waves are longitudinal in nature.

In transverse wave generation, in addition to longitudinal or compressive stress, there is a bending moment induced by differential expansion between the top and bottom of the resonator. The magnitude and importance of this bending moment depends on whether the beam is metallised and the dimensions of the beam relative to the absorption length of light and the thermal or electronic diffusion length (for the corresponding period of oscillation).

The thermal diffusion length, L_{th} ,is the distance away from the light source for the temperature to decay to 1/e of its peak value in the period of oscillation and is[77]:-

$$L_{th} = \sqrt{\frac{\tau C}{\rho S}} \qquad (11)$$

Where τ is the period of one oscillation, C is the thermal conductivity, and S is the specific heat capacity.

There is a corresponding electronic diffusion length which is given by[77]:-

$$L_{El} = \sqrt{D\tau} \qquad (12)$$

Where L_{El} is diffusion length, D is the electronic diffusion constant and τ is the period of oscillation.

These characteristic lengths are important since they define the volume of material that undergoes significant induced stress during one cycle. A long length will reduce the peak compressive stress and differential stress across the thickness of the beam, although the volume of material under stress will be greater. Section 3.5 discusses the theoretical efficiency of actuation using the thermal diffusion length to estimate the peak temperature. These equations may also be used to calculate a characteristic time to achieve equilibrium, given a particular length (for example the thickness of the beam).

The design parameter which determines the size of the bending moment induced by light, relative to the bending moment required to produce sufficient curvature, is the thickness of the beam. It is possible to calculate an optimum thickness with respect to the characteristic electronic or thermal diffusion length by maximising the ratio of induced bending moment to stiffness. The induced bending moment is calculated by finding the stress at a given distance from the top of the beam. This stress is determined by the penetration depth of light in uncoated silicon and, working from the incident flux density, the reflectivity of the material. This stress is then integrated, with positive stress above the neutral axis and negative stress below. It is assumed that in the case of electronic strain, the excess carrier lifetime is long with respect to the time taken to achieve equilibrium

across the beam. This diffusion time determines the effective induced differential stress. In the calculation for optimum thickness for electronic strain, the thermal contribution is ignored because is is assumed that the electronic mechanism is dominant and for simplicity.

The bending moment for a given deflection in a bridge structure is;

$$\text{Moment} = \frac{2bt^3E}{l^2} \times \text{Deflection} \qquad (13)$$

where b, t and 1 are the width, thickness and length of the beam respactiviely and E is the Youg's modulus of the material. This must be balanced against the induced moment about the neutral axis of the structure;

$$\text{Induced Moment} = \int_t^0 bl\sigma E\left(\frac{t}{2} - x\right).dx \qquad (14)$$

where σ is the strain and x is the distance from the top of the beam.

The reflectivity of a material is given by[78];

$$\text{Reflectivity} \approx \left(\frac{n-1}{n+1}\right)^2 \qquad (15)$$

where n is the refractive index (about 3.4 in silicon) yielding a reflectivity of about 0.3.

The flux density at a given depth in the silicon is then;

$$\text{Flux Density} = I_0(1-R)e^{-\frac{x}{d}} \qquad (16)$$

where R is reflectivity (as defined above), d is the penetration depth of light in silicon and I_O is the flux density of light at the surface.

If equation 8 is used for the number of carriers generated and the strain produced per carrier, and where the time to reach equilibrium across the beam (equation 12) is used to find the energy (the effective non-equilibrium state lasts for the diffusion time and flux is Joules/second);

$$s = \left(I_0(1-R)e^{-\frac{x}{d}}\frac{\lambda}{hc}\right)\left(-\frac{1}{3}\frac{dE_g}{dP}\right)\frac{t^2}{D} \qquad (17)$$

where λ is the wavelength of light (typically 750nm -810nm for a laser diode) h is Planck's constant, c is the speed of light, t is the thickness of the beam, and x is the distance from the top.

This may then be substituted into the integral to find the total bending moment, as shown below:

$$\text{Total Moment} = K\int_{1}^{0}\left(\frac{t}{2}-x\right)e^{\frac{-x}{d}}.dx \qquad (18)$$

where all constant values are included in K.

For a given beam length, the bending moment (controlled by the exponential and the diffusion time) becomes larger with thickness, but the deflection decreases by (thickness)^3. The optimum thickness can be found by differentiating the expression for the deflection using the above expression for the bending moment i.e., if the integral for the total moment is called T, and the thickness is t, differentiate for T/t^3. A numerical method for solution of the equation yields an optimum thickness of 2.7xpenetration depth (d). This relates the thickness to a physical property of the silicon (electronic diffusion constant) but only takes into account one form of strain generation.

A similar argument may be used with metallised structures where the thermal diffusion constant is used to calculate the effective temperature difference across the beam. The relative sizes of the electronic and thermal diffusion constants will affect the relative importance of thermal and electronic strain. In silicon, the electronic diffusion constant is typically ten times the thermal diffusion constant, so a thin structure will favour the thermal mechanism.

Another mechanism that affects metallised structure actuation is the 'bi-metallic' effect, where differential thermal expansion between the metal and silicon generates a bending moment in the beam. This is a function of metallisation thickness and again there will be an optimum ratio of metallisation thickness to silicon thickness which will be related to the Young's moduli of the materials and the increase in damping by the metal. It has been shown [63] that actuation efficiency increases as metallisation thickness increases up to a

limit where the extra damping becomes important and the structure becomes too thick.

A simple expression for the total bending moment due to differential expansion of the metal and silicon, neglecting the bending moment in the aluminium is;

$$\text{Moment} = \Delta T(\alpha_{Al} - \alpha_{Si})E_{Al}.A.\frac{t}{2} \qquad (19)$$

where A is the area with a temperature difference (from the thermal diffusion length and illuminated area size), ΔT is the temperature difference and α is the coefficient of thermal expansion with subscripts of Al and Si indicating aluminium and silicon respectively, and E_{Al} is the Young's modulus of aluminium.

Again, the deflection at resonance will be Q times this value. Any attempt to predict the optimum thickness of aluminium should also take into account the internal acoustic losses of metal which will significantly reduce the Q[64].

In addition to an induced bending moment, there is the overall expansion of the beam which is more like the conventional photoacoustic wave generation discussed above. The longitudinal strain in the neutral axis of the beam, bending for a deflection of h and a beam length l, making the assumption that it forms a perfect arc is;

$$\text{Strain in Beam} = \frac{\tan^{-1}\left(\frac{2h}{l}\right)}{2\sin\left(\tan^{-1}\left(\frac{2h}{l}\right)\right)} \qquad (20)$$

and the strain due to the rise in temperature or excess carrier density per cycle should be 1/Q of this.

The actual deflection produced by the two mechanisms (acoustic wave and differential strain) will not give the same deflection for a given strain. It may be possible to optimise the resonator design to favour the most efficient mode of deflection generation. For a metallised beam, the thickness of the metal layer may favour differential

expansion over acoustic wave generation or, because of more efficient thermal conversion, favour acoustic wave production.

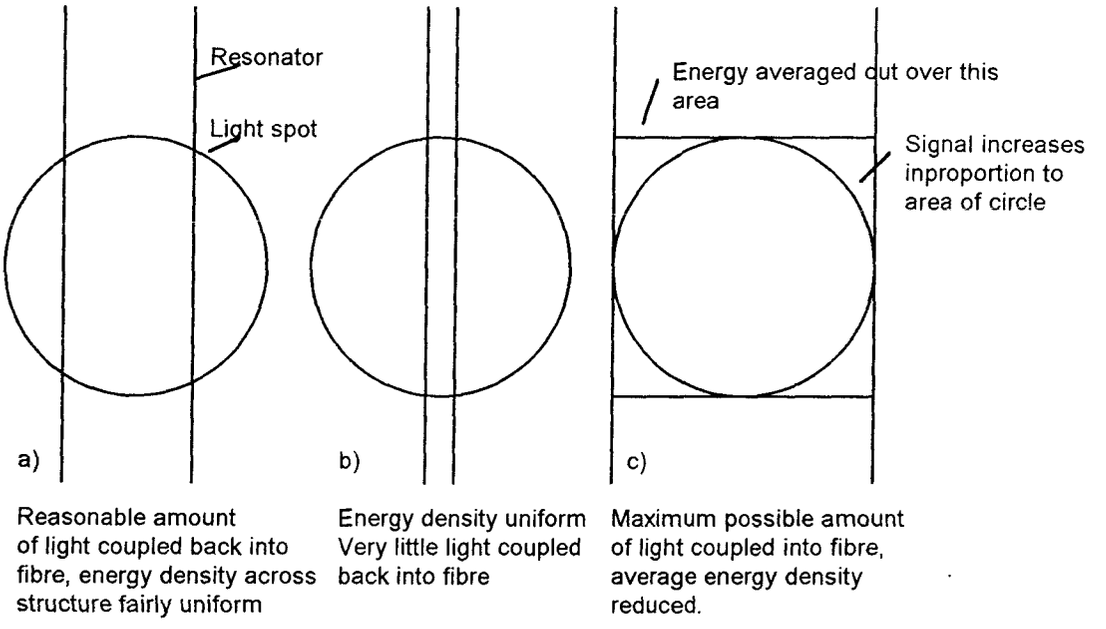

Figure 3.4 Energy Density -Optical Signal Balance

3.4.3 Energy Density-Optical Signal Balance and the Resonator Width

If the energy density for actuation is fixed and the resonator is operating under vacuum, the width does not effect either deflection size or frequency. If the light is coming from the bare end of a fibre without focussing optics, it will be spread over an area that will depend on the fibre-target separation and the angle of the cone of light from the fibre (determined by its numerical aperture). The amount of light from the fibre that misses the resonator (if it is assumed that the fibre system is aligned along the axis of the resonator correctly) depends on its width. If the fibre end to sensor distance is small compared with the core diameter of the fibre, the amount of light returned from the resonator depends only on the width. If the resonator is wide, the maximum possible amount of light is coupled back into the fibre but the length of resonator near the edge that is illuminated is reduced, so the average energy density on the resonator is less. The square on figure 3.4(c) illustrates the area over which the energy dendity is calculated. So, the width of the resonator in an evacuated system has an upper limit which is set by the energy density required for actuation, and a lower limit which is set by the need to couple sufficient light back into the fibre for

interrogation. The resonator must also be wide enough to suppress any lateral modes of vibration which means that the energy required to excite 'side-to-side' movement of the beam is far greater than the energy required to excite 'up-and-down' modes. This is necessary for stable, single frequency resonance of the structure. The relative sizes of the light spot and the resonator are illustrated schematically in figure 3.4, where the circle represents the illuminated area and the straight parallel lines represent the resonator width.

For both types of optical interrogation being considered here (phase modulation and amplitude modulation of the reflected light are discussed in section 3.6), the signal increases with the amount of light returning to the fibre. For interferometric interrogation, where the signal increases with the square root of the amount of returning light, the optimum resonator width is 0.7 times the width of the illuminated area.

The results presented here will be used in the analysis of results which will be used to optimise the design of the resonator in Chapter 6. The controlling parameters for the length of the resonator are dicsussed in section 3.10.

3.5 Actuation Efficiency

This section approaches the actuation mechanism by presenting a method for calculating the efficiency, considering the maximum theoretical efficiency as a heat engine, the energy input to the oscillator and the energy necessary to maintain oscillation after dissipation. This is intended to give some idea of the energies involved in sensor actuation and perhaps suggest a way of improving the efficiency.

3.5.1 The Efficiency of an Ideal Heat Engine

Since the underlying effect of the "actuation mechanism" is to take one form of energy and convert it, by heating, into movement, the system of modulated laser and vibrating microstructure may be considered to be a heat engine and is thus limited in its efficiency by the maximum temperature change achieved during a complete cycle.

This maximum efficiency can not exceed that for an ideal heat engine as described by the Carnot cycle and is:

$$E_{max} = \frac{(T_1 - T_2)}{T_1} \qquad (21)$$

Where T_1 is the maximum and T_2 is the minimum temperature in Kelvin.

A rough estimate of the temperature change is from the temperature rise necessary to conduct the energy away to the bulk material.

To a first approximation (assuming the beam to be long in comparison to its depth, i.e. an insignificant temperature gradient going down from the aluminium to the silicon) the thermal conductivity of the composite bridge may be found by adding the parallel thermal conductivities of the silicon and aluminium:-

$$\frac{1}{C_T} = \frac{1}{C_{Al}} + \frac{1}{C_{Si}} \qquad (22)$$

where C_T, C_{Al}, and C_{Si} and the conductivities of the composite beam, aluminium and silicon respectively.

Using this conductivity and the expression for the thermal diffusion length (equation 11) the volume of silicon and aluminium that is heated by the energy in one pulse may be calculated and from this, the maximum temperature rise. This is used to calculate the maximum theoretical efficiency. These results are used in the discussion, section 6.3 to calculate the efficiency of actuation of the devices used in this work.

3.5.2. Calculation of the Efficiency From the Mechanical Q and Stored Energy of the Resonator

The energy necessary to maintain oscillation at the observed amplitude is equal to the energy loss per resonator cycle. The mechanical Q of a resonator is defined as:-

$$Q = \frac{\text{Total Stored Energy of Resonator}}{\text{Energy Lost per cycle}} \qquad (23)$$

For a given Q, a fraction of 1/Q of the total energy of the resonator must be added per cycle to maintain steady oscillations.

The energy of an oscillator may be found by evaluating the generalised integral[71]:-

$$U = \frac{1}{2}\int EI\left(\frac{d^2y}{dx^2}\right).dx \qquad (24)$$

Where the beam deflection (y) is a function of the distance along the (in this case) beam (x) and U is the energy. EI is the flexural rigidity and is constant for all values of x and y relevant to this example (y is defined in equation 1).

For a rectangular section bar [72],

$$I = \frac{bt^3}{\sqrt{12}} \qquad (25)$$

and by a numerical method the integral is reduced to:-

$$U = \frac{1}{2\sqrt{12}} Ebt^3 I A^2\beta^4 \qquad (26)$$

Where A is the amplitude of oscillation and β is determined by the mode of oscillation and boundary conditions, see section 3.3. By inspection of equation 25, the energy of the oscillator increases dramatically as the number of nodes, the amplitude or the thickness increase. Since for a given mode, (β × length) is constant, if the length is reduced to increase the frequency, the amplitude of oscillation must also drop for the same energy in the resonator.

The energy input to the bridge for a metallised device, per cycle, is given by:-

Energy = Power from fibre end
x absorption coefficient of aluminium
x period of oscillation.

From this relationship, the (measured) Q and the energy stored in the device, an experimental value for the efficiency of actuation may be calculated and these expressions are used for the results obtained in this work in sections 6.3 and 6.4.

3.6 Optic Fibre Vibrometry

3.6.0 Introduction

There are at least two possible but fundamentally different methods that could be used for the optical vibrometer. They are the more usual interferometric technique[14-19,67,68] and a reflectometric technique[69]. The second of these two is only possible because of the controlled geometry of the sensor and the large movement of some devices.

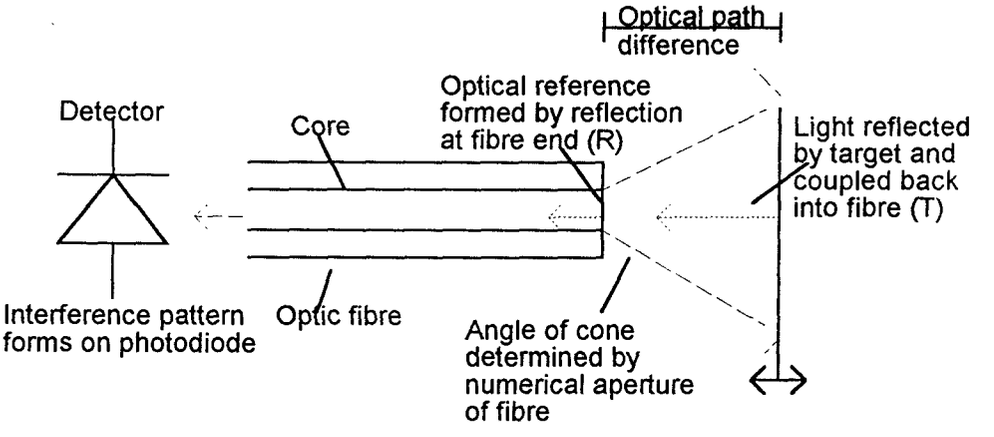

Intensity of light from fibre = I
Intensity of light from target = IxT
Intensity of light from reference = IxR

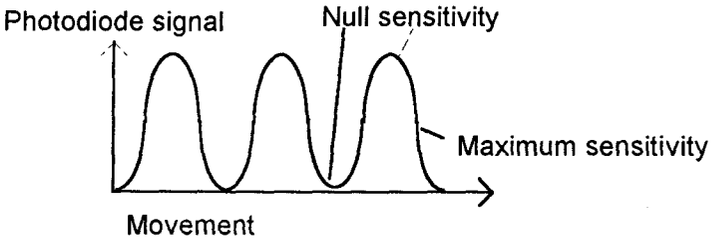

Interference fringes. Maximum signal is proportional to the square root of TxR.

Figure 3.5 Important Dimensions in Interferometric Vibrometry

3.6.1 Interferometric Vibrometry

Vibration may be detected optically using a Michelson-Morley interferometer arrangement. Figure 3.5 illustrates schematically an optic fibre placed close to the target surface. An optical reference signal is reflected from the end of the fibre, and some of the light that is reflected from the target is coupled back into the fibre. As

the target moves, the interference pattern that is formed on the photodiode changes in intensity. This change is shown by the graph of movement against photodiode signal. As the target moves there are regions of null sensitivity where the change in signal is small for a small amount of movement and regions of maximum sensitivity where the gradient of the graph is high. The basic variations of interferometer are illustrated below in figure 3.6. Each version has its own distinct advantages and disadvantages but perhaps the best compromise between cost and high frequency performance is the simple single mode fibre version.

The two systems using frequency shifted reference beam techniques both avoid the problem of null sensitivity points i.e. points where the signals have the same phase, and the change in intensity with the change in phase of one of the components is very small. They achieve this by 1) tracking the phase change and maintaining the optical path difference at its optimum sensitivity or 2) by frequency shifting one arm of the interferometer, the vibrational information is seen as a modulation of the beat frequency between the two components. Without some phase modulation of the light in one arm of an interferometer, there will always be a range of phase differences (between the two optical paths) where the change in intensity of light at the output of the instrument for a given change in the phase difference is very small. This is obvious when it is considered that the output intensity is proportional to the $\sin^2$ of the phase difference between the two optical paths.

The simple single mode interferometer is easy to build and gives a good signal when the path length is adjusted properly. A lower cost version is the very simple multimode fibre interferometer. The problem with multimode fibre is it has many different optical paths each of which may interfere, if the light is coherent, producing modal noise. If the coherence length of the light source is short, interference in the fibre is prevented once the modes have travelled far enough to become incoherent. Successful operation as an interferometer requires that the distance between the reference (fibre end) and target (silicon resonator) is less than the coherence length. This may be realised by using a multiple transverse mode laser diode, which is

designed to have a short coherence length (less than 1mm) to avoid mode noise in the laser cavity.

More recently, white light interferometers have been developed that use broadband sources. These can work if a second interferometric system is used to retrieve the signal (optical path length matching) or if the distance between the optical reference and the signal is less than the coherence length of the light source. The problems with this is that the fibre must be mounted very close to the resonator, and the power available may not be enough at the required wavelength (even with the required power from the light source, coupling efficiency to the fibre can be poor). Potential light sources include the newer 'non-coherent' laser diodes which demonstrate similar efficiency to a laser diode but do not have an effective optical cavity[80].

Irrespective of the particular type of light source used, a simple interferometer of the Michelson-Morley arrangement will not be sufficient for closed loop operation of a sensor, since there is no fixed optical phase reference. This causes an ambiguity in the signal, where its direction with respect to the direction of movement of the resonator may change by 180° as the cavity size changes. Unless the cavity is stable to better than a quarter of a wavelength over the temperature range of the sensor or the optical system is more sophisticated (figure 3.6 a and b illustrate typical systems) a non-interferometric vibrometer will have to be used. A possible, low cost solution to this problem based on the stabilisation of self-resonant devices[29] is discussed in Chapter 8 where development of a similar system is proposed for further work.

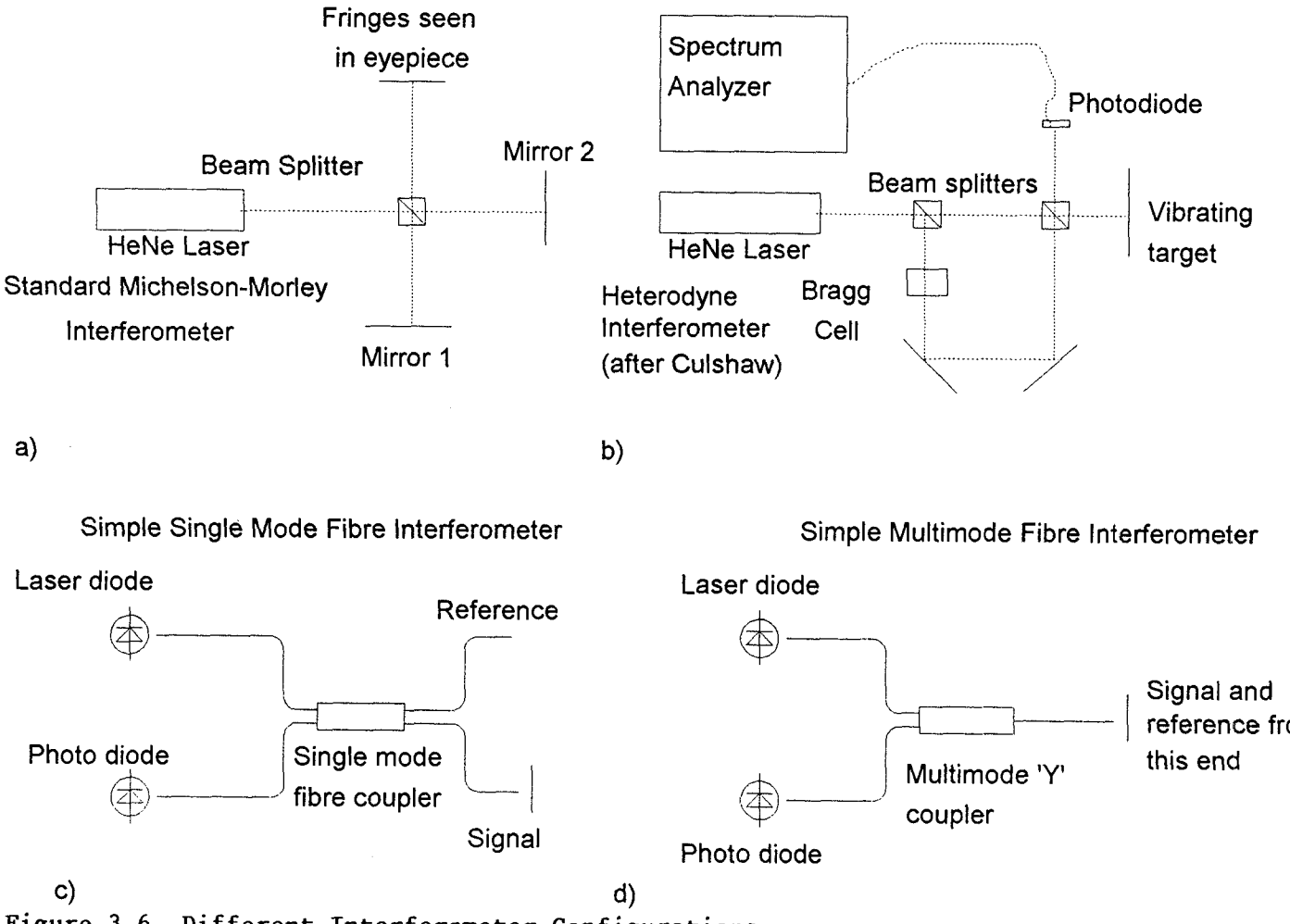

Figure 3.6 Different Interferometer Configurations

A second problem with an interferometric system is that the signal is limited by the amount of light available from the optical reference. This is typically 4% from a glass-air interface which is then further reduced if a 50% optical splitter/coupler is used.

If the size of the interferometric signal is given by[81];

$$\text{Interferometric Signal} = 2I\sqrt{RT}\cos\left(\phi + \frac{2\pi(\text{pk - pk movement})}{\lambda}\right) \quad (27)$$

where I is the intensity of light from the fibre, T and R are the proportion of this light that is returned to the fibre (where R<<T) from the fibre end and target respectively, ϕ is a phase which is dependent on the optical path difference and λ is the wavelength of the light. These terms are illustrated in figure 3.5. As may be seen from this equation an increase in the size of the reference intensity will increase the signal significantly, and the amount of light available for actuation will only be reduced by a small fraction. If the coherence length of the light source is long enough, the fourth port of a single mode coupler could be used to provide a reference signal at least as large as the target signal to achieve the maximum possible fringe visibility. Since the shot noise from the photocurrent is dependent on the total photocurrent (not the product), increasing the smaller optical reference will have no effect on the noise (because the intensity frmo the target is reduced by the same amount). Taking into account the shot noise of the photocurrent and the dark current of the photodiode, the signal to noise ratio is given by:

$$\frac{Signal}{Noise} = \frac{\text{Interferometric Signal} \times \text{Photodiode Response}}{\left(\left((2I(R+T)\times e + (\text{Dark Current})^2\right)\times BW\right)^{\frac{1}{2}}} \quad (28)$$

where the interferometric signal is defined in equation 27, the photodiode response is the photocurrent per watt of optical power, I, R and T are illustrated in figure 3.5, e is the charge on the electron, the dark current is the leakage current produced by the photodiode and BW is the bandwidth of the optical detection system. This is limited by the capacitance of the photodiode and the size of the resistor that is used to convert the current into a voltage

signal. If the peak to peak movement is small compared to the wavelength, the system is adjusted to its maximum sensitivity at $\pi/2$ phase difference and the light reflected from the fibre end is small compared to the light reflected from the target and coupled back in to the fibre, this expression can be reduced to;

$$\frac{Signal}{Noise} = \frac{4I(RT)^{\frac{1}{2}} \times (\text{photodiode response})}{\left(\left(2I(R+T)e + (\text{dark current})^2\right)BW \times \lambda\right)^{\frac{1}{2}}} \times \text{Peak to Peak Movement} \quad (29)$$

3.6.2 Calibration Procedures

Coarse calibration (sufficient for this work) of an interferometric vibrometer is fairly simple. Assuming that the device will be used over its most sensitive range, then its output may be assumed to be linear with distance. If a suitable target is moved by more than $\lambda/2$ the output goes through one complete cycle. The maximum electrical signal achieved is then equivalent to $\lambda/2$ movement. The most sensitive point of the interferometer is mid-way between the maximum and minimum signal.

3.6.3 Reflectometric Vibrometry

Since the geometry of the sensor is fixed it may be possible to detect the motion of the resonator from the change in the amount of light coupled back into the fibre by reflection from the target. This frees the system from the problems associated with maintaining a suitable optical phase reference but may not be sensitive enough. Transmission noise would not be a problem because the resonator frequency will be above any acoustic interference and the absolute amplitude of the signal is not important . The main problem may be finding a light source that will couple sufficient light into the fibre for actuation but has a sufficiently short coherence length to avoid optical interference. A super radiant diode SRD[72] may be suitable for this. Also, because this technique is much less sensitive it may require reflection from the edge of the device to get a larger change in the amount of light coupled back into the fibre (i.e., amplification of the signal by using some discontinuous reflector).

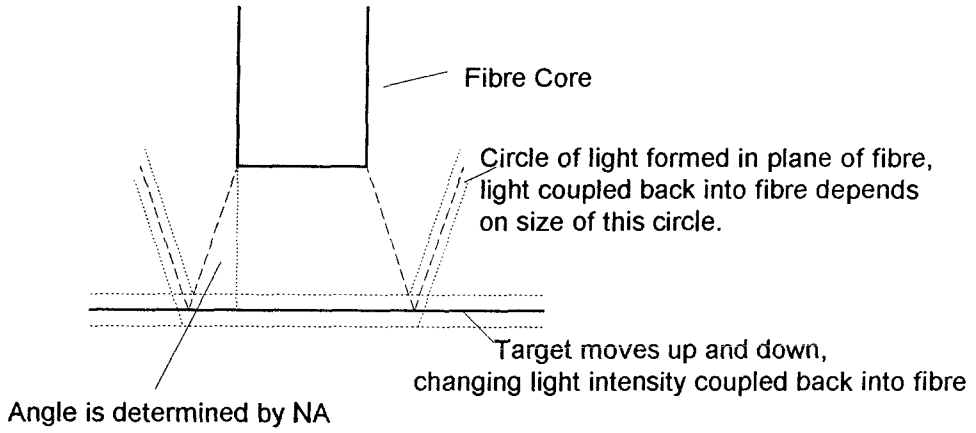

Figure 3.7 Reflectometric Vibrometry

Light diverges from the end of a fibre at an angle determined by the numerical aperture (NA) of the fibre, as illustrated in figure 3.7. The area of the target that is illuminated is then determined by the NA of the fibre and the distance from the target. This area then acts as a light source, emitting light with the same NA as the fibre. For a fibre to target distance of d;

$$\text{Light Coupled Back into Fibre} = \frac{(\text{core radius})^2}{(\text{core radius} + 2d\tan(\sin^{-1}\text{NA}))^2} \qquad (30)$$

This assumes that the target is as wide as the illuminated area. For a resonator, the signal will be reduced by the ratio of the two areas.

This expression gives a dependence for the signal with distance that indicates a higher sensitivity as the fibre becomes closer to the target. This may have to balanced with coherence length considerations since the interferometric signal could be 180° out of phase with the reflectometric signal. This could be solved by using an anti-reflective coating on the end of the fibre. Curvature of the beam is not considered in this treatment since it is negligibly small for the geometries in this work.

From the alternatives of interferometry and reflectometry, the first is more sensitive but the simplest configurations are unstable with respect to the phase of the oscillator, making closed loop operation impossible. This situation may be alleviated by using a long wavelength, stable communication diode and a single mode fibre, allowing a greater change in optical cavity size and maintaining

fringe visibility. The alternatives to this are active adjustment of the laser diode, or a more sophisticated interferometer (perhaps using a Bragg cell for phase shifting of one interferometer arm) which would be far more expensive. Effective reflectometry needs adjustment of the mechanical arrangement such that a movement of the reflector causes a discontinuous or non-linear change in the back-reflected siganl to become effective.

3.7 Silicon Bonding Techniques

3.7.0 Introduction

There are many methods that are used for bonding to silicon in sensors. This section concentrates on the theory of forming silicon-to-glass and silicon-to-silicon permanent bonds. A glass mounting is desirable because of its ability to be moulded for interface to the rest of the system (perhaps incorporating a lens) and its chemical stability. Silicon mounting for the sensor has the potential for an ideal match between the silicon sensor and the sensor housing, as well as providing a means of accurate location of the sensor by matching micromachined features if allignment of an optical system is required. In Chapter 6 other possible techniques for mounting the silicon chip are discussed as well as the whole problem of packaging a silicon sensor.

3.7.1 Mallory Bonding[5,43,44]

Conditions for anodic or Mallory bonding were initially researched in 1969 and have recently merited further attention because of the potential for stable, hermetically sealed mounting of silicon sensors.

The theory of the bonding mechanism is that when the glass is heated it becomes conductive. An electric field is applied that drives alkali atoms away from the silicon interface to leave free oxygen atom bonds in the glass which then bond to surface silicon atoms. The temperature can be selscted to reduce the residual stress after bonding to a minimum, and if the electric field is removed before the assembly is cooled, there is no residual rlectric field which could also cause drift

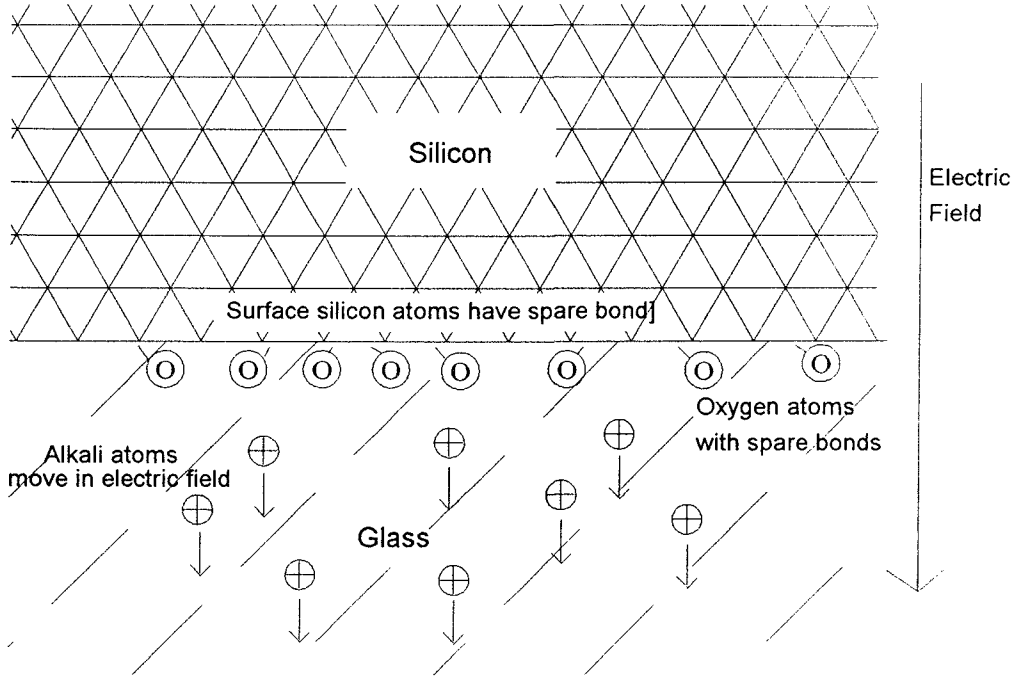

Figure 3.8 Schematic of Electrostatic Bonding

3.7.2 Silicon to Silicon Fusion Bonding

Silicon-to-silicon or silicon fusion bonding may be used to produce a continuous bond between two pieces of silicon with no impurities in the bond region. Atomic microscopy has shown that the only evidence of the bond is a discontinuity of the lattice orientation. The advantage of silicon to silicon bonding is that no pressure or field is required to achieve the bond. The main problem is the temperature required. This is high enough to preclude the use of an aluminium metallised structure (chromium may be suitable). One of the reasons why an understanding of unmetallised actuation is that it may be required to realise the full potential of this bonding technology.

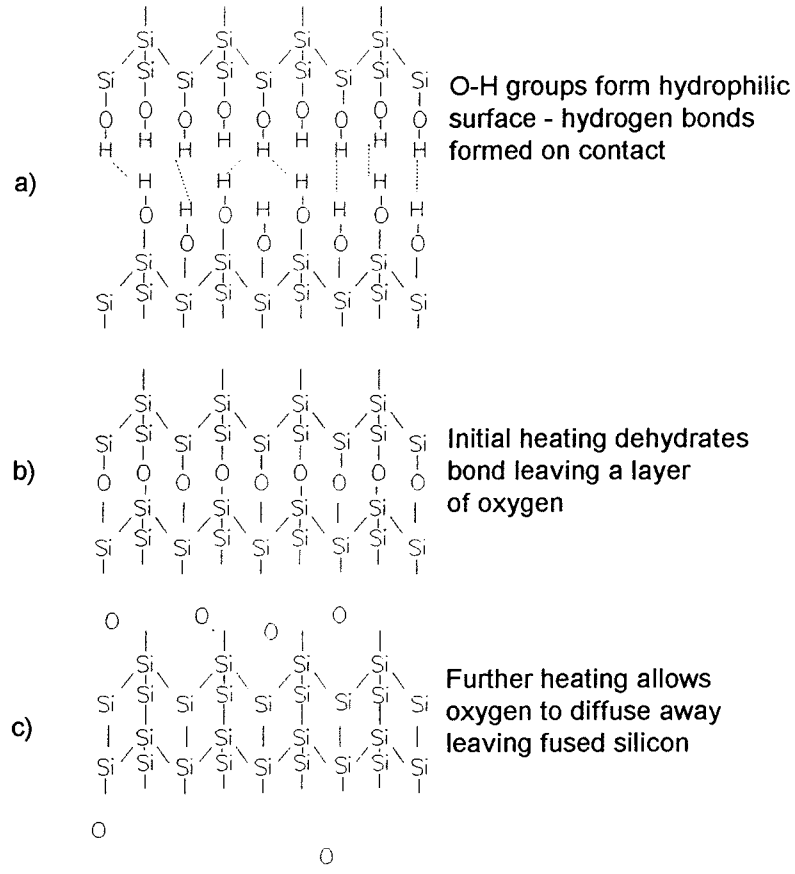

Figure 3.9 Silicon Fusion Bonding Mechanism

The only surface preparation required for reliable bonding is that the silicon surfaces must be hydrophilic and clean. The hydrophilic layer is fomed by a layer of -O-H groups attached to free silicon bonds on the surface (called silane). At room temperature, these groups form a strong bond on contact with another similar surface. The assembly is then baked. At high temperature, (800°C) water diffuses from the interface, leaving a layer of Si-O-Si which is stable. At 1100°C the oxygen diffuses away from the bond to leave fused silicon. Figure 3.7 illustrates the mechanism. Chapter 8 discusses the advantages of this and other bonding techniques. If the same type of silicon is used (e.g, ‹111› or ‹100›) the mechanical properties of the sensor and its mounting will be the same, thus preventing thermal mismatch and stresses across the bond which could lead to increased thermal sensitivity or drift.

3.8 Material Properties of Micromachined Silicon and Micromachining Techniques

Shapes for microcomachining in silicon may be defined by diffusing high ($10^{25}m^{-3}$) concentrations of boron into the surface of the silicon and removing (possibly with plasma etching) silicon around the desired shape. Etching under the required structure is then achieved using a chemical that does not etch the boron doped silicon but does etch normal silicon. Whilst this technique is compatible with integrated circuit technology the boron doped silicon has a high residual stress which places the structures under tension and reduces the stiffness of the material. These effects may be reduced by annealing. If the physical properties change in a short time during annealing the possibility of sensor drift due to a relaxation of this tension over a long period of time must be considered. Annealing would therefore be recommended as part of the normal manufacturing process.

The amount of residual tension in boron doped silicon is proportional to the level of doping and is approximately equal to 2.3×10^{-24} times the doping concentration (for boron).

Silicon has a high Young's modulus, comparable with steel and about a fifth of that of diamond and it also has a high tensile strength. The Young's modulus of silicon depends on the material condition and the crystal orientation. Values have been are measured for bulk silicon and microcomachined resonators. The problem encountered with silicon is its low dislocation mobility which prevents it from deforming plastically and causes it to fail catastrophically instead. Since silicon pressure gauges measure the stress in the diaphragm directly rather than the strain, this is not a problem and the high Young's modulus and yield strength allow silicon sensors to have a very good overpressure capacity.

3.9 Resonant Frequency Tracking Using A Phase Locked Loop and the Signal to Noise Ratio

The frequency output of a voltage controlled oscillator (VCO) is used to measure the resonant frequency of the mechanical pressure dependent resonator at the other end of an optical fibre. In order to determine

how accurate this is, it is necessary to understand how the VCO is controlled and how accurate the method of control is.

A phase sensitive detector (PSD) is used to sample the frequency output of the resonator. By integrating the output of a multiplier, it is effectively summing samples of half cycles of the signal. Each of these samples has an error caused by the noise in the system. By summing and averaging a number of samples in this way, the noise in the output is reduced by a factor;

$$\left(\frac{\text{Noise}}{\text{Signal}}\right)_{\text{OUTPUT}} = \frac{1}{\sqrt{N}} \sum_{0}^{N} \left(\frac{\text{Noise}}{\text{Signal}}\right)_{\text{INPUT}} \qquad (31)$$

where N is the number of resonator oscillations in one PSD integration interval. This expression does not take into account any systematic errors which would distort the signal and increase the error in the PSD output. As can be seen from equation 31 the signal-to-noise ratio improves as the number of samples increases. The required signal to noise ratio from the vibrometer (which will be a sum of all the noise sources to that point, i.e. a sum of the squares of those contributions) may be calculated from the frequency of the resonator and the required response time of the system.

3.10 Frequency Range and Resonator Length

In order to optimise frequency measurement within the physical constraints of the system (such as alignment of the optical system and manufacturability), it is important to select the optimum frequency operating range. This process has to take into account the required response time, amplitude of oscillation, intended accuracy of the transducer and bandwidth. Starting from equation 31, the uncertainty in the output of the PSD depends on the number of oscillations in a given integration time, the amount of noise and the amplitude of the signal. In order to find the best frequency, the dependency of equation 31 on frequency must be found by deriving the components of the differential shown by;

$$\frac{dU}{df} = \frac{\partial N}{\partial f} \cdot \frac{\partial n/\partial f}{\partial S/\partial f} \qquad (32)$$

where n and S are the noise and signal amplitudes respectively, U is the uncertainty in the output of the PSD, N is the number oscillations in the sample time and f is the frequency of the resonator. Differentiating equation 31 with respect to N gives an expression for the change in the uncertainty with the number of oscillations of,

$$\frac{\partial U}{\partial N} = -\frac{1}{2}N^{-\frac{3}{2}} \qquad (33)$$

and substituting the dependency of the first term in equation 32 on frequency this becomes;

$$\frac{\partial U}{\partial f} = -\frac{T}{2}f^{\frac{-3}{2}} \qquad (34)$$

The noise depends on the bandwidth of the system, which will be determined by the capability of the electronics to track the frequency over a given range and the frequency at zero pressure (base frequency). The sum of these (i.e. the highest frequency that the system will operate at) is the bandwidth (BW), and if the change in the frequency is small this is the same as the frequency of the oscillator;

$$\text{Total Noise} = n_o \times \sqrt{f} \qquad (35)$$

where n_o is the noise/$\sqrt{}$Hertz for the light detection components in root mean squared (RMS). This gives a dependency of the noise on frequency of;

$$\frac{\partial n}{\partial f} = -\frac{1}{2}\frac{n_o}{\sqrt{f}} \qquad (36)$$

where n is the total noise. The dependence of the signal amplitude on frequency is rather more complex, as it depends on both the thickness and the length of the resonator. Since the thickness of the device is used to optimise actuation or may be restrained by silicon processing parameters a change in the length only will be considered here. From equation 26 and assuming that the vibrational energy is constant, the signal size is proportional to the length squared which, in turn is inversely proportional to the frequency. This gives an expression for the change in signal if the length is used to change the frequency;

$$\frac{dS}{df} = -\frac{k}{f^2} \quad (37)$$

where k is some constant of proportionality.

This gives a total expression of;

$$\frac{dU}{df} \propto T \times n_o \quad (38)$$

which, within the limitations of this analysis, is independent of frequency and depends only on the sample time T and the noise per root Hertz of the optical source and detectors.

This means that the signal to noise ratio from the interferometer is independent of the length of the beam, so length may be used to optimise device size to the requirements of the optical system (detection and actuation) and achieve a frequency which is separated from any low frequency noise and is compatible with the available electronic components. The thickness is used to maximise the deflection size which is more important than frequency when improving signal to noise ratio. An alternative approach would be to maximise the amount of energy incident on the beam by reducing the length until all of the central section (positive strain) is heated by the light from the fibre. Any reduction in length beyond this point would mean that parts of the beam in negative strain would be heated, reducing overall curvature. Any increase reduces the energy density for the whole beam. The thickness could be chosen to balance the sensitivity, actuation efficiency and frequency. This approach is less complex than an analysis of actuation mechanisms, but may cause problems if the necessary thickness (scaled down from larger devices) causes difficulties in production.

3.11 Resonant Systems

There are two oscillating systems in the transducer. The first is the sensor which is a forced oscillator being driven at or near its resonant frequency. The second is the VCO-PSD-sensor system which is a pressure and temperature dependent oscillator. Since actuation and detection of the resonator are being switched, it will not be in a steady state. The minimum response time for the system must be known

and the system must be stable if there is a sudden change in pressure. If the phase between the drive and the response changes this will produce an error in the output of the PSD which will affect the VCO frequency so any phase shifts in the system must be either stable for all frequencies or at least repeatable within the system tolerance. If the transient and driven behaviour of the resonators used in this work is similar to the behaviour of a simple harmonic oscillator, they can be described by[81];

$$\frac{d^2y}{dt} + 2b\frac{dy}{dt} + \omega^2 y = F\sin\omega' t \qquad (39)$$

where y is position along the bar, t is time, F is the driving amplitude, ω and ω' are the natural and the driving frequencies respectively and b is some damping factor. This equation has a transient and a steady state solution for different levels of damping. The lightly damped solutions (small b) are relevant in this case. The transient solution is;

$$y = Ae^{-bt}\sin\left(\left(\sqrt{\omega^2 - b^2}\right)t\right) \qquad (40)$$

where A is the amplitude at time t=0. This equation tells us that the resonator does not resonate at its natural, undamped frequency but is shifted by an amount that depends on the Q of the device. If the Q is the number of oscillations that it takes to decay to 1/e of the original amplitude, then b is Q^{-1} times the resonant frequency. This means that the value b may be measured experimentally, so the undamped frequency may be found. This can be used to find a more accurate value for the residual stress or other mechanical property of a relatively low Q resonator. This equation also tells us that if the amount of damping changes, the resonant frequency of the device will change, causing drift.

The steady state solution for driven simple harmonic motion is;

$$y = \frac{F}{\sqrt{\left(\omega^2 - \omega'^2\right)^2 + 4b^2\omega'^2}}\sin(\omega' t - \phi) \qquad (41)$$

where ϕ is some phase difference. For driven oscillations, the maximum response is achieved at resonance where the driving frequency is ω^2.

$2b^2$. This is not the same as the natural damped frequency, so the measured frequency of a sensor using a self-resonant system of actuation or separate drive and detection systems operating in a closed loop will be different from the resonant frequency measured by pulse train actuation followed by free decay. This should not cause any problems for the stability or accuracy of the system since there is no feedback of the response of the resonator during the actuation cycle. It will mean that if the system is operating under closed loop conditions, and the frequency of the VCO is the same as the undriven frequency of the resonator, the actuation efficiency will be reduced because this is not the frequency at which the resonator has maximum response. It may be possible to account for this in the phase shifter between the reference and the signal inputs to the PSD to achieve the maximum signal possible.

For a pulse train driven system, the drive frequency can not be a pure sine wave since it is not infinitely long. The width of the drive frequency is related to the length of the pulse train and this will obviously affect the observed Q of the device. The fundamental relationship is[80]:-

$$\Delta\omega\Delta t \geq 1 \qquad (42)$$

3.12 Noise Sources[81]

There are both optical and electronic noise sources in the system. The optical 'noise sources' are associated with the nature of the optical source and the vibrometer used and are covered in section 3.6. The electronic sources can be broken down into each component and then summed.

The sources of noise in electronic components are shot (current) and Johnson (voltage) and may be calculated for discrete components. Integrated circuits such as operational amplifiers have a noise contribution which is generally documented in data sheets in volts or amperes per √Hertz. Photodiodes have a dark current which is normally stated in nanoamps per √Hertz or this is also expressed as a a quality factor called the noise equivalent power (NEP). This is the amount of light that would produce the same current as the dark current and is

given in W/√Hz for a wide range of frequencies and wavelengths to characterise the device.

$$\text{Shot Noise (RMS)} = (2qI_{dc}B)^{\frac{1}{2}} \qquad (43)$$

$$\text{Johnson Noise(RMS)} = (4kTRB)^{\frac{1}{2}} \qquad (44)$$

Shot noise is caused by the quantised nature of charge and, because of the square root (from statistical 'random walk' of electrons) is less significant for large currents. It will be more significant, therefore for the small current flowing in the photodiode. When dealing with small perturbations of a larger signal such as the output of the interferometer, the dark current will be due to the dc component but will affect the small ac vibration signal. For improved performance this dc component should be kept as small as possible.

Johnson noise is caused by electron-phonon interactions and is a thermal effect. It only becomes important when there is a large value resistor present in the system or when certain types of high input impedance devices are used.

Both sources of noise may be reduced by increasing the throughput of light in the system. Low noise operational amplifiers should be used in the electronics and the bandwidth should be kept as small as possible. In a system with a high amplitude ac signal in one part of the circuit, and a second circuit detecting small signals of the same frequency, electrical cross-talk may be a problem as well as electrical pick-up. These may be avoided by isolating the two circuits (through careful power supply design) and by shielding the detection circuit in a Faraday cage. Whilst the system will still operate under noisy conditions, as shown in section 3.10 the uncertainty in the output of the PSD will increase, leading to a loss of accuracy. Non-stochastic noise of this type affects the output of a PSD more than shot or Johnson noise.

For a system which detects low levels of light, th dark current of the photodetector may be the most important noise source. This can only be reduced by careful selection of a low noise photodetector and reduction of the bandwidth of the system.

3.13 Conclusions

Analysis of the physics of photogenerated strain has shown that there are two strain generation mechanisms that may be used for actuation of resonance, electronic strain and thermal strain. Electronic strain, for the same amount of light produces a greater volume change than thermal strain, but the light is absorbed in a greater volume of silicon, whereas thermal strain is generated from a metallisation layer on the silicon, concentrating the strain and preventing light from passing straight through the thin silicon beam. Expressions have been derived which demonstrate the balance between increasing the thickness of a resonator to increase the induced bending moment, and the increase in the moment required to produce a given deflection. The efficiency of actuation may also be calculated from the size of the deflection and the light absorbed by the structure, and this may be compared with the efficiency of an ideal heat engine operating at the same temperature change. This comparison is useful as a guide to the validity of some of the assumptions being made in this work. The relationship between the width of the beam and the core diameter of the optical fibre has also been determined, and it has been shown that for a constant thickness, the signal to noise ratio is independent of the length a frequency of the beam, which means that the length may be used to match the frequency and size of the beam to system requirements other than signal quality from the interferometer.

Chapter 4: Experimental Prototype

4.0 Introduction

Before making a complete transducer design, it was necessary to build and characterise a sensor system based on the published work and theory already available. The intention was to make the prototype as close as possible to a perceived design solution, such that problems in the mounting of the sensor or operation of the optical system could be anticipated. This chapter describes that work, and is followed by a description of experimental technique and the measurements that were taken to characterise this sensor and operating technique.

4.1 Design Considerations

It was decided to build a prototype pressure sensor using a single mode fibre optical actuation and detection system since this offered better reliability than a multimode system as discussed in section 3.6. In order to achieve reasonable accuracy and stability this was to be of a 'closed loop' type, whereby the measured resonant frequency of the sensor could be fed back into the actuation stage. Previous sensors of this type had used a dual optical system, employing separate optical sources for actuation and detection. It was perceived that the main way of reducing the cost of such a system was to use a single optical source for both actuation and detection and that this should be the main objective of the first stage of sensor design, being both original and giving a subsequent transducer a cost advantage over other systems. The technique used was to switch the laser between actuation and detection of oscillations, since the considerable Q of the resonator enabled the frequency to be measured accurately without a simultaneous actuation signal. A publication describing this technique is included in Appendix C.

A second requirement of the project is to devise a suitable method of temperature compensation, and a cantilever beam (which would be independent of pressure) was provided on the silicon wafer for this purpose. All previous reports of micromachined silicon cantilevers with optical actuation and detection of vibrations required two

optical fibres pointing on to the cantilever[72]. Since the detection system that had already been chosen precluded this, it was decided to actuate the second harmonic of the cantilever, which should only require a single fibre (see figure 3.3). If this can be achieved, it will also be an important original step, since it will make cantilevers easier to integrate into an optical system, with repercussions in accelerometer technology as well as temperature measurement where coupling to pressure is not required. It will be possible to drive a long sensor at a high frequency, and be independent of pressure.

A temperature measurement technique using the same optical actuation and detection system and silicon technology proposed in this thesis would be preferable to the technologies described in Chapter 2 for temperature compensation. The match of the two temperature characteristics would be excellent since the structure of the two resonators would be the same and this would reduce the demands on the signal processing. Oscillating at around 420kHz, (see Chapters 3 and 6) its would occupy a separate part of the frequency spectrum from the pressure sensor, thus preventing cross-talk.

The basic design considerations for the experimental system to investigate the basic sensor characteristics were:-

1) Cost

It was obviously necessary to maximise value for money from limited resources. Silicon processing was one of the two major capital expenditure items and it was decided to place two resonators on each device as this doubled the flexibility without incurring any additional costs. A pre-assembled optical system was chosen as at the time it offered good value for money for a single mode fibre system although it has little flexibility.

2) Useability

At this initial stage it was important to build a prototype that allowed the components (sensor and optics) to be easily changed and there were facilities for operating the sensor under vacuum, with or without a pressure applied to the back side of the sensor for measurement of its characteristics.

4.2 Silicon Design

4.2.1 Resonator Shape

Before calculating the resonant frequencies and sensitivities for any device, shape and material composition must be considered in terms of stability, sensitivities and manufacturability. This last point will place limitations on the shape and size of the device which all other considerations must work within. A particularly complex shape may well be mechanically ideal but the cost of developing a manufacturing process for it may be prohibitive. Since normal silicon manufacturing processes will be used, the shape must be planar and require as few steps as possible (this is the case in all manufacturing processes). It is also preferable if there is only one critical thickness to control in the device manufacture. Considering the sensitivity of the physical characteristics of silicon to temperature, some means of temperature measurement in the sensor head is also preferable. The simplest design that meets these criteria is to have a bridge and a cantilever etched into the surface of the silicon. The presence of two resonators does not add to the complexity of manufacture, and it gives a non-pressure dependent resonator on the device which may be used to measure temperature. Some micromachined devices have a micoromachined diaphragm[13,20] as well as the resonator but this makes fabrication of the devices difficult[73] and should be avoided.

The silicon design was partly based on previous results obtained by the other groups undertaking similar work, and the known characteristics of silicon. Data from other groups was essential as the efficiency of the laser-vibration coupling is only known experimentally. Equations of motion for a fixed-free (cantilever) and a fixed-fixed (bridge or encastré) resonator were obtained from standard texts on material properties[76,77]. The intention was to design a structure which could be actuated with or without metallisation. A theoretical study was undertaken to establish the optimum thickness for the device in order to obtain maximum strain through its thickness. Other dimensions were calculated with a desired frequency of oscillation in mind. The resonant frequency of the bridge is chosen to be 104kHz and the resonant frequencies of the

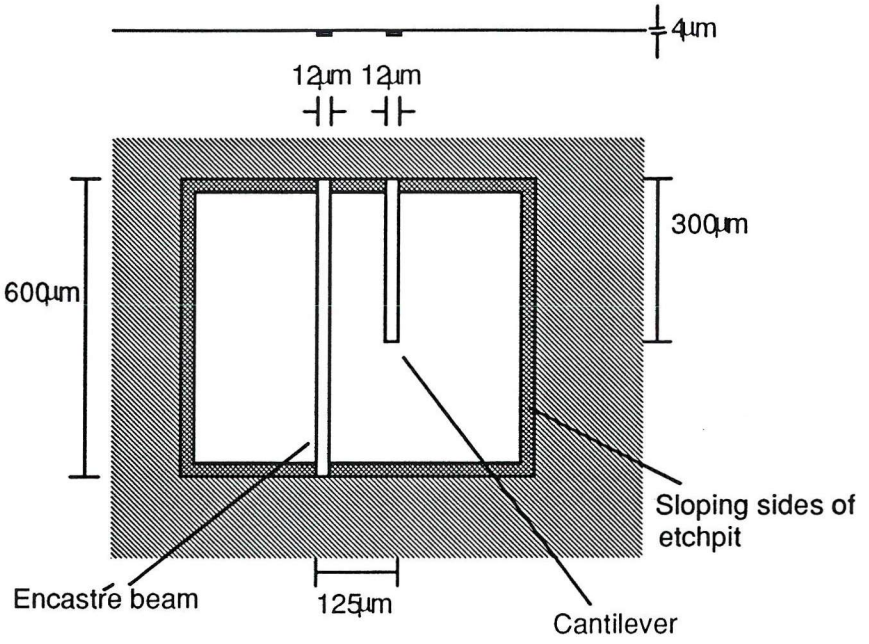

Figure 4.1 Silicon Resonator Design in Middle of Wafer.

first and second harmonics of the cantilever are 55kHz and 450kHz respectively. The fundamental frequency of the bridge was chosen to be above any acoustic interference, without being too high for the available electronics or too small to see.

It was decided to place a bridge and a cantilever on each device with sufficient spacing for them to be addressed by separate optic fibres of either 50/125 or 62.5/125 types.

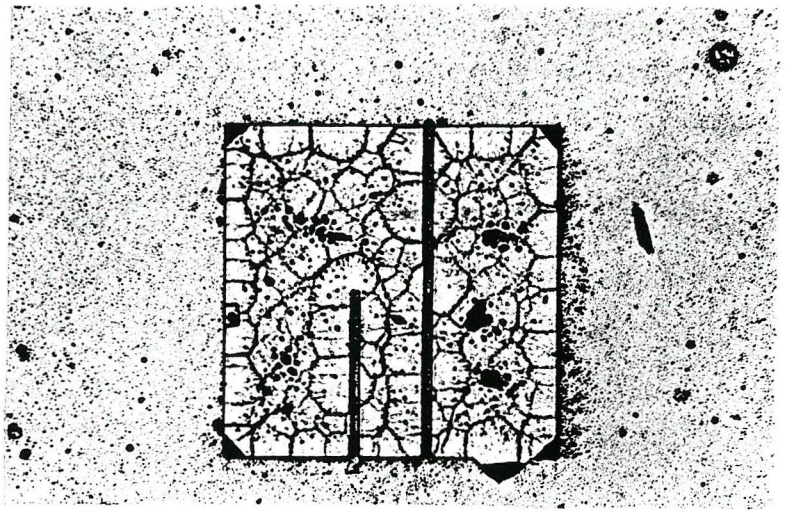

Figure 4.2 Photograph of Silicon Resonators

The photograph of the resonators above shows the separation and width of the devices in the 0.6mm square etch pit. The optical technique used for taking the photograph also shows the relative roughness of the silicon at the bottom of the pit.

It is expected that the second harmonic of the cantilever will be difficult to maintain once the drive frequency stops, but it may continue for sufficient oscillations to be seen and measured. There is a reported oscillation of a bridge of smaller dimensions oscillating at higher frequencies than 450kHz[18] so the evidence is quite promising, (figure 3.3 shows the shape of the oscillators at resonance). The optimum position for actuation of oscillations by thermal expansion is the place for maximum strain for a given mode. The optimum position for detection of oscillation by an optical technique is the place of maximum movement. For the first harmonic of a fixed-fixed (bridge) resonator, the only place where there is a maximum of both strain and movement is in the middle. For the first harmonic of the cantilever the position of maximum strain is at the fixed end and the position of maximum movement is at the free end of the bar. For the second harmonic these positions converge in the middle making it suitable for actuation and detection by a single light source.

4.2.1 Silicon Resonator Manufacture

The following is a brief list of the necessary processes for manufacture of this device. The plasma etch is used to achieve the depth of cut and gives a structure which has clean, straight sides.

1 - RCA clean of silicon wafer[49]

2 - Boron deposition at 1150°C for 90 minutes

3 - Remove Boron glass by dry etching

4 - Low Temperature Oxide (LTO) deposition

5 - Photolithography of mask

6 - Plasma etch LTO

7 - Plasma etch 6μm or 4μm of silicon anisotropically

8 - Remove resist in HNO_3

9 - KOH etch for 1-2 hours (40% wt KOH 60-70°, 20μm per hour)

10 - Remove oxide in HF

4.3 Laser Delivery System

There are basically two simple options available for this prototype and these are a single mode, and a multimode system (figure 3.6, c and d respectively). There are documented examples of each type of system in the literature [13-20,61]. Since it is not the primary objective of this research to develop a fibre optic vibration probe it was decided to use the simplest all-fibre version available that maintained integrity as a vibrometer.

Initially it was decided to use a single mode system, since it had potentially fewer problems as a vibrometer, and although it is possible to couple much more light into a multimode system, vibration detection was seen to be more important than power throughput. A switch to multimode fibre was seen as the next development, once a basic working system was achieved, since it offers lower cost and is easier to use.

The fibre system consists of (see Figure 3.6(c)):-

1) Monomode Fibre Coupler
This is a fused single mode fibre coupler, which evenly distributes light from one arm into the two arms at the other end.

2) Laser diode
A Sharp laser diode type MD27 was used as it has a low astigmatism and a single transverse mode which make it especially suitable for coupling to single mode fibres to be used in an interferometric application.

3) Laser monitor output

This was originally cut and polished to Brewster's angle in order to minimise the light returning back up the fibre and interfering with the interferometric process. A photodiode was later added to directly monitor the laser diode output.

4) Laser output

This is terminated by a SELFOC graded index lens (without anti-reflection coating so that an interferometric reference is generated at the lens face) to generate a well collimated beam. This is the easiest form to take the laser light in before focusing and it provides a convenient interface for reflecting light back into the fibre. Four percent of the light at the outer face of the selfoc lens is reflected back into the fibre. This serves as the reference for the interferometer.

5) Interferometer output

The light returning back up the fibre interferes at the photodiode. The intensity here provides information on the phase difference between the reference and the returning light. As the phase difference depends on the distance travelled outside the fibre, any change in the output signal is interpreted as a change in the distance between the fibre end and the target and therefore provides information on motion perpendicular to the end of the fibre. Obviously, with the light from one end coupled evenly between the two opposing outputs only a maximum of 25% of the original signal will appear at the interferometer output after reflection from the target (in this case the sensor). The signal size of the interferometer for one complete fringe is limited by the 4% back-reflected reference signal which is halved at the coupler to give a maximum signal of 0.5% of the light originally coupled into the fibre.

The response of the vibrometer was measured by pointing it at a low frequency vibration source (a speaker cone) moving more than one half wavelength of the laser and measuring the peak-to-peak voltage obtained (a sinewave). The output change per nanometre of movement was calculated and this figure was later used to calculate the movement of the bridge at resonance. The peak-to-peak voltage for one nanometre was then simulated at 100 kHz by adding a small modulation to the laser drive current. The visibility (i.e., whether or not the

signal was swamped by noise on the oscilloscope screen) could then be tested after passing through the bandpass filter.

4.4 The Electronics

4.4.1 Laser Driver

A proprietary Sharp laser driver chip (number IR3C01N, see Appendix A) in the typical recommended circuit was used to drive the laser diode. The driver chip generates a steady current which is controlled by a voltage applied to one of the pins. This current flows through a current limiting resistor to the laser diode. Feedback from the photo diode passes through a low pass filter and reference voltage before returning to the current driver. Since there is a peak hold this circuit responds to the peak power levels. The decay constant of the peak hold is adjusted to respond to changing power requirements of the laser diode, while removing the modulation signal from the feedback. See Appendix A for circuit diagrams.

4.4.2 The Detector Circuit.

All that was required for the detector circuit was an amplifier and band pass filter. Sufficient amplification was necessary to make the signal visible on the available oscilloscope. The bandwidth of the filter was designed to cover the full possible operating range of the resonator. The high pass characteristic cut out acoustic noise, while the low pass filter reduced electronic noise from both the circuit and photodiode.

4.4.3 Prototype Actuation and Detection System

In order to realise a system for single fibre operation as quickly as possibe, a system using switched signal generators and an oscilloscope was used. It was possible to trigger the oscilloscope such that only the detection cycle was displayed, making the drive cycle transparent to the observer of the oscilloscope. Figure 4.3 is a schematic illustrating the system.

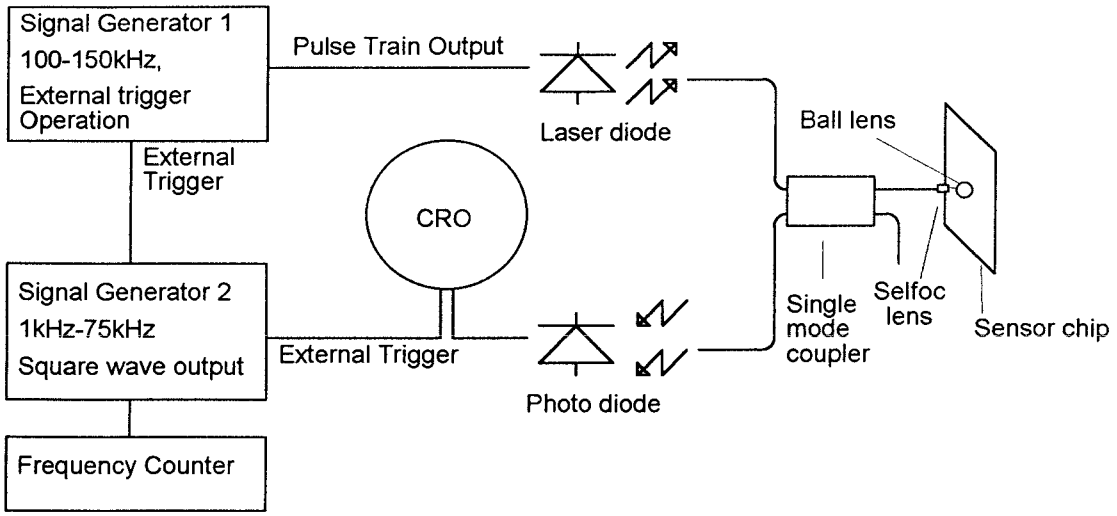

Figure 4.3 Experimental Prototype Schematic

Using this system it is possible to investigate a wide range of actuation frequencies and pulse train lengths, in order to ascertain the best way of operating a stable closed loop system with the best response and accuracy available for the method.

4.5 Wafer Holder and Beam Focus.

The assembly to direct the laser onto the silicon is designed to be as rigid as possible, to minimise vibrational noise. Five - axis control is maintained over alignment of the components. A vacuum seal between the silicon and the holder is provided by a polished metal surface againxst the smooth surface of the silicon, with silicon vacuum grease bonding the two together. Sealing between the glass window and the wafer holder is provided by a lightly greased 'O'-ring. A pair of screws provide a fine adjust for the ball lens (see figures 4.5 and 4.6). Adjustment of the laser beam is controlled by the 6-axis holder purchased from Melles Griot. All other apparatus was custom built. A UV- curable adhesive was used to fix the lens into the window. A ball lens was used as it has a very short focal length and low f- number, which give it a very small beam waist, sufficient to confine most of the laser light to the resonator when correctly aligned. As the optimum distance between the lens and silicon is constant, this was set by careful machining and is only slightly adjustable by applying more or less pressure on the glass and compressing the 'O' ring which forms the vacuum seal. The wafer holder can be evacuated and pressure may be applied across the silicon. There is, unfortunately, no simple

method for fixing the diaphragm boundary to simulate an anodically bonded sensor so the results presented here are for a metallised silicon chip independent of the effects of packaging (apart from any stress from clamping during pressure or vacuum application) and for an unclamped diaphragm. Figure 4.7 is a photograph of the complete assembly, with the pressure reservoir and gauge to the right of figure 4.6. Figure 4.8 is a photograph of the custom window, with the screws that are used to adjust the focus and position of the lens.

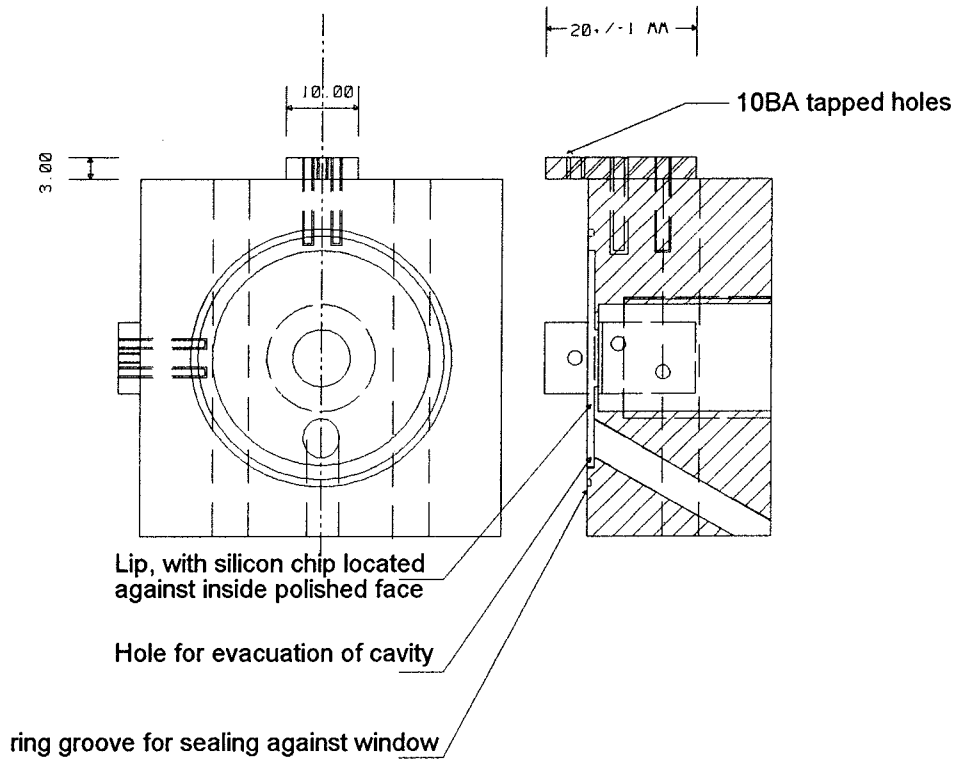

Figure 4.4 Wafer Holder

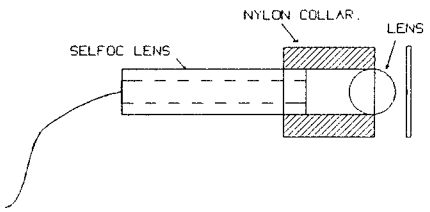

Figure 4.5 Initial 'Easy' Scheme for Optical System Focus

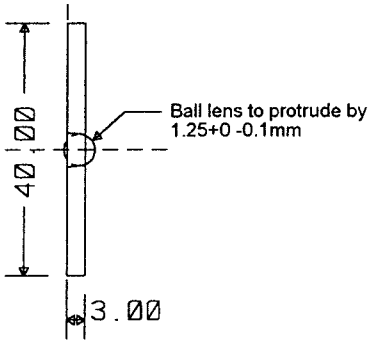

Figure 4.6 Window with Ball Lens

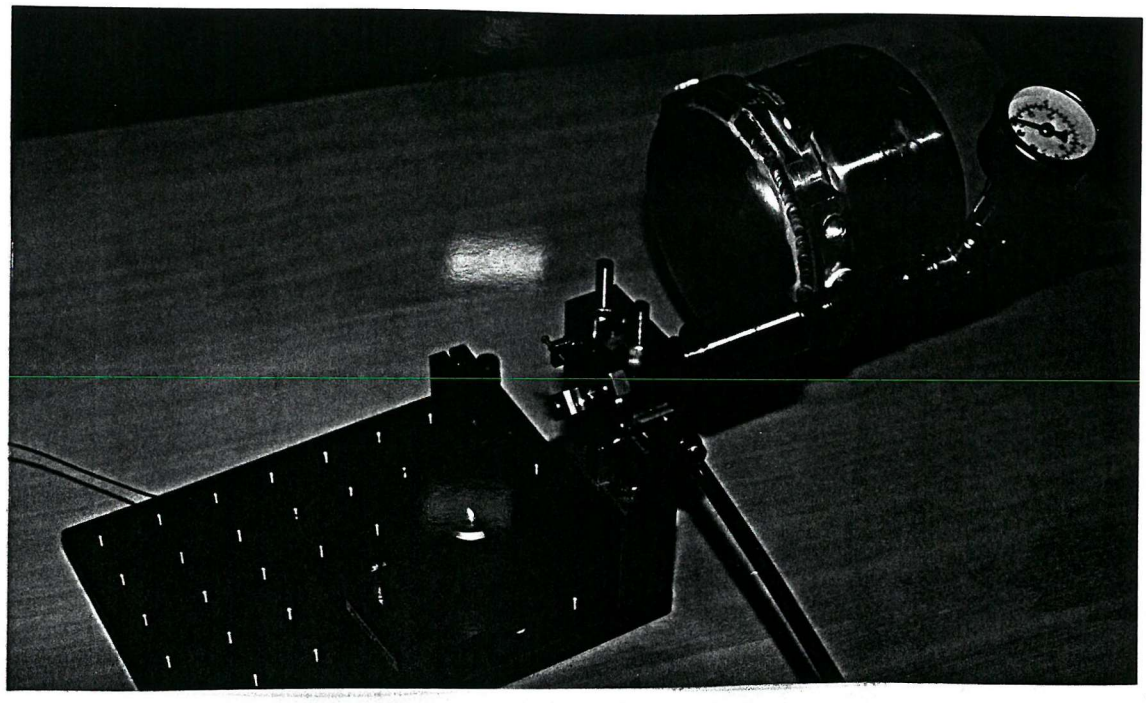

Figure 4.7 Photograph of Prototype Silicon Chip Holder

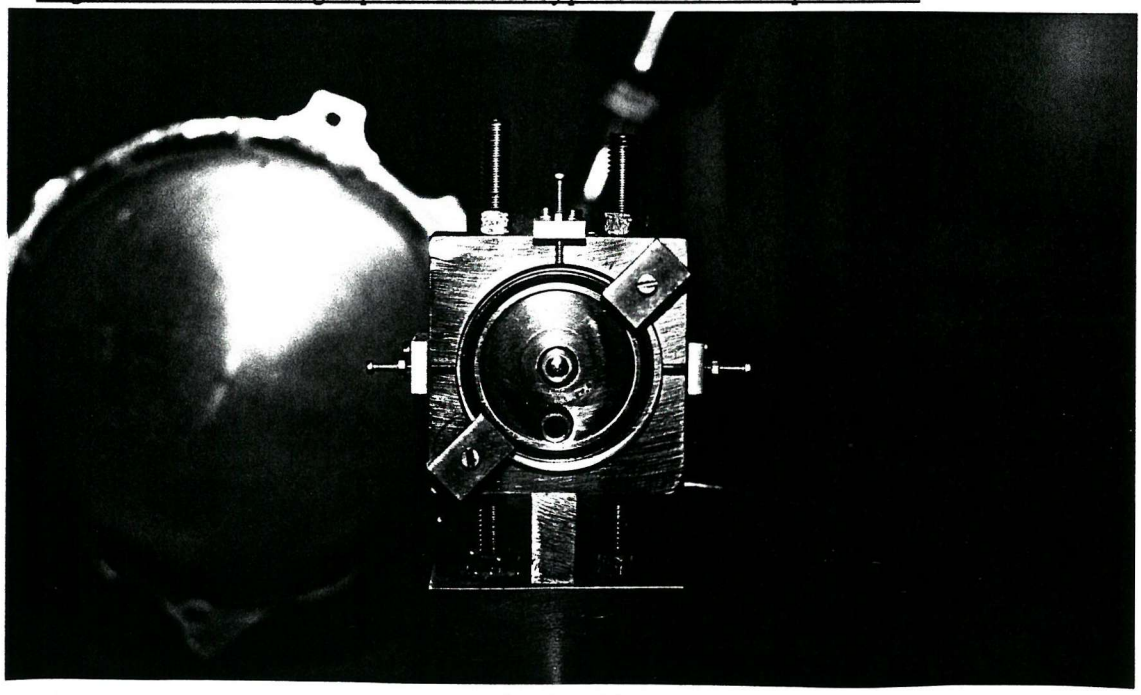

Figure 4.8 Photograph of Optical Alignment

4.6 Anodic Bonding

Anodic bonding is used to join silicon to glass. Glass is seen as a potential mounting material for the silicon sensor because it is chemically very stable and will allow visual allignment of the optical system with the resonator. A small trial anodic bonder was built to assess the difficulties involved. Figure 4.9 is a photgraph of the

anodic bonder, with a sample of pyrex glass between the top and bottom plates and leads for the thermocouple and heater power to the left.

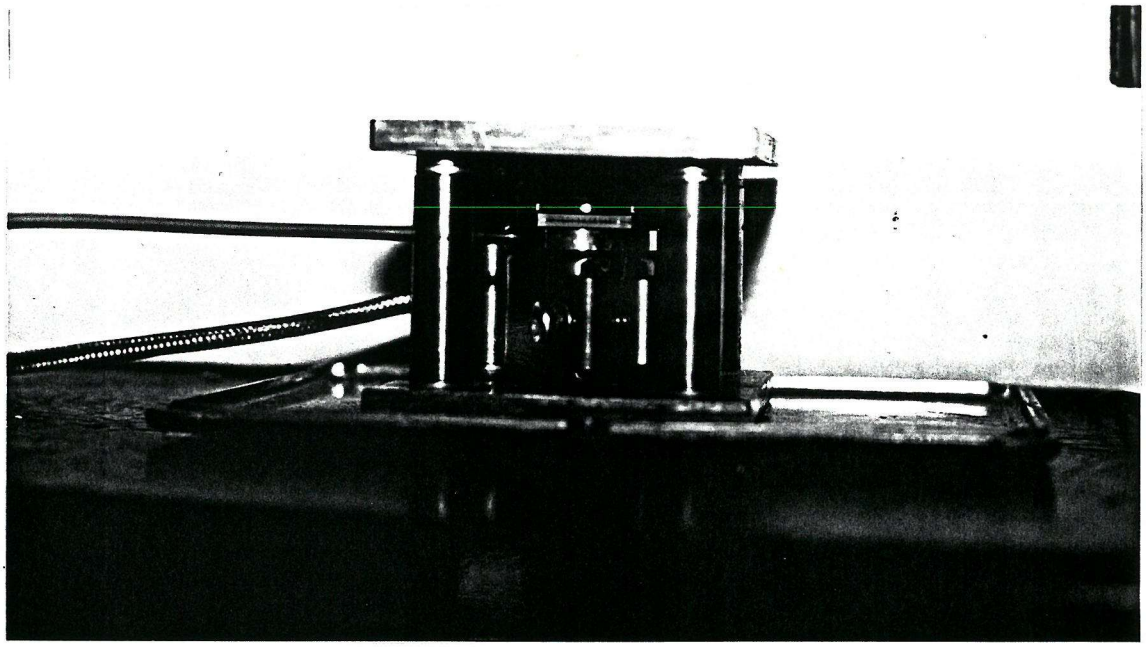

Figure 4.9 Photograph of Trial Anodic Bonder

Chapter 6: Discussion

6.0 Introduction

It should perhaps be remarked at the outset of this discussion that there were unusual features in this project as an academic research exercise. Initially the work was industrially funded and later on a part time basis by the author. The circumstances of the sponsoring company changed during the progress of the research, which put pressure on both the funding of the project and the time made available to the author. Nevertheless, despite these, at times severe, constraints on time and resources significant progress has been made in the advance of a novel variation in an important technology, and the outcome of the investigations and the associated design exercise are felt to make a worthwhile contribution to the developing technology.

The principal targets for the design of the transducer described in this work are reduced cost and improved temperature performance. These have been approached by developing an optical drive which reduces the optical components and by including a pressure insensitive cantilever beam for temperature measurement of the silicon chip. The transducer system has been broken down into distinct functional areas, with the performance of each area being either calculated or set by known physical parameters such as the core diameter of an optic fibre. The design points for this transducer are illustrated in Figure 6.1. The first part of this chapter discusses a systematic approach to transducer design for this technology, in the light of the techniques for sensor interrogation and drive that have been investigated in this work, with a resonator design that takes into account both the physical properties measured here and the theoretical aspects of sensor actuation that are explored in Chapter 3. The section on sensor packaging takes into account the short study of anodic bonding and discussions that took place with a potential manufacturer of batch produced sensor heads. All the basic components of this transducer are described in the previous chapters, and critical parts of the system are demonstrated experimentally in Chapters 4 and 5. The problems encountered in this particular project are then discussed, and the lessons learned about the technology are presented. Finally,

the prospects for this type of transducer in the context of other recent developments are discussed.

6.1 Transducer Design

This section contains a design process for the transducer technology developed in this work. The fundamental requirements for the design are set out in section 6.1.1 and are aimed the production of a transducer that will equal the accuracy of current industrial transducer technology but with the advantages of optical operation and improved long term stability.

The design process is taken in stages that follow the scheme illustrated in Figure 6.2. Each system parameter is considered in the context of environmental conditions (e.g. acoustic noise setting the low operating frequency), device availability (e.g. dark current in photodiodes, laser power, coherence and coupling efficiency) and overall design targets (cost reduction in the optical system and temperature calibration).

6.1.1 Design Boundary Conditions

The boundary conditions for the sensor operation within its performance limits are set by the design objectives and known device characteristics. The main design areas are illustrated in figure 6.1, and figure 6.2 illustrates the process of defining component tolerances from the required system performance. The design objectives are:-

1) High Performance

Accuracy of 0.1% full scale from -50° to +125°C, with a settling time of less than 100milliseconds. The device should have a useful range, i.e. 0 to 3 bar absolute for avionic applications. Within the context of existing technologies, this would constitute a high, but not exceptional performance device.

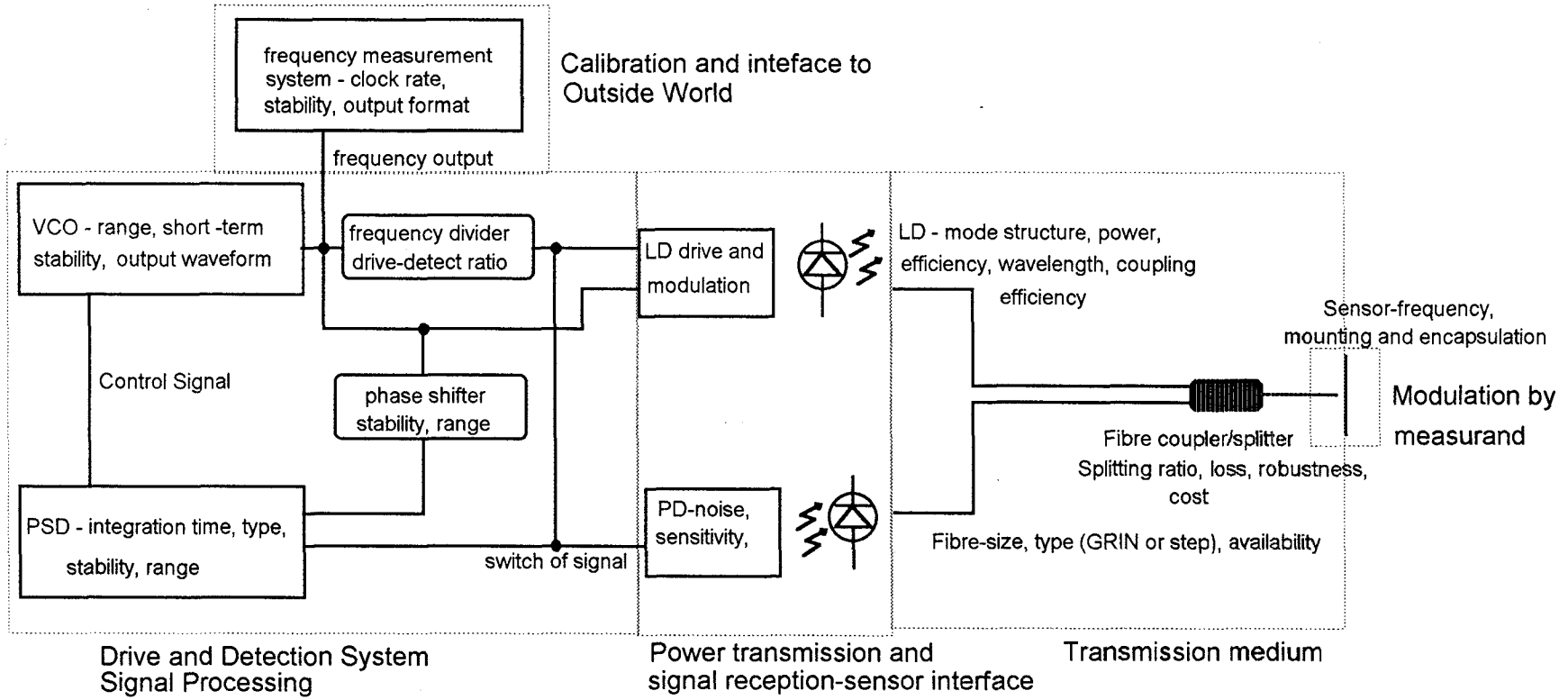

Figure 6.1 Design Points to Cover

This was designed for simplicity for bonding of SCS to pyrex out of vacuum. The three conditions required for bonding are:-

1) Pressure in excess of 400kPa.

2) Temperature of between 300 and 400 degrees Centigrade.

3) Up to 500 Volts.

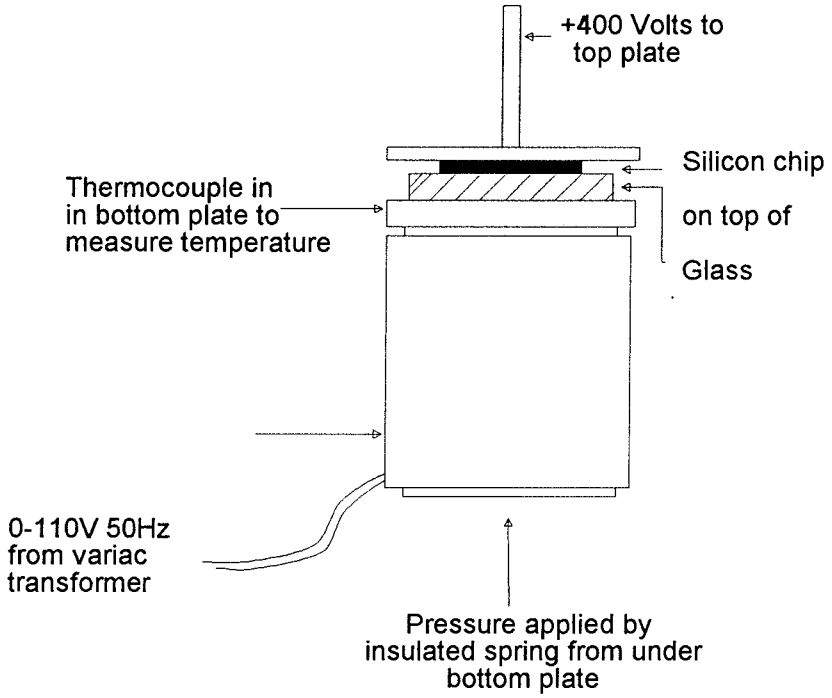

Figure 4.10 Anodic Bonder Schematic

These conditions were satisfied by (see Figure 4.10) :-

1) A spring pushing the lower platen (adjustable compression of the spring gives a variable pressure).

2) A 50 Watt, 110 Volt heater around the lower plate. The platen is designed to give a temperature profile which is as uniform as possible across the glass and is insulated from the spring and hence thermal contact with the main metallic structure of the bonder by a ceramic filler. Temperature is monitored with a thermocouple that is as near to the bottom of the glass as possible, in a hole in the lower platen.

3) The main structure and the heater are all attached to ground. A positive voltage is applied to the upper plate, which is only connected when a lid with an ammeter is placed over the assembly. The top plate is electrically and thermally insulated with a disk of thermoplastic, glued to the metal using a high temperature epoxy resin. Observation of current is important in assessing bond completion (since bonding is due to migration of positive ions in the glass, see Chapter 3).

The advantages of using glass as a packaging material are the range of techniques for machining glass and bonding optic fibres to it or even moulding a glass mount for the sensor with a suitable lens in it, similar to the window used in the experimental prototype. Since the Young's modulus of glass is lower than silicon, any mount must be large enough for the sensor to be insensitive to a change of ambient pressure on the glass face and the glass samples used for testing should, if possible, take this into account.

4.7 Further Development of Electronic System

A switched PSD was built to test the viability of this type of circuit, a diagram is included in Appendix A. The main problem with this system was preventing crosstalk from the frequency generator. Initially separate power supplies were used but these could be replaced by independent DC to DC converters. In order to avoid a ground loop an optical isolator was used for connection of the reference signal to the PSD. The system for switching the reference worked well when tested using a signal generator to simulate a small signal from the photodiode, and the reference and switch from the laser modulation driver.

Chapter 5: Experimental Work and Results

5.0 Introduction

The requirement to actuate and interrogate a micromachined silicon resonator with a single optical source was identified, micromachined silicon resonators of suitable dimensions for optical operation were designed and manufactured and a simple chip holder for the resonators was constructed. A single mode fibre coupler was purchased, terminated with a suitable light source, detector and optics for the early experimental work (see figure 3.6(c)). It was intended that a multimode 'Y' coupler (see figure 3.6(d)) should be developed as a lower cost alternative to the single mode system in the later stages of the project in conjunction with suitable electronics for closed loop operation of the resonator drive and detection system.

The observations and measurements of the micromachined resonator presented here were all made with the single mode fibre system and the electronics described in figure 4.3 for pulsed actuation and detection. The pressure and temperature characteristics of the sensor were measured, the Q was measured in and out of vacuum using different techniques and the signal-to-noise ratio with the existing electronics was also measured. These results are for a device 4μm thick, 12μm wide and 600μm long, with a 0.5μm thick aluminium metallisation layer.

It was fortunate that measurements to establish characteristics of resonator response to pressure and temperature were completed at an early stage, as the progress was brought to a premature end. This was due to a failure of the laser diode in the single mode fibre optic system and under the pressure of time and cost on the priject it was not possible to perform the test that the author had planned. This project has perhaps been unusual in that much of the effort went into system design, device fabrication, and parameter optimisation for the long term aim of a complete transducer product. This left the remaining experimental programme vulnerable to the sort of catastrophic failure that occurred.

The measurements of resonator response to pressure and temperature that were taken demonstrated the potential sensitivity of the device,

it was possible to characterise the pulsed actuation and detection system for the best mark-space ratio and pulse train frequency and some evidence was gathered for systematic variation in sensor characteristics. These measurements enabled the design and construction of a suitable modulation frequency generator and resonance detector circuit.

The optical system characteristics are presented first, since these provide some calibration data for the deflection size and actuation efficiency. Sensor characteristics and calculations of device parameters are presented last.

Since the signal-to-noise ratio of the output of the interferometer determines the accuracy and response of the transducer, it was important to have an understanding of noise sources in the detection system. These can be broken down into three basic types:

1) Mechanical Noise

Owing to the small size of the vibrations that are being measured, it was important to keep the linkage between the vibrometer optical reference and the vibrating sensor as stiff and as short as possible. This reduced differential movement to very low frequency distortions in the structure (such as differential expansion caused by a change in temperature) or acoustic vibrations of shorter wavelength than the distance between the optical reference and the target. This excluded speech but included noise caused by impacts to the bench. Both the silicon chip holder and the fibre holder were firmly bolted to a small optical bench made from half-inch thick mild steel. Any remaining noise was removed by the high pass filter in the detection circuit. Without the filter, small mechanical disturbances such as leaning on the bench or the noise from the pump reduced the visibility of the signal on the oscilloscope, sometimes quite severely.

2) Electronic Noise

The most important sources of electronic noise were shot noise, dark current from the photodetector, and noise from the integrated circuits. This was reduced by minimising the bandwidth of the system. Low noise operational amplifiers were used and there were no large value resistors so Johnson noise was not important. Electrical pick-

up was only a problem without the bandpass circuit and consisted mostly of signals at 50Hz with some at 1MHz.

3) Optical Noise

There were two types of optical noise in this experiment. The first was the normal shot noise which was indistinguishable from the other electronic noise and could be reduced by a bandpass filter. The second was noise caused by instabilities in the laser diode. These consisted of quantised jumps in the output intensity of the diode which may have been accompanied by jumps in the frequency, although this effect was not separable from a jump in amplitude. This type of noise in lasers is called mode noise, and is caused by the laser changing its mode of oscillation. This change may be caused by a

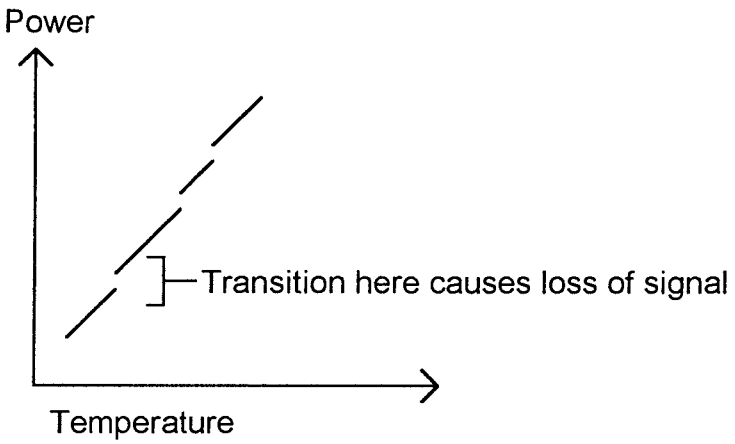

Figure 5.1 Change in Laser Diode Output With Temperature

change in the optical cavity length or refractive index, or by light reflecting back into the optical cavity favouring a different mode of oscillation. The characteristics of the laser diode[87] show a variation in output intensity with temperature. This variation includes a series of discontinuous jumps of power and frequency which were responsible for the severe mode noise found in the laser diode. This mode noise is sensitive to both temperature and to the laser drive current (which also affects the temperature and refractive index). Cooling with an aerosol spray changed the mode noise, but did not stabilise the diode. Following analysis of the problem a thermoelectric cooler was installed to stabilise the diode at a lower controllable temperature, so that the mode noise would be reduced.

Running at a lower temperature is also supposed to increase the reliability of a laser diode.

5.1 Optical System and Alignment

5.1.1 Vibrometer Calibration and Performance

The interferometer was initially tested with a simple low-noise operational amplifier for signal recovery. The output optic (SELFOC collimating lens) was targeted onto a vibrating surface (a speaker

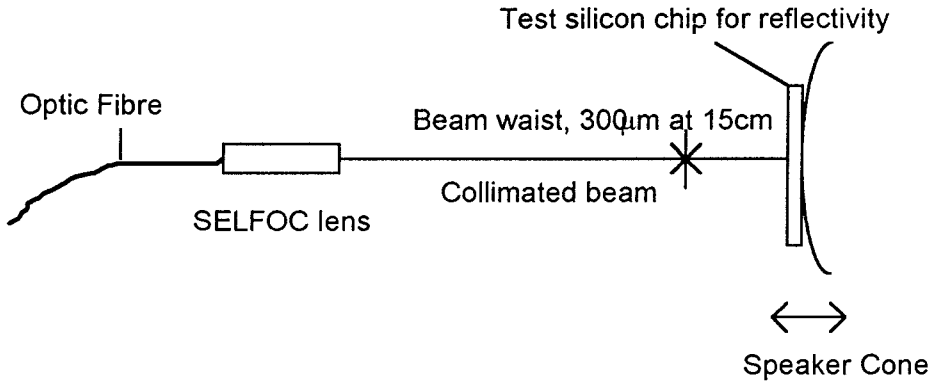

Figure 5.2 Test Set-up for the Vibrometer

cone with a test chip mounted on it) and oscillations were detected

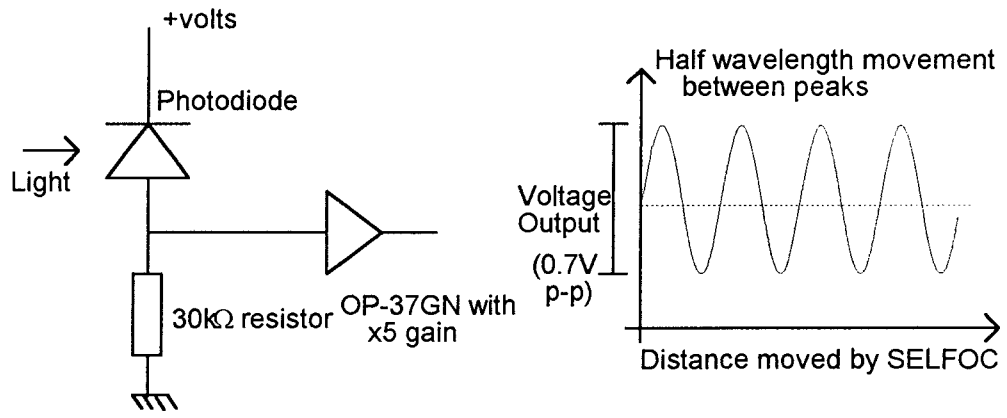

Figure 5.3 Initial Simple Circuit for Vibrometer Tests

from a distance of several centimetres, the light from the SELFOC being sufficiently well collimated to couple light back into the fibre as shown in figure 5.2. This test gave initial calibration values for the vibrometer.

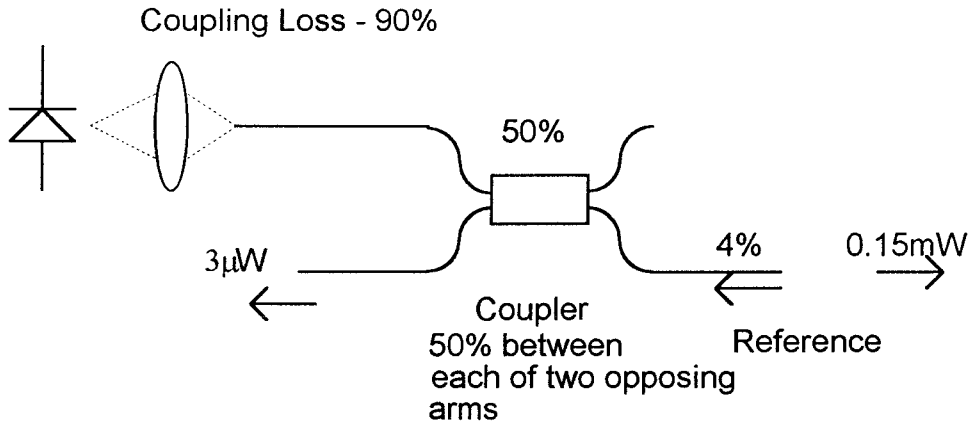

Figure 5.4 Optical System Throughput

When the vibrometer was tested with the speaker cone and the simple amplifier illustrated in figures 5.2 and 5.3, a signal of 1.8mV per nanometre movement was achieved.

After initial calibration, the visibility of any possible vibrations on the display of the amplifier output on the oscilloscope was assessed by adding a small amount of amplitude modulation to the laser diode output to simulate a true interferometric signal at the photodiode. The amount of modulation was calculated from the peak-to-peak change in the output of the amplifier associated with the full scale output of the interferometer. Levels of modulation were added corresponding to movements from one nanometre up to ten nanometres and the visibility (a result of optical throughput and noise levels) was subjectively assessed to give a minimum detectable movement of not more than 5nm, depending partly on the behaviour of the laser diode. This proved that should oscillations be actuated, the system was capable of detecting tham above the noise floor.

Figure 5.4 illustrates the optical system throughput. The initial coupling efficiency was estimated from the typical power output of the laser diode and the measured power from the SELFOC lens. Measurement of this power indicated that the amount of reference signal reflected from the SELFOC was greater than that expected for normal incidence reflection at a glass-air interface. This had the experimental advantage of increasing the available interferometric signal and may have been caused by the high refractive index of the SELFOC or by multiple reflections inside the lens assembly.

After these initial calibration measurements, a high pass filter was added[84], and the gain in the system was increased which yielded an improvement in signal-to-noise of 25%. The gain-bandwidth product of the additional amplification limited the high pass frequency to 1MHz, a sufficiently high frequency for detection of the second harmonic of the cantilever. The disadvantage of this broad bandwidth was the amount of relatively high frequency noise present in the measurement of 100kHz signals.

In a preliminary experiment this simple optical arrangement was targeted at the microresonator devices but failed to detect oscillations from any of them. The two reasons for this were insufficient energy incident on the resonator for actuation, and not enough light from the resonator returning to the SELFOC, as shown in figure 5.5.

5.1.2 Optical Alignment

In order to focus the light to a small spot a 5mm diameter ball lens was attached to the end of the SELFOC lens with a simple nylon collar. A ball lens has no axis which means that problems with angular alignment were avoided. The simple nylon collar (see figure 4.5) held the lenses about the same concentric axis. This system of SELFOC and ball was used for all the measurements described here.

A considerable amount of time (a few hours each time the equipment was used over a period of several weeks) was spent re-aligning the optical

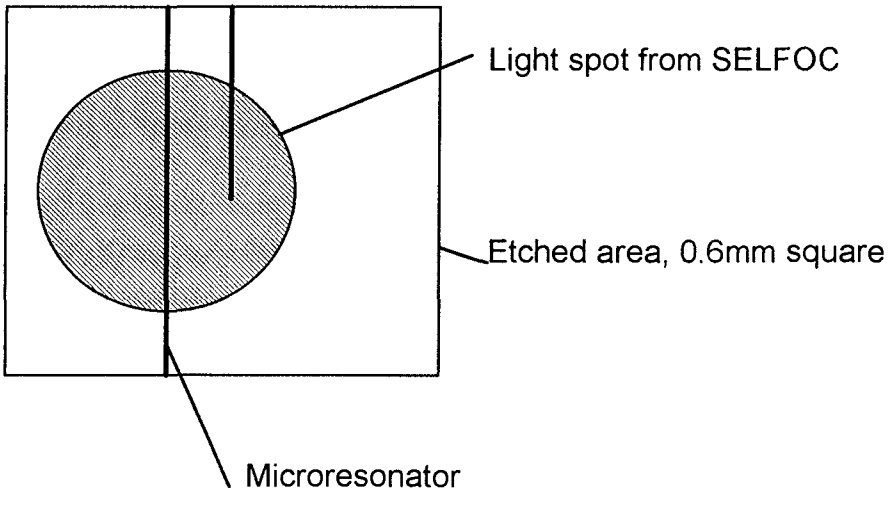

Figure 5.5 Relative Sizes of the Light Spot and Resonator

system to achieve the maximum possible signal. It was important to achieve such a level of confidence that the system could be aligned without relying on the presence of a resonance signal from the sensor. This work had dual benefits. The first was to develop a method of alignment that saved time (potetially several hours). The second and more important benefit was the confidence of being able to say that the actuation and detection system were inadequate for certain types of resonator, not just that the system was not aligned properly. Without a high degree of such confidence, no conclusions could be drawn about the successful operation of the different types of device. Changing the chip and realigning the system was practised so that a new device could be set up in the holder (figure 4.4), aligned, and the first sweep of drive frequency would detect some oscillation which could then be optimised. This was achieved in about 70% of the cases, so that for a new device, relatively few attempts at actuation and detection were sufficient to assess whether or not the device would be successful.

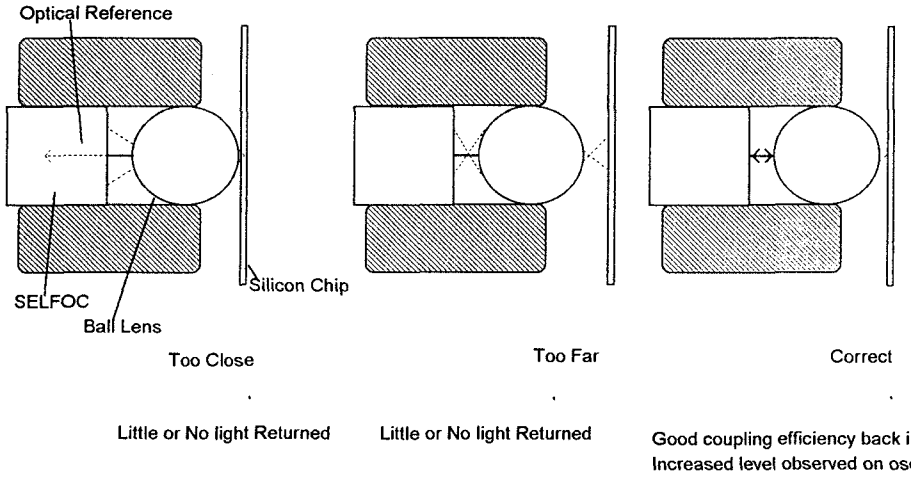

Figure 5.6 First Stage of Alignment Process

For the first set of measurements, in order to align the optical system with the resonator the fibre and lens assembly was moved up to the silicon using a five axis positioner (see figure 5.6 above). Then the angle and spacing were adjusted until the maximum amount of light was detected at the photodiode. At this stage a faint point of light was visible from the surface of the wafer. This was moved down until it was level with the middle of the resonator. Motion was then only required in one axis, with frequent checking of the frequency for the

first few attempts. In the etched area of the silicon, the background was rough and there was a noticeable drop in reflected light as the focal point of the optics moved across. The reflected light increased slightly when the focal point passed over the resonator and this could be monitored on an oscilloscope, following initial coarse alignment by eye (see figure 5.7). During this process, it was noticed that when the system was correctly aligned, the spot of scattered light became brighter, probably because the focused spot was wider than the beam, and there was light reflected from the sides. This was used as a guide for faster system alignment. The major difficulty in aligning the system was that the resonant frequency of the device was not accurately known, so every new possible position had to be tested by scanning the frequency across the set of likely values (i.e., 90-120kHz). This had to be done slowly enough for any signal not to be missed in the noise, especially with a high Q device. This developed in later stages to the application of short tone bursts to increase the width of the response and make alignment easier.

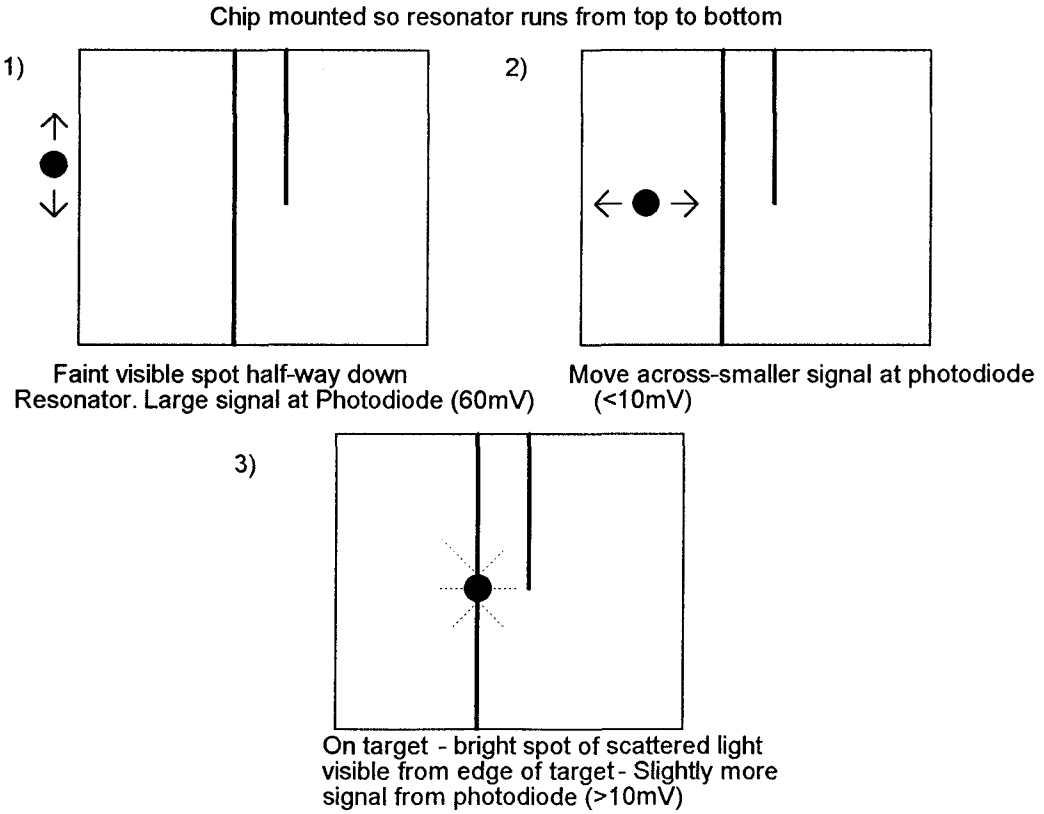

Figure 5.7 Second Stage of Alignment Process

In vacuum, alignment was a three variable adjustment process. Initial alignment was achieved by placing the lens approximately in the region of the beam and aligning the laser with it to achieve a visible point of light somewhere near the microstructures. Since the light spot position was sensitive to the angle of light from the fibre, most repositioning of the fibre after lens adjustment was in the X-Y plane, and not angular. Again, after each possible alignment was achieved, it had to be tested with a range of frequency inputs. A single fine screw was used to push the lensed window along the length of the structure (vertically), whilst a pair of opposing screws were used to move the lens across it (horizontally), achieving fine control through flexure of the aluminium supports. It was found that the movement available was sufficient to achieve alignment within 30 minutes, with a stable laser diode. Again, a certain amount of practice was required with this system in order to achieve some confidence in the correct alignment in order to assess whether or not a resonator was functioning. If part of the system was not functioning properly, the previous simple nylon collar could be used to check that if the system was not working, the problem was not associated with alignment.

In an attempt to achieve alignment of the optical system more reliably, the change in the amount of light being coupled back into the fibre was observed as the focus of the optical system was moved across from the un-etched part of the wafer to the resonator. Although these measurements are intended as a guide for alignment, they also give an idea of the spot size generated on the device which is required for a more accurate assessment of actuation energies. The returning light level as measured on the oscilloscope dropped from around 65mV outside the etched area to 10mV when aligned over the microstructure. These readings indicate, for a device width of 12μm, a focused spot size of approximately 50μm which indicates that the possibility of actuation with a multimode fibre is good (assuming sufficient light may be coupled using the low cost optics available) since the energy density is not high.

Throughout this work, the interferometric signal from the system depended heavily on the behaviour of the laser diode, and the prevalence of mode noise in its output which could make interferometric readings impossible.

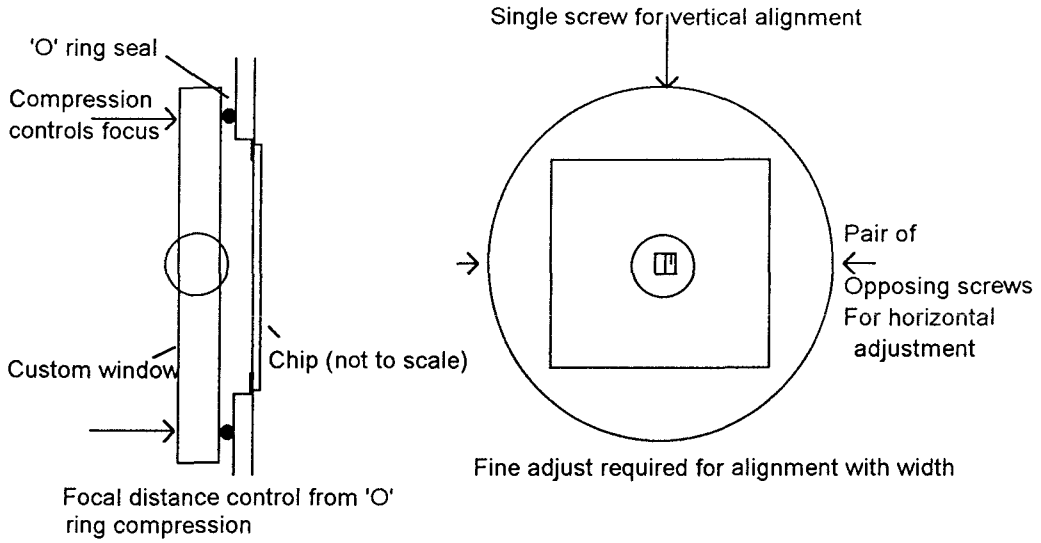

Figure 5.8 Alignment of Window with Lens

5.2 Measurements of Resonator Characteristics

After development and adoption of the optical alignment procedures described in section 5.1 oscillations of a metallised encastré beam were observed. The table below gives the characteristics.

Device 1	Frequency	Peak - Peak movement	Q
	90±3kHz	220±25nm	100±20

The time to decay below the noise floor was about two milliseconds. This large peak to peak deflection was achieved with short, in-phase tone bursts that gave the resonance a width of about 13kHz.

5.2.1 Investigation of the Effects of Pulse Train Length and Frequency

Successful actuation and detection of a resonance demonstrated that the system functioned and could be used to drive a micromachined resonator. The main disposable characteristics of the electronic system were the mark-to-space ratio of actuation time to detection time and the length of a complete cycle. The illustrations of oscilloscope traces below illustrate the different types of actuation signal used and the effect they had on the amplitude and Q of the system.

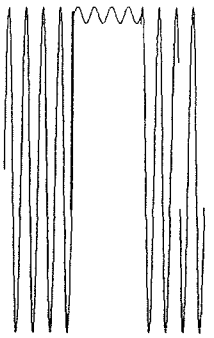

Short bursts-broad response Large amplitude Oscillations when successive bursts in phase

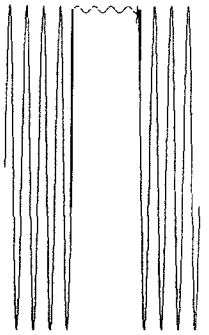

Small amplitude response when successive bursts out of phase

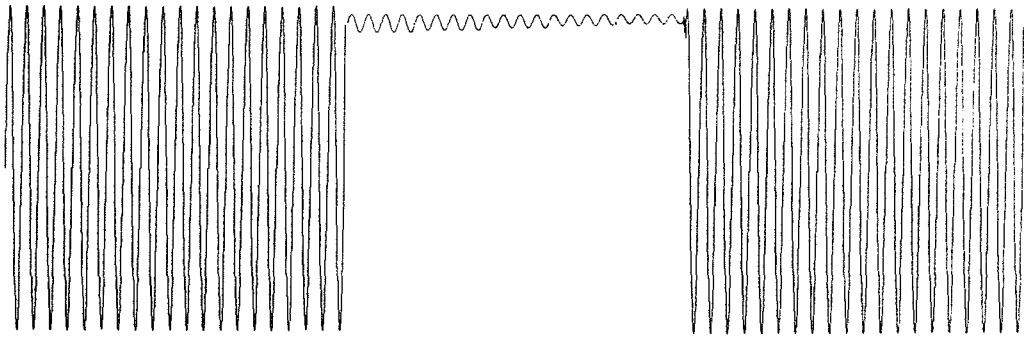

Long Tone Bursts - sharp response, oscillations decay during detection cycle

Figure 5.9 The effect of Long and Short Actuation Tone Bursts

5.2.2 Measurements of 'Q'

Higher amplitude oscillations were observed where successive pulse trains were in phase, i.e. the resonant frequency was an even multiple of the pulse train repeat frequency. The Q was measured by two techniques. The first was to measure the time to decay to 1/e of its original amplitude, which determined the Q of the device independently of any effects from the drive frequency. The second was to measure the 3dB points of the response, which is a convolution of the frequency content of the drive and the frequency response of the resonator.

Measurements of Q	Vacuum (10^{-2}Torr)	Air
Decay to 1/e	250±20	100-150
	30 cycle Tone burst	100 cycle tone burst
3dB	35±5	100±5

By the decay of oscillations method, the Q in vacuum was found to be around 250, and this was reduced to 100 in air. The best vacuum that was achieved was between 10^{-2} and 10^{-3} Torr. At this pressure, the mean free path of air is about 1mm, which was greater than the largest dimension of the resonator. The resonator would see a reduction in the viscosity of the gas and therefore a reduction in the amount of air damping. Since there was no cold trap in the vacuum system, there may well have been some oil contamination of the resonator which may have reduced the resonator Q. The uncertainty in the measurement is due to the amount of noise in the signal, and the difficulty of finding the point at which the signal dropped to its 1/e point for a long pulse train in a significant amount of noise. See Chapter 6 for further discussion of these results.

5.2.3 Sub-Harmonic Actuation of Resonance

An alternative method for single light source drive of the resonance is to use pulses at a fraction (1/2, 1/4, 1/8) of the fundamental frequency of the oscillator. This was attractive because it could be implemented using a very simple circuit if no ÷100 frequency divider or similar device was available for simple generation of longer tone bursts. A second device was investigated for these measurements. Its characteristics are displayed in the table below. The amplitude dropped in proportion to the frequency, making lower frequency measurements impossible since they disappeared below the noise. Figure 5.10 illustrates some typical waveforms.

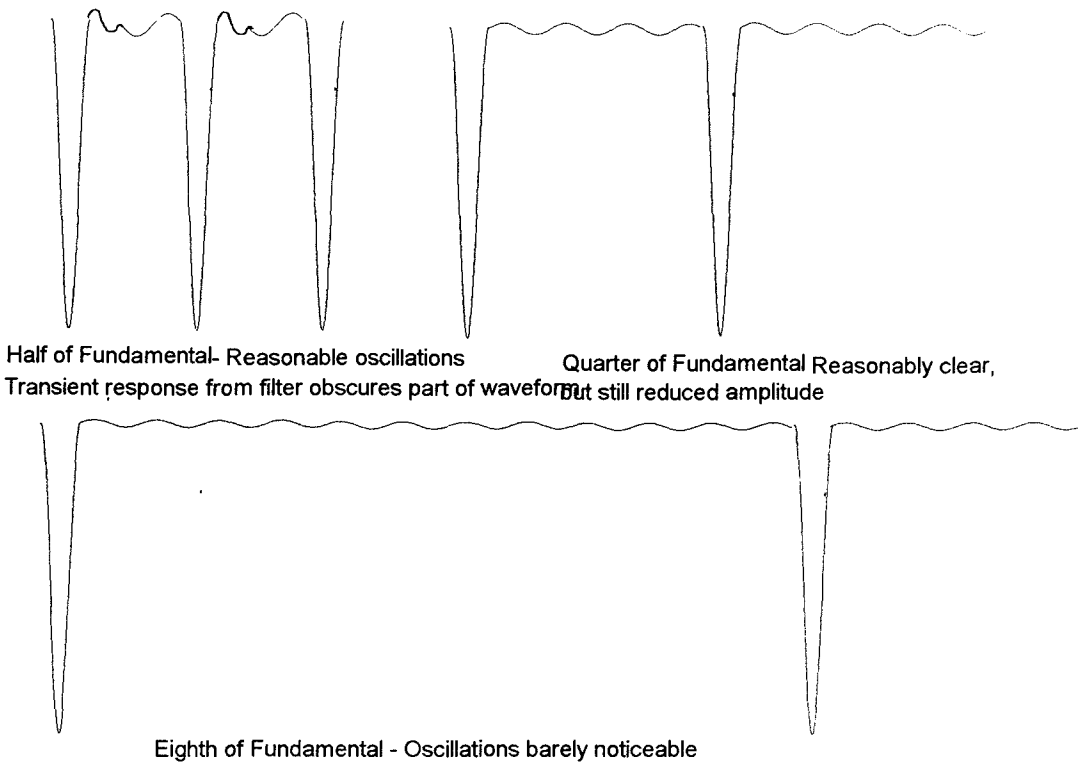

Figure 5.10 Subharmonic Actuation of Resonance

Device 2	Frequency	Peak - Peak movement	Q
	105kHz	165nm	100

5.3 Measurements of the Pressure and Temperature Characteristics

A third device was used for measurement of the pressure and temperature characteristics. The devices had a limited lifetime in the chip holder, partly from contact with the resonators during handling and installation in the wafer holder, and partly from a build up of contamination from dust and oil (vacuum pump) over the course of a few weeks.

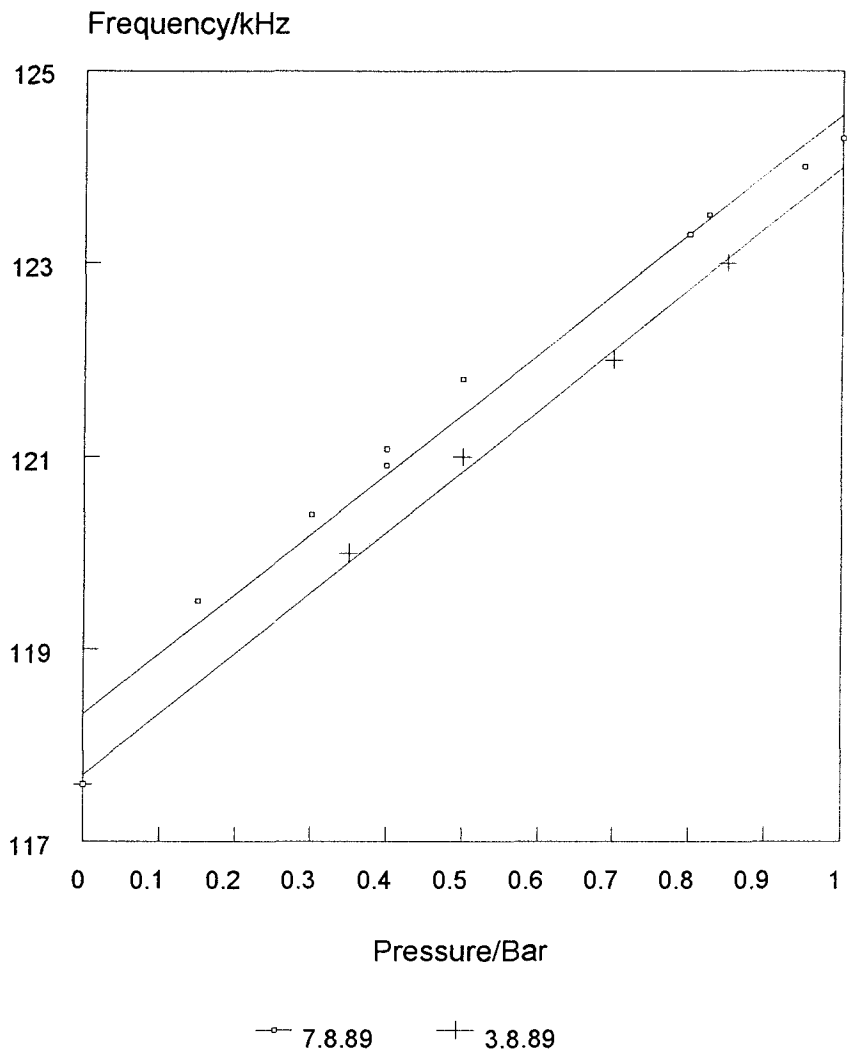

Figure 5.11 Frequency vs. Pressure

Device 3	Base Frequency	Peak to Peak Deflection	Q
	117kHz	50nm	150

Pressure and vacuum fittings were added to the original chip mount to permit measurement of pressure and temperature characteristics and the effect of operating the sensor under vacuum. Initially the wafer was

clamped, which generated stresses that proved unrepeatable (due to the structure of the apparatus) but in the initial test increased the resonant frequency of the device to 131kHz. With care, this could be reduced to a much less significant change and all the values of base frequency are for unclamped devices.

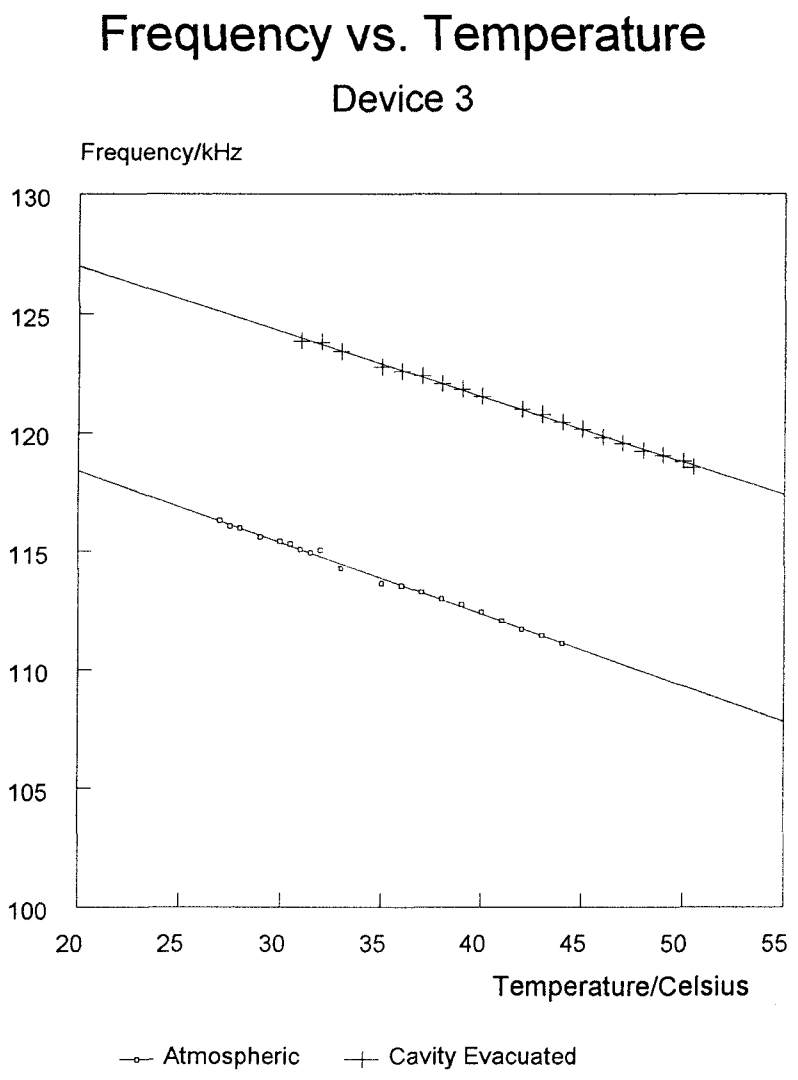

Figure 5.12 Frequency vs. Temperature for device 3

The results presented here were all obtained using a tightly focused spot of light and an aluminium coated silicon bridge. The observable scatter in the readings for pressure was identified as being due to the limitations of the means of pressure maintenance (i.e., leaks in the pressure system and a low quality pressure gauge). The technique adopted to measure the temperature characteristics was to warm the sensor holder and sensor up to the high temperature and, with a thermocouple in contact with the back side of the sensor, take

measurements as the assembly cooled down. The scatter in these readings is due to the temperature moving during measurement and to the time constant of the thermocouple making accurate measurements impossible. The main objective of taking these measurements was to observe the direction of the temperature characteristic and to prove that the measurement technique was feasible. The same device was used for the measurements, with mounting stresses and ambient temperature changing between the sets of results.

5.4 Pressure and Temperature Characteristics

The theoretical gauge factor and base frequency may be calculated from the dimensions of the devices and the physical properties of silicon and aluminium. These figures can be compared with the measured values to yield some information about the actual physical state of the resonators.

	Theoretical Unmetallised	Theoretical Metallised	Measured (unclamped)	Measured (clamped)
Base Frequency	102kHz	103kHz	108kHz	117kHz
Gauge Factor, Clamped Diaphragm	4.24kHz/bar	4.16kHz/bar		6kHz/bar
Gauge Factor, Unclamped Diaphragm	5.5kHz/bar	5.4kHz/bar		6kHz/bar

Equations 2 and 5 (Chapter 3) give values for the base frequency and gauge factor respectively. These values together with the experimental results are shown in the table below. The base frequency is also given for an diaphragm without additional stresses from the wafer holder. The gauge factor is not available since it was not possible to make measurements.

The values for a clamped and unclamped diaphragm are both included because the diaphragm in this case was held firmly between two flat

pieces of metal, so some movement would have been possible, but not free movement.

This table shows a reasonable agreement between the measured and theoretical values of the gauge factor for a metallised unclamped diaphragm. The gauge factor has increased by a similar factor to the base frequency.

The temperature sensitivity measured here is the same (within experimental error) for the device with no pressure across the diaphragm and with one atmosphere across the diaphragm. This yields an uncomplicated compensation algorithm.

The measured value of the temperature sensitivity for this work and measured values from [65] (also unclamped) are shown in the table below for comparison.

Unmetallised	Metallised[65]	Measured in this work, metallised
-30ppm/°C	-1200ppm/°C	-3000ppm/°C

The temperature sensitivity for this device is significantly higher. See Chapter 6 for further discussion.

5.5 Variation of Sensor Characteristics

Apart from the early examples tested in this work, the devices seemed to be reasonably consistent in the deflection size, Q and frequency (several devices were tested during some early work on signal processing). It might be conjectured that, over time, the frequency increased and the deflection size decreased. Figure 5.13 displays the product of deflection with frequency for the devices recorded in this chapter. There is some evidence to say that the values show a tendency for the frequency to increase and the deflection to decrease, since the devices came from the same section of wafer, and the early results were not reproduced later in the work. The values of 117kHz-120kHz recorded above were due to stress from the clamping mechanism. These devices exhibited the same deflection as the later device in the graph, but to include the data in this case would be misleading.

These results are discussed further in Chapter 6 where they are considered to be caused by the aluminium metallisation. An increase in the frequency and a decrease in the deflection is consistent with an increase in the stiffness of the beam. The actual change in the relationship depends on the precise mechanism causing the change.

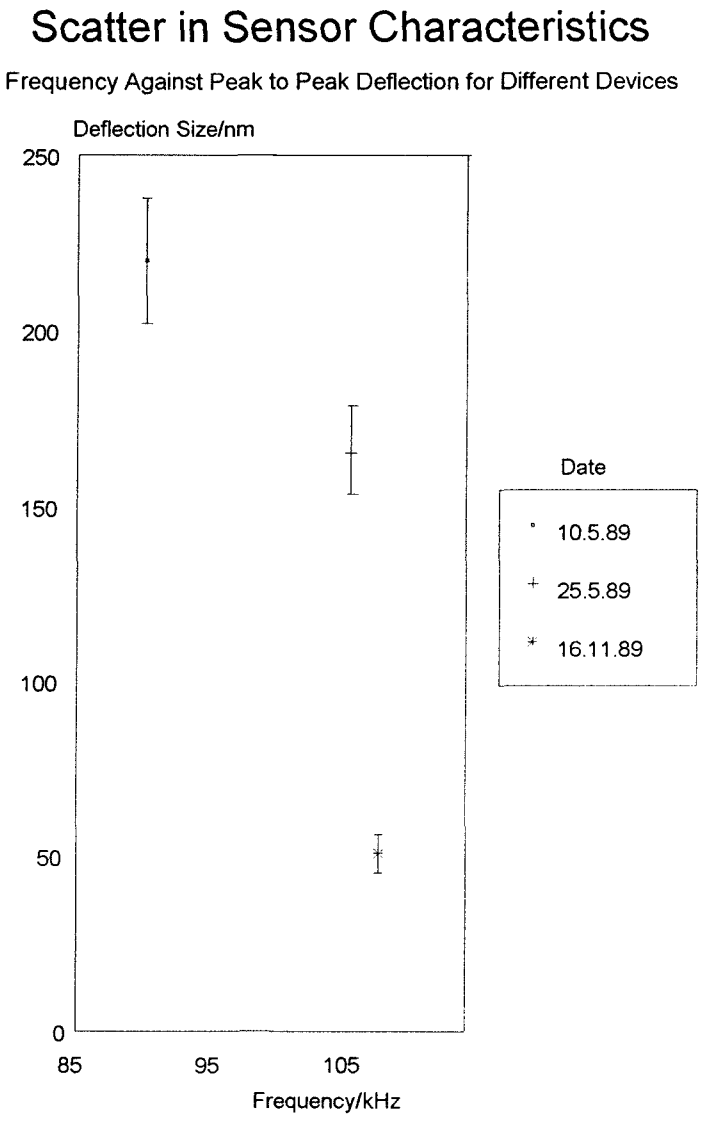

Figure 5.13 Systematic Variation in Sensor Characteristics

5.6 Anodic Bonding

A short study of anodic bonding was undertaken with the apparatus described in figure 4.10. Initially, the equipment was arranged with the silicon in contact with the heater. Bonding was attempted at the recommended parameters (350°C and 500Volts) but with no success. The

polarity of the applied voltage was reversed and the glass was placed in direct contact with the heater. After temperature stabilisation, the voltage was applied and a small current flowed (0.4mA) which decayed to 7μA after 5 minutes. That this bond was successful was due to the glass being allowed to warm up properly before bonding, so the arrangement was adopted for all subsequent tests.

Figure 5.14 shows three successfully bonded silicon and Pyrex glass samples, one of which is bonded to the 0.5μm aluminium metallisation layer. The samples displayed interference rings around contaminated areas that demonstrate bond strength (i.e., the glass was not heated above its annealing temperature, so if the two surfaces were being pushed apart,there must have been considerable stress present normal to the plane of the bond) . It was not possible to separate any of these samples and with the exception of the first attempt, all bonds were successful.

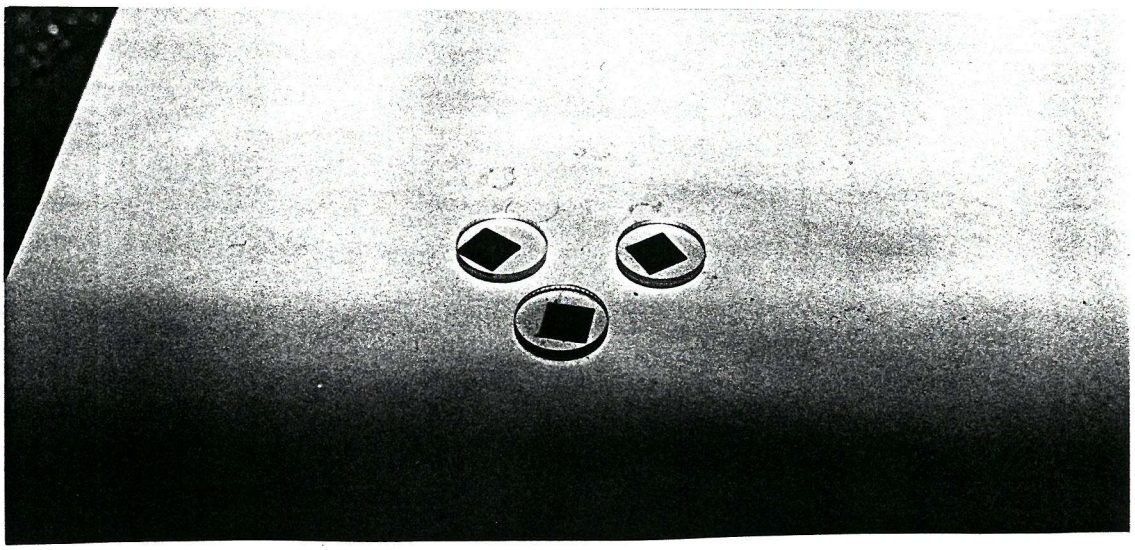

2) Stability

Sensor calibration must remain within tolerance for at least 10 years. If re-calibration is required, it must be made as simple as possible. This point is important for cost of ownership of the sensor and for its overall reliability.

3) Temperature Calibrated

The output must be insensitive to temperature for the limits set out in (1). This may be achieved through careful design of the sensor head as well as active compensation techniques.

4) Cost

The transducer must offer significant cost benefits over competing technologies to be accepted into the marketplace, and have the potential for cost reduction in the future.

Significant progress has been made in achieving these objectives through reduction if the optical component in the transducer and analysis of the limiting factors of the beam dimensions. Futher progress will be made through careful analysis of vibrometer performance, new materials technology and manufacturing techniques in the sensor head, temperature measurement using a cantilever resonator (pressure insensitive) next to the bridge (pressure sensitive) and cost reduction through batch production of the sensor.

6.1.2 Base Frequency and Full Scale Change

The operating frequency of the sensor places a boundary on the number of cycles over which the frequency can be measured, and is also related to the interferometric signal from the resonator. The total change in frequency for the full scale of the measurand is determined by the ability of the Phase Locked Loop to track it, and this depends on the operational bandwidth of the phase sensitive detector (see figure 6.1, drive and detection system). The lower limit of the base frequency is set by the upper limit of any possible acoustic interference. The upper limit is set by the size of deflection that will be achieved by the resonator. A working frequency is required in order to determine the other system parameters. From the experimental work, 100kHz will allow a reasonable separation from acoustic

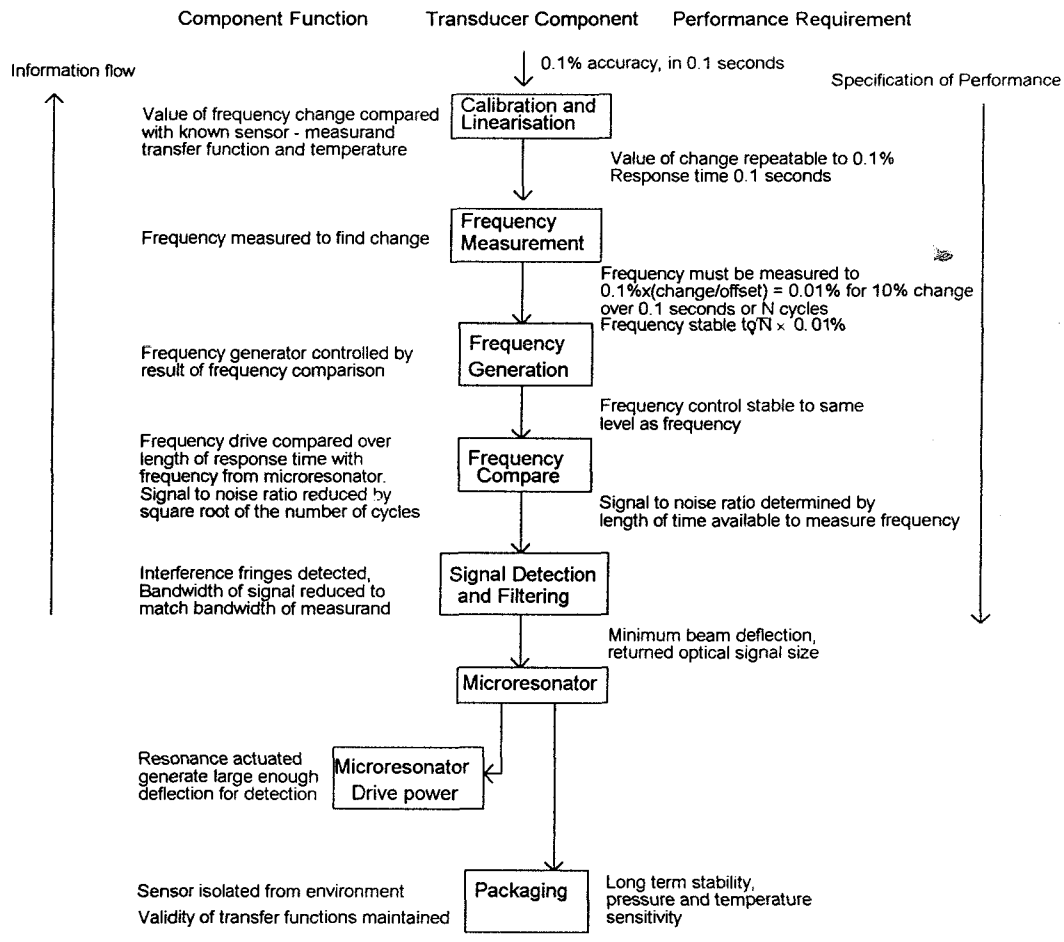

Figure 6.2 Determination of System Component Tolerances from Design Targets

interference, and a full scale reading of 10kHz will be within the working range of a phase locked loop. The accuracy of the transducer is determined by how accurately this change can be measured, so the accuracy to which the absolute frequency must be measured is increased to:

$$\text{Required Accuracy} = \text{Transducer Accuracy} \times \text{fractional change in frequency}$$

Which gives a required absolute frequency measurement accuracy from the high performance target in section 6.1.1 of 0.01%.

6.1.3 Stability of Frequency Output of VCO

From Figure 6.2, and the frequency set in section 6.1.2 the maximum error in this output is:

$$\text{Percentage Uncertainty in Frequency} = \sqrt{\text{Response time} \times \text{Frequency}} \times \text{Percentage Accuracy}$$

This gives a percentage accuracy of the output of the VCO with respect to the actual resonant frequency of the resonator of:

$$\sqrt{0.1\times 10^5}\times 0.01\% = 1\%$$

Which is a 40dB signal to noise in the output of the VCO, averaged over the response time of the transducer. This figure is determined solely by the error in the control input from the PSD and is independent of any changes in the transfer function of the VCO if the frequency output is measured over at least the same length of time as the integration interval of the PSD.

6.1.4 Uncertainty in the Control Output of the PSD:Mark-Space Ratio and Pulse Train Length

For a normal phase locked loop, the signal-to-noise ratio of the signal into the PSD is the same as the time averaged error in the output, in this case, 1%. Here, the role of the loop is switched between drive and detection of oscillations. There are three parameters that determine the performance of the PSD in monitoring the resonant frequency of the sensor and controlling the VCO. These are:

1) Drive-detect cycle length.

This is the time taken for one complete drive-detect cycle. If this time is long (compared to the frequency and Q of the device), the drive frequency is well defined (frequency width of the drive is inversely proportional to the length of the tone burst) but the integration time is either reduced or oscillations decay excessively during the detection cycle. If the time is short (compared to the frequency and Q of the device), the amplitude of the detect signal is large but the drive frequency is less well defined, leading to a broadening of the frequency response of the resonator, as seen in the experimental work.

2) Mark-space Ratio.

This is the proportion of the cycle time that is divided between drive and detection of oscillations. If the drive time is longer than the detect time, the average signal is larger and the frequency is better defined, but the integration time is reduced. If the detect time is longer, the integration time is increased, but the average amplitude

is lower and the drive frequency is poorly defined, giving a broader frequency response.

The optimum combination, as seen in the experimental work, is to use a 1:1 drive detect ratio, with a total cycle time that is matched with the Q of the resonator. This will give a frequency response from the resonator that is only slightly wider than its optimum value, and the signal will be measured over the maximum possible amount of time before it decays completely, with an average amplitude of about two thirds of the maximum at the start of the cycle.

6.1.5 Power and Signal Transmission System - Choice of Optical Fibre and Light Source

From the 1:1 drive detect cycle of the PSD (only half the time is spent in signal detection), the signal to noise ratio of the output from the interferometer is increased to 43dB (0.7% noise). This figure will determine the necessary optical throughput of the system and the deflection of the resonator. A suitable optical fibre, coupler, and laser diode must be selected in order to define the necessary performance from the resonator.

The target optical system for this transducer must use multi-mode fibre because of the reduced cost and higher coupling efficiencies that can be achieved over an equivalent single mode system. Although the additional coupling efficiency is not important for actuation (where energy density determines deflection size) the total amount of light returning to the photodetector from the fibre end and target will be significantly larger and as long as the conditions for efficient multimode fibre interferometry are met by the coherence length of the diode and the fibre end to target separation (see Chapter 3), signal quality will improve.

An unterminated (no connectors) multimode fibre coupler was purchased for this work (CANSTAR, 'Y' coupler with 50/125μm fibre, 0.2NA) and some time was spent studying the feasibility of coupling sufficient light into the fibre using the sources and optics that had been acquired some time previously, since no pre-terminated optics were available. Although a small reference signal was detected at the photodiode, the power coupled into the system was less than the power

from the original single mode system and was found to be insufficient to detect oscillations. Future work with this multimode system must rely on pre-terminated optical systems which, although expensive, deliver guaranteed performance and for the system described here, only one device is required.

The ideal light source is a low coherence, high power diode with a fibre directly attached or a suitable connector for joining to a mating fibre. A visible output is preferable for safety and checking the alignment.

The fibre system used in this work was ideal for the original experimental arrangement. The light was of high coherence, allowing a large separation between the fibre end and resonator, and the power output, in a well collimated beam, was sufficient for the application. The collimation of the light from the fibre allowed a simple lens arrangement to be used and this was incorporated into the vacuum cavity without undue difficulty. The system was purchased fully terminated and performed to expectations. The laser diode (SHARP, LTO26MD) was selected because of its short astigmatic distance and suitability for coupling to single mode optic fibre. The mode noise, although inconvenient, did not prevent measurements. A low coherence light source would remove mode noise in any future system.

6.1.6 Silicon Design

The order in which the dimensions of the device are calculated is set by their limiting conditions. The table below summarises these.

Dimension	Minimum	Maximum	Determined by:
Width	Reflected light must be sufficient to detect oscillations. Resonator must have lateral stability to prevent parasitic oscillations	Average power density across the width must be high enough to actuate oscillations.	Fibre core diameter, Relative thickness
Thickness	Physical strength, actuation efficiency, frequency	Deflection size, frequency, sensitivity	Diaphragm thickness, actuation mechanism
Length	Upper limit of frequency, central section of beam has to be more than illuminated length	Lower limit of frequency. Relative size of strain caused by own weight	Fibre core diameter, Frequency, Thickness

The width is controlled by the core diameter of the fibre and calculated first, to define the average energy density. From section 3.4.3 the best balance between optical signal and enrgy density is

achieved when the resonator is 0.7 ties the core diameter. For 50μm core fibre, this gives a resonator width of 35μm.

This width, since it defines the amplitude of the optical signal, is used to calculate the necessary deflection from the resonator to achieve the specified signal to noise ratio. From equation 29, if the bandwidth of the electronics up to the PSD is limited by the time constant of the photodiode (capacitor) and the resistor (to 110kHz), the power from the fibre is 1mW, the response of the photodiode is 0.5A/W, the wavelength is 750nm, and the reflectivity of the fibre end and resonator surface are 0.04 and 0.7 respectively, at least 100nm of movement (peak-to-peak) is required from the resonator. This value is compatible with deflections recorded for devices early in this work, but is greater than the later results, and other reported deflections for simple microbridge structures.

The optimum length and thickness are partly determined by the actuation mechanism. For a silicon microresonator there are three basic types of strain which are dominant in three different types of structure. These are:-

1) Bare Silicon.
The total induced strain is the difference between the thermal and electronic contributions and this depends on carrier lifetime and the frequency of oscillation of the beam. The relatively long absorption length of light in silicon means that there will be a significant amount of light absorbed throughout the thickness of the beam. This reduces actuation efficiency by reducing the strain gradients between the top and bottom of the device and letting some light through.

2) Thin Metallisation.
A thin (compared to the thickness of the silicon) metallisation layer restricts absorption of light to the top surface and acts as a heater of the silicon. This increases actuation efficiency because all the (non-reflected) light is captured and the resulting strain is all generated in the same thin layer, but the Q is decreased by damping in the metal.

3) Thick Metallisation.

A thick metallisation layer means that the metal itself is mechanically important. Actuation occurs through the 'bi-metallic' effect and is an order of magnitude more efficient than thin metallisation. Despite the accompanying decrease in the Q and increase in the temperature coefficient of the device this is the most effective actuation mechanism for encastré beams.

In each type of structure, there are also two different types of strain:-

1) Bending Moment.

All three of the strain generation mechanisms produce a strain gradient down the thickness of the device. Differential strain about the neutral axis of the resonator generates a bending moment which causes the beam to deflect.

2) Longitudinal Strain.

All three mechanisms also produce an overall expansion of the illuminated part of the beam. Compression of this zone produces a longitudinal wave which propagates along the structure. Although this wave has no component in the transverse mode, the bending moment will couple some in. In encastré beams this expansion serves to make bending easier by reducing the stiffness caused by residual tension.

The most important example of an unmetallised structure is a coupled pair of resonators with both ends free[13]. It is quite large compared with other devices and despite exhibiting a Q of up to 20000, still only undergoes an optically induced deflection of a few nanometres. A thin metallisation layer decreases the Q by a factor of five but the deflection is increased by an order of magnitude, demonstrating the inefficiency of unmetallised actuation.

The dominant mechanism for the resonator under investigation in this work is bi-metallic expansion. Some simple calculations may be made of the induced bending moment and resulting deflection for comparison with experimental results. If there is good agreement, then the dominance of differential expansion is confirmed. Substituting values for the diffusion length, incident energy and the dimensions of the beam, the calculated induced bending moment is approximately half of

the moment required to produce the observed deflection. For the simple theory presented in section 3.4.2 this is a reasonable agreement. The overall strain in the beam is 1.5×10^{-9} and the thermal expansion is about a tenth of this so it can be concluded that differnetial expansion is the dominant effect. Both of these calculations use the Q of the device in vacuum (250).

If the thickness of this device is reduced, the induced bending moment becomes smaller (less leverage from the surface to the middle) and the bending moment for a given deflection decreases. The volume of silicon as a proportion od the volume of the beam also decreases, so the Q drops (damping from the metallisation becomes more significant), also reducing the deflection at resonance and the stability of the frequency. Other reports[64-66] describe thin, long resonators with similar actuating power and beam deflection as in this work, but a lower Q (30 instead of 100). This demonstrates the requirement to balance the Q with induced deflection size, so there is some minimum silicon thickness for bi-metallic actuation.

Following a similar process as above, but for electronic strain, the required actuation efficiency is much less, since the Q is an order of magnitude higher. The electronic diffusion length is larger than the thermal diffusion length in silicon and the absorption is spread through a greater thickness so the bending moment is correspondingly smaller. The effect of longitudinal strain can only be assessed if the amount of coupling of this mode of oscillation by the bending moment into the transverse mode is known but should be relatively more important (than in thermal expansion) because the whole beam absorbs the light.

It is obvious that for a full understanding of the actuation mechanism to be achieved, the system must be modelled using finite element techniques. This work has demonstrated that it is possible to achieve large beam deflections (50nm peak-to-peak or greater) and maintain a reasonable Q without requiring a mechanically complex resonator which is difficult to manufacture. A suitable resonator design may be a larger version of the resonator used in this work, with an increased length and silicon thickness, but the same thickness of aluminium. This structure could have the same frequency as at present, and would

resuire the same bending moment for the same deflection, but because of the relative increase in the mass of silicon, would have a higher Q and this would increase the peak-to-peak signal and stability of the device.

6.2 Sensor Packaging

6.2.0 Introduction

The materials used for mounting of the silicon chip and isolation of the resonator are important factors in determining sensor stability and temperature sensitivity. Manufacturing techniques are limited by the need to protect the sensor and align the optical system. Since there are no electronics and potentially no metallisation on the silicon it should be possible to construct a sensor package that will survive high temperatures, minimise temperature sensitivity and have good stability. By using active temperature compensation, the prime consideration in construction of the sensor head becomes its stability since temperature sensitivity may be removed in the electronics as long as the calibration constants for the transducer remain constant.

The three techniques that are considered here for sensor encapsulation and mounting are anodic (silicon to glass) bonding, silicon to silicon fusion bonding and plasma enhanced chemical vapour deposition. Aspects of each technique to consider are the actual manufacturing process, stability of the material and its thermal expansion characteristics. Mechanical design is determined by the need to align the optical system and maintain a hermetically sealed vacuum cavity around the resonator. The problem with maintaining a vacuum will be outgassing into a very small volume, although techniques for reducing this exist[]. The design proposal at the end of this chapter was discussed with a potential manufacturer and was based on a combination of their existing capabilities.

6.2.1 Anodic Bonding

The early experimental work described in Chapters 4 and 5 demonstrated the basic technique and the ease with which a suitable bonder may be constructed. This technique was attractive due to the relative stability of the bonds (when compared to conventional techniques using

adhesives or mechanical fixings) and the compatibility of glass with a wide range of machining, moulding and etching techniques, as well as its resistance to chemical attack. The possibility of sensor drift due to relaxation of any residual electric field and the nonlinear expansion coefficient (which would produce a non-linear temperature characteristic) make it worth while investigating other possiblities as well. If it was necessary to use a lens for interfacing with the sensor then a glass moulded sensor mounting would be ideal.

6.2.2 Silicon to Silicon Fusion Bonding

If it is not necessary to be able to see the resonator, then silicon of the same orientation and type as the sensor would provide a better match with less bond drift (single crystalline structure) and better thermal matching. Silicon is also attractive because features may be etched into the bonding face to align the two halves automatically before bonding. Since it is not necessary to heat the two halves in order for initial bonding to take place the equipment required becomes greatly simplified.

6.2.3 Plasma Enhanced Chemical Vapour Deposition (PCVD)

PCVD may be used to deposit reasonably thick layers (200um of SiC[]) of any chemical that may be deposited from a vapour phase chemical reaction on to a suitable high temperature substrate. Compounds that may be deposited using this technique include diamond, polysilicon and silicon carbide. This is an attractive technique for forming materials that are normally difficult to machine onto irregular shapes to a controllable thickness. Silicon carbide is attractive as a material for holding the optic fibre onto the back of the sensor since it is chemically stable and has been used to form optic fibre ferrules (using sacrificial carbon formers [private communication, Tony Rogers]). It may also be possible to use SiC as a passivation layer for the exposed side of the silicon diaphragm. Although this would inevitably reduce the sensitivity of the device, it might be preferable because of its high stability compared with isolation with an oil-filled secondary diaphragm.

Forming the cavity under vacuum at temperature will help prevent outgassing and subsequent deterioration of the vacuum reference.

Infra-red optics and/or micromachined features on the silicon may be used for silicon to silicon allignment (see Chapter 8.

6.2.4 Proposed Sensor Head Design

In order to achieve maximum long term stability of the sensor, it is proposed that silicon fusion bonding should be used to join the sensor and fibre alignment chip. This should be hermetically sealed using PVCD silicon carbide that will also coat a piece of sacrificial carbon to create a suitable fibre holder (see diagram 6.2).

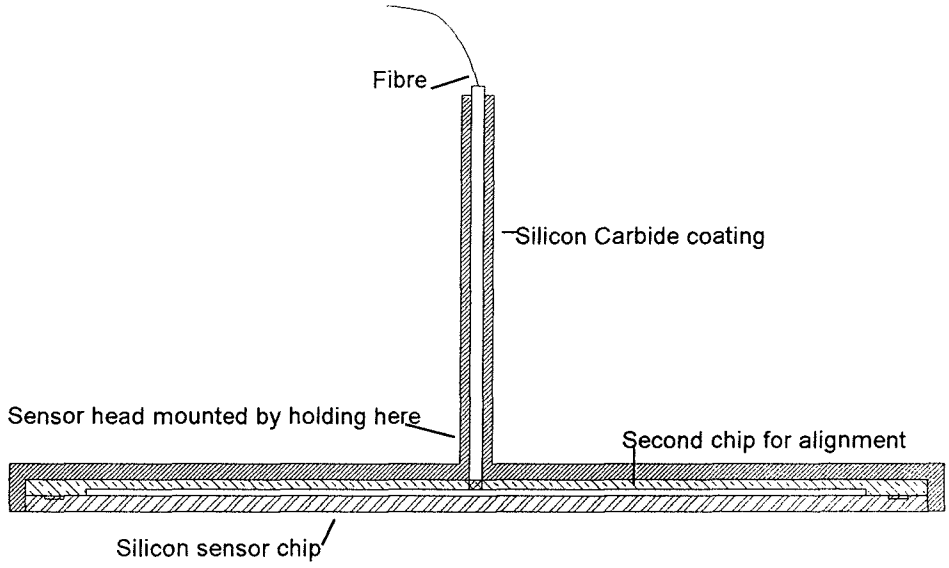

Not drawn to scale The silicon chip is a maximum of 10mm across and 0.5mm thick, the silicon carbide coating can be up to 0.2mm thick, and the fibre is 0.125mm in diameter.

Figure 6.3 Proposed Sensor Head Design

These techniques make it possible to create an entirely ceramic, covalently bonded structure that will couple the optic fibre with the sensor and isolate it from the effects of interfacing with a pressure vessel. Deposition of the SiC occurs before bonding of the micromachined silicon so that the fibre end may be polished and terminated at the correct length. Bonding of the two halves may then be done at room temperature, with a low temperature (300°C) bake afterwards. This leaves the possibility of using a metallised vibrating element if necessary.

This design has the advantage of compatibility with batch fabrication processes and with temperature being measured in the device for

digital compensation the structure may be optimised towards stability with no compromise towards softer materials with a closer thermal match to silicon. Even so, the manufacturing techniques allow the use of the same type of silicon as the immediate mounting for the sensor, which will obviously have an ideal thermal expansion match. Silicon Carbide has a thermal expansion roughly twice that of silicon. Under the right processing conditions it may be possible to reduce the temperature coefficient because differential expansion of the silicon carbide will increase the frequency, couteracting the intrinsic reduction in frequency from silicon but other factors should not be compromised to achieve this goal.

6.3 Calculation of Actuation Efficiency

The actuation efficiency may be calculated using the two methods described in Chapter 3. These calculations assume a good match of the focused spot size with the width of the beam. Any increase in this width will decrease the theoretical efficiency and increase the experimental efficiency.

From equations 11 and 22, the thermal diffusion length for the composite beam at 100kHz is 20μm.

This gives an average temperature rise during one cycle of the central length of beam (50μm long) of 0.02K (absolute temperature is used to calculate efficiencies). This gives a maximum theoretical efficiency of approximately 0.006%.

From equation 25 (energy in the oscillating beam), the total stored energy for a deflection of 25nm is 36nJ. For a Q of 250 (in vacuum), the loss per cycle is 13fJ so for an input per cycle (using the same parameters as above) of 0.5nJ, the efficiency from experimental data is of the order of 2.6×10^{-3}% or approximately one half of the maximum theoretical efficiency. This calculation assumes that all of the light is incident on the beam but is a useful guide for the validity of any assumptions that are being made about the structure. If the numbers were unreasonable (experimental efficiency much greater than theoretical efficiency for example) then some of the assumptions that are being used for other actuation calculations may also be incorrect.

6.4 Actuation Efficiency and the Temperature Coefficient

The actuation mechanism for a beam with thick (significant compared with the silicon) metallisation relies on differential thermal expansion between the two layers to generate a bending moment. The actuation mechanism is more efficient when the difference between the coefficients of thermal expansion is large, and that a small temperature change generates a large differential strain in the resonator. The same condition is true for the ambient temperature, and devices that use differential expansion to excite oscillations have exhibited a correspondingly high temperature sensitivity. This need not be a problem, if the high actuation efficiency produces a system with a high signal to noise ratio, and the ambient temperature sensitivity is stable. With local temperature measurement available, full compensation can take place in digital electronics.

6.5 Aluminium Metallisation and Sensor Drift

Early measurements of resonator characteristics revealed devices with lower than expected resonant frequencies and high deflections as illustrated in figure 5.13. Although this is consistent with variations in processing parameters all the devices came from the same region of the wafer and despite the strong variation in the first two resonators, these characteristics were not observed later in the course of the project. This indicates that there was some decay in performance of the resonators with time which was caused by a change in the physical characteristics of the beam. Single crystal silicon is known as a stable material, so it is likely that the aluminium was responsible. The possible causes are slow oxidation of the aluminium due to its porous nature (it was and evaporated and was not annealed) or relaxation of residual stress from the manufacturing process. This emphasises the importance of careful annealing of this type of sensor after production and further investigation is required to ascertain how effective stabilisation of the metallisation could be.

Chapter 7: Conclusions

Modern pressure measurement has developed from early mechanical devices that relied on corrugated diaphragms or Bourdon tubes to convert movement to voltage via a potentiometer. These early devices have proven reliablity and still find a market in areas where robustness and immunity to electrostatic damage is of prime importance[85]. Bonded strain gauge pressure transducers, which measure the strain in a thin steel diaphragm, offer improved accuracy, cost and size over the older mechanical transducers while maintaining some of the advantages associated with a metal diaphragm. Silicon strain gauge pressure transducers have a much better accuracy and temperature performance than either mechanical or bonded strain gauge transducers and may be fabricated with batch production techniques for low cost and consistency, but are susceptible to electrostatic damage and are less mechanically robust. The silicon diaphragm also needs protection from corrosive environments (usually from an oil-filled cavity and a thin stainless steel diaphragm). Development of high accuracy and stability pressure transducers have concentrated on resonating devices, made from quartz or metal that although extremely stable, tend to be expensive and susceptible to mechanical damage. With the advent of silicon processing it became possible to manufacture a silicon resonating pressure sensor which would be robust, low cost and very accurate. Optical drive of these devices has developed as a method for removing the electronics from the sensor, making construction of the silicon easier, and permitting remote operation in hazardous and difficult conditions.

This work has approached the optically-driven resonant silicon sensor with the aim of developing a low cost, stable device, with an optimised silicon resonator design that could meet a target specification. The main cost in the technology was identified as the optical system. Consequently a method for single optical source drive of the resonator was developed. The method is suitable for closed-loop driven operation of the sensor, and takes advantage of the high Q exhibited by these devices through time sharing the single optical source and fibre coupler between actuation and interrogation. A prototype pressure sensor was demonstrated and the pressure and the temperature characteristics of a silicon micromachined resonator were determined. The operating characteristics of the system were investigated, so that suitable electronics for automatic tracking of the frequency could be developed.

A system comprising a switched phase sensitive detector combined with a voltage controlled oscillator was devised for closed loop operation. This would allow multiplexing of several devices onto the same fibre by splitting a main fibre between many sensors, each pressure sensitive oscillator (PSD, VCO and silicon resonator) occupying its own part of the frequency domain. The narrow bandwidth of the system would prevent crosstalk as long as the full scale deflection of the devices did not cross over.

A design method for the transducer was developed which, from the system framework, defined the performance of each of its components from a target specification. The response time and accuracy was used to define the signal to noise ratio required from the interferometer, and from this the signal size and frequency of the resonator were calculated. Linking the target specification to the physical capabilities of the microresonator enabled predictions to be made about the possible future performance of the technology.

A theoretical analysis of optical actuation and detection was undertaken to optimise resonator dimensions and determine what the maximum performance of the sensor could be. The limiting factors and optimising parameters for the dimensions of a simple microbridge resonator were identified. These parameters are unique for an optically actuated and interrogated device and take into account the actuation mechanism and relative dimensions of the fibre. The width of the resonator is governed by the core diameter of the optic fibre. The length may be used to match the device size with the requirements of the optical system (for alignment) and to achieve a target frequency which maintains the operating range of the sensor beyond susceptibility to acoustic disturbance. The thickness of the device is determined by the actuation mechanism and the actuation mechanism is determined by the structure of the resonator. Thin silicon resonators with thick metallisation exhibit low Q, high actuation efficiency and a high thermal sensitivity, the mechanism being dominated by differential expansion between the metallisation and silicon (the bi-metallic strip effect). Thick silicon resonators with thin metallisation layers are actuated from the generation of photoacoustic waves and exhibit higher Q, lower actuation efficiency and lower temperature sensitivity. Optimum thicknesses for each of these actuation mechanisms have been calculated. For a given thickness, different device lengths could be manufactured in the same process to give a range of resonant frequencies making them suitable for multiplexing onto the same optical system.

The appropriate packaging technology for an optically driven sensor has been considered. The objective was to design a stable sensor head with the minimum number of materials in contact with the sensor yet compatible with batch processing techniques. Discussions with a potential manufacturer led to the development of a design that could be manufactured by available techniques, augmented by automatic alignment of the optical system with the resonator. The fibre could be integrated into the head by forming a ferrule from plasma enhanced chemical vapour deposited silicon carbide, which could also be mounted in a sensor head housing with the minimum amount of stress transmitted to the sensor itself. The central design criterion for the sensor head is that it is stable, and it is assumed that active temperature compensation will be applied by by measurement of the sensor temperature with a pressure independent resonator driven in parallel with the pressure sensitive microbridge.

The design solutions to the problems outlined for a transducer in the introduction are set out in Figure 7.1.

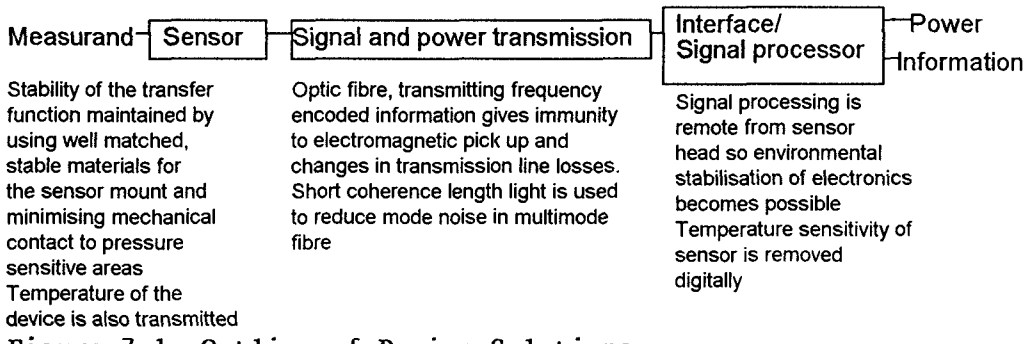

Figure 7.1 Outline of Design Solutions

Compromises are reached by considering noise contributions throughout the system and aiming to reduce these as far as possible. The design has the potential for a low cost construction using batch fabrication techniques that generate a complete sensor, not just the sensing element. The prime requirements for this sensor head are its long and short term stability and manufacturability. Accuracy, temperature sensitivity and dynamic range are important, but are secondary considerations compared to the repeatability. The first criterion determines the lifetime of the sensor and the second promises lower cost production in the future.

Although the technology has the potential for high accuracy operation, the limitations of optical detection of vibrations reduce this, leading to a less favourable accuracy or response time. An optically driven transducer of this type is suitable for intrinsically safe applications, and in a distributed network of sensors powered from the same fibre, but the signal processing would have to be adjusted to increase the accuracy to a level which would compete with pressure calibrators and other high accuracy devices. For these applications, a non-optical technique would be more suitable.

A prototype pressure sensor has been demonstrated. Through this, and other work reported in the literature an understanding of the technology has been established and a comprehensive design process for the transducer has been developed, which predicts the future performance and ideal construction for a simple micromachined silicon bridge.

During the course of this work, the following points have been covered:-

1) A pressure and temperature sensor was constructed with sensitivities of +6kHz/bar and -0.3kHz/°C

2) A system of driven, single optical source actuation and detection was devised which time multiplexes the optical system between drive (tine burst) and detect (interferometer) cycles.

3) The 'tone burst' actuation system is only made possible by the high Q of the resonator

4) The best ratio between drive and detect durations is 1:1, with each cycle time matching the Q of the resonator (ie, its decay time).

5) There was some evidence of relaxation of residual stress or long term oxidation of the aluminium metallisation layer early in this experiment. This must be investigated further.

6) Limiting parameters which optimise the resonator for optical actuation and detection have been identified. The width must 0.7 times the fibre core diameter, the thickness must maximise actuation efficiency and Q and the length must be chosen to match the requirements of the thickness (for a given frequency) and optical system.

7) The manufacturing technology permits incorporation into the pressure sensor desing a temperature sensor of the same construction, but without a coupling mechanism to pressure, thus permitting excellent match between the thermal characteristics of the two devices.

8) The on-board temperature sensor removes temperature compensation requirements from the packaging design, so the emphasis can change to stability and manufacturability.

9) A sensor packaging system using current technology has been identified that would fulfil the requirements of this sensor.

Chapter 8 Further Work

8.0 Introduction

As this project has progressed, the development emphasis has moved from the central aspects of the transducer (actuation, detection, optical system) to the outer parts (signal processing and sensor head construction). These aspects must be the focus of further work in addition to further characterisation of the dynamic behaviour of the transducer system itself and improvements to the optical system.

8.1 Phase Stabilisation for Closed Loop Operation

A method for stabilisation of the phase of the detection signal must be developed. One possibility is to adapt a technique used for self-resonant sensors[31] where the position of the interferometric signal in the fringe is maintained by adjusting the laser diode power and therefore the frequency in a closed loop, low pass control system. This could be adapted to control the interrogation level of the laser without affecting the drive cycle. An alternative to this is to use a non-interferometric interrogation system which would have to rely on the detection of changes in the intensity of the reflected light. It may be possible to observe the scattered light with a second fibre (without its own light source) and in this way, improve the geometry without affecting actuation. This would still require switched operation from the light source.

8.2 Sensor Packaging

The sensor packaging, as described in Chapter 6 should be developed. If isolation of the diaphragm is required, the surface could be coated with a suitable passivation layer instead of the more usual oil-filled diaphragm which would unduly compromise the performance of the sensor. Finite element analysis of the structure could be used to ascertain the best position for mounting the head. It is suggested that the silicon carbide around the fibre (the 'ferrule) should be held firmly, allowing the pressure to surround the sensor. This would make it immune to ambient pressure on the outside of the and isolate the assembly from any instability in the mounting. The use of this scheme

could be broadened to house other silicon sensors, with the wires replacing the optic fibre.

8.3 Sensor Characterisation

The variation in sensor characteristics observed in the ealy part of the project must be investigated further. The work should aim to establish the exact cause of the drift through examining the relationships between the rates at which sensor characteristics (Q, frequency and actuation efficiency) change. In order to collect as nuch information as possible, freshly metallised structures must be used. Also, if the aluminium is unstable, the importance of this instability must be assessed, especially if the sensor is operating at high temperature. If it can be proven beyond doubt that it is possible to stabilise the aluminium, this would make the technology more accessible through the increased actuation. The damping mechanisms in the aluminium should be quantified, and if possible reduced through suitable thermal or chemical conditioning. These measurements should be correlated with other acoustic absorption measurement techniques to gain a better understanding of the mechanisms involved. If the performance of the earlier devices in this study could be reproduced and maintained (perhaps by forming a stable layer of oxide on the aluminium shortly after deposition, as practiced in the electronics industry) the improvement in transducer performance would be considerable.

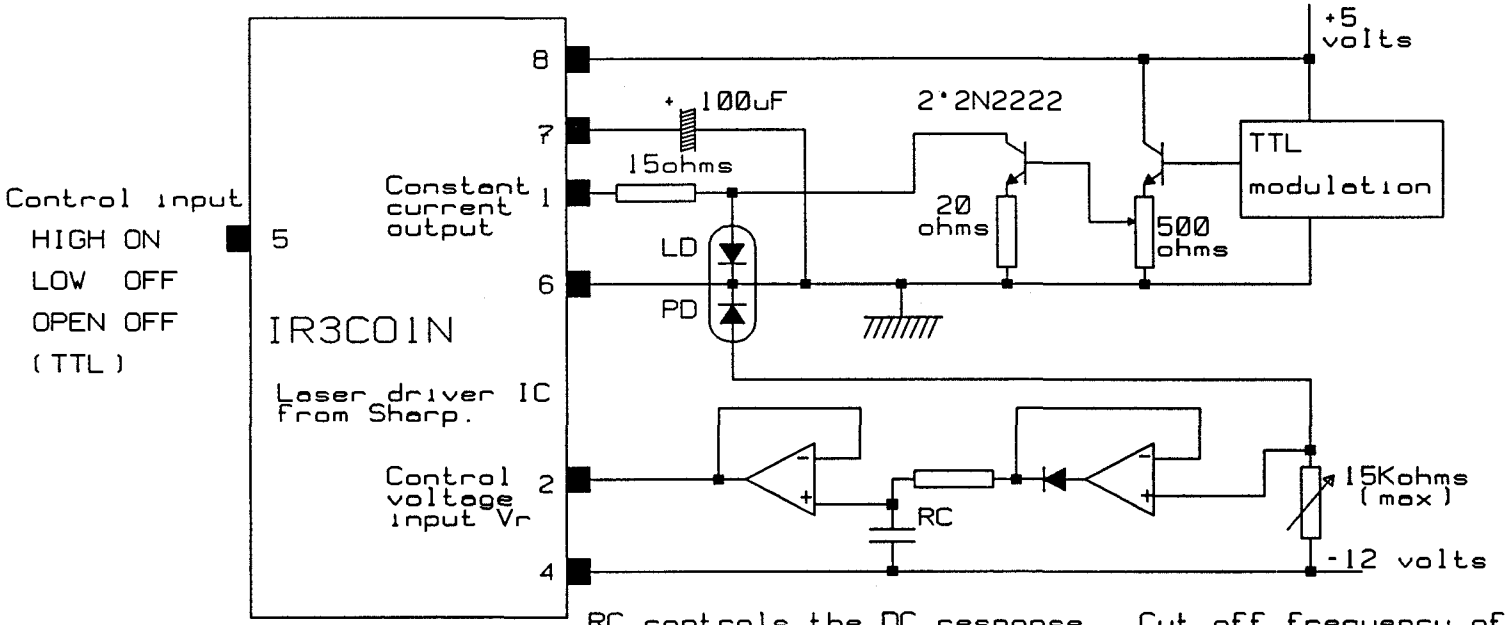
Control input
HIGH ON
LOW OFF
OPEN OFF
(TTL)
5
IR3C01N
Laser driver IC
from Sharp.
8
7
1
6
2
4
Constant
current
output
Control
voltage
input Vr
+100uF
15ohms
LD
PD
2*2N2222
20
ohms
500
ohms
+5
volts
TTL
modulation
RC
15Kohms
(max)
-12 volts
RC controls the DC response.
Vr controls the DC level.
Cut off frequency of
low pass filter
designed to be 1kHz

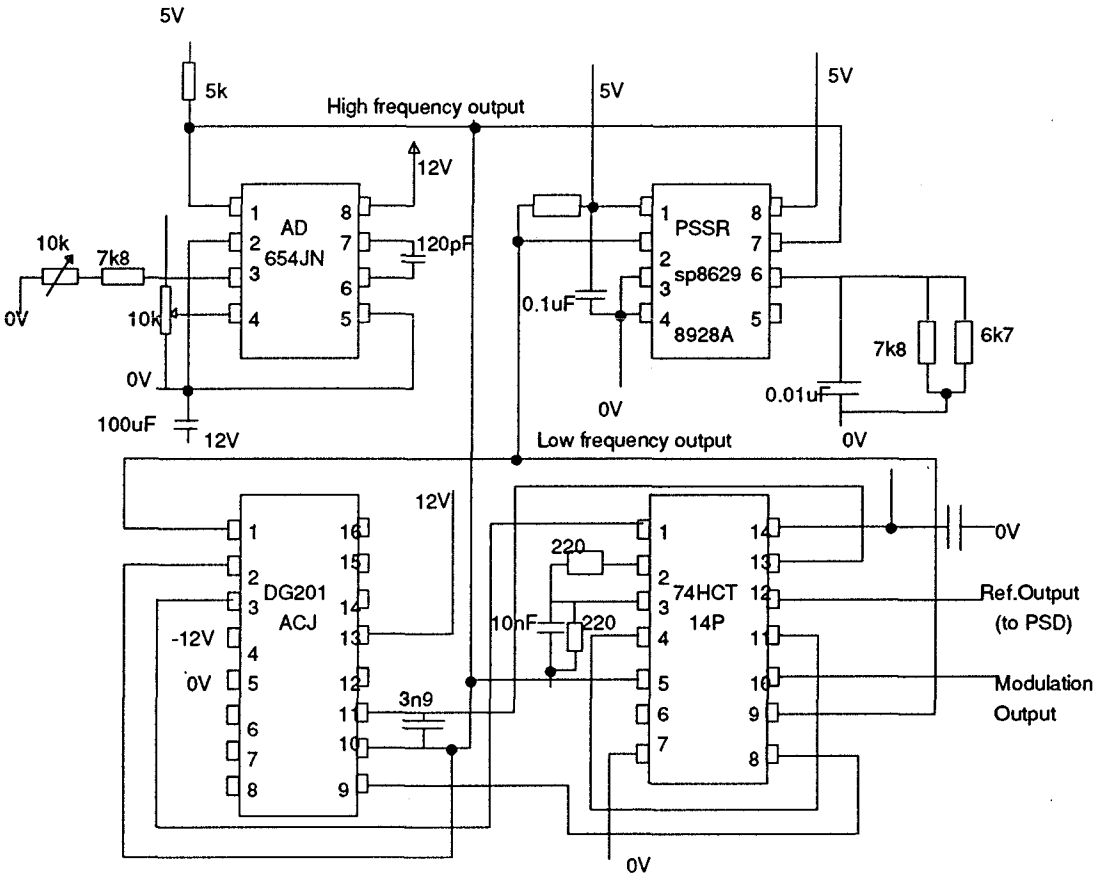

VCO-Switch Circuit for Laser Diode Modulation and PSD reference.

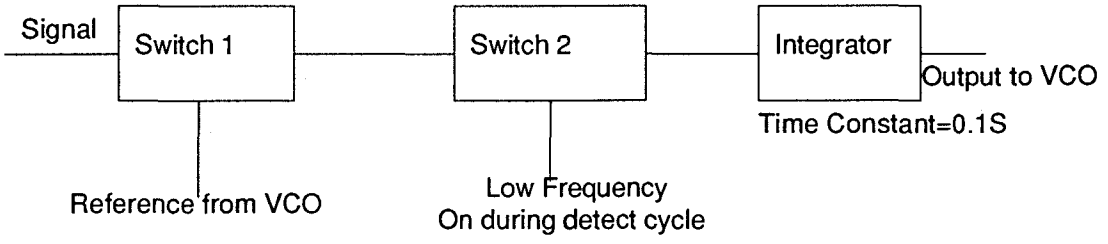

Switched PSD - Uses DG201ACJ FET array for switches

Appendix B - Photographs of Resonant Sensors

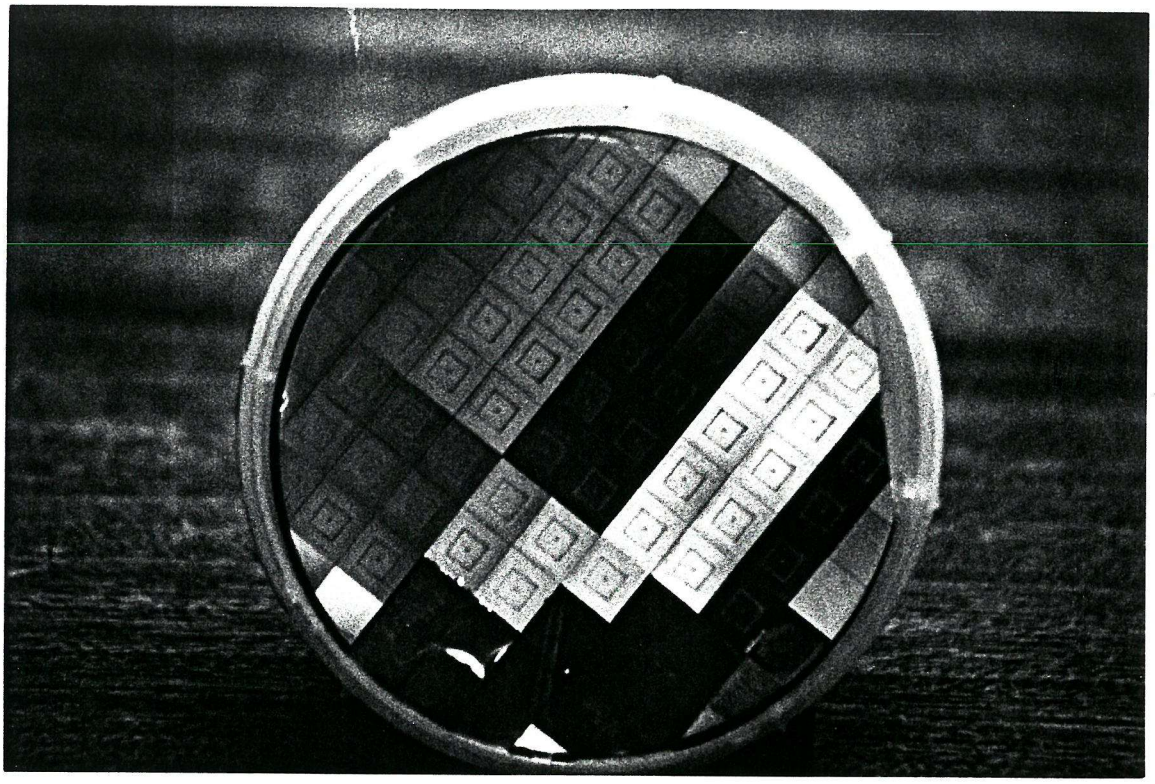

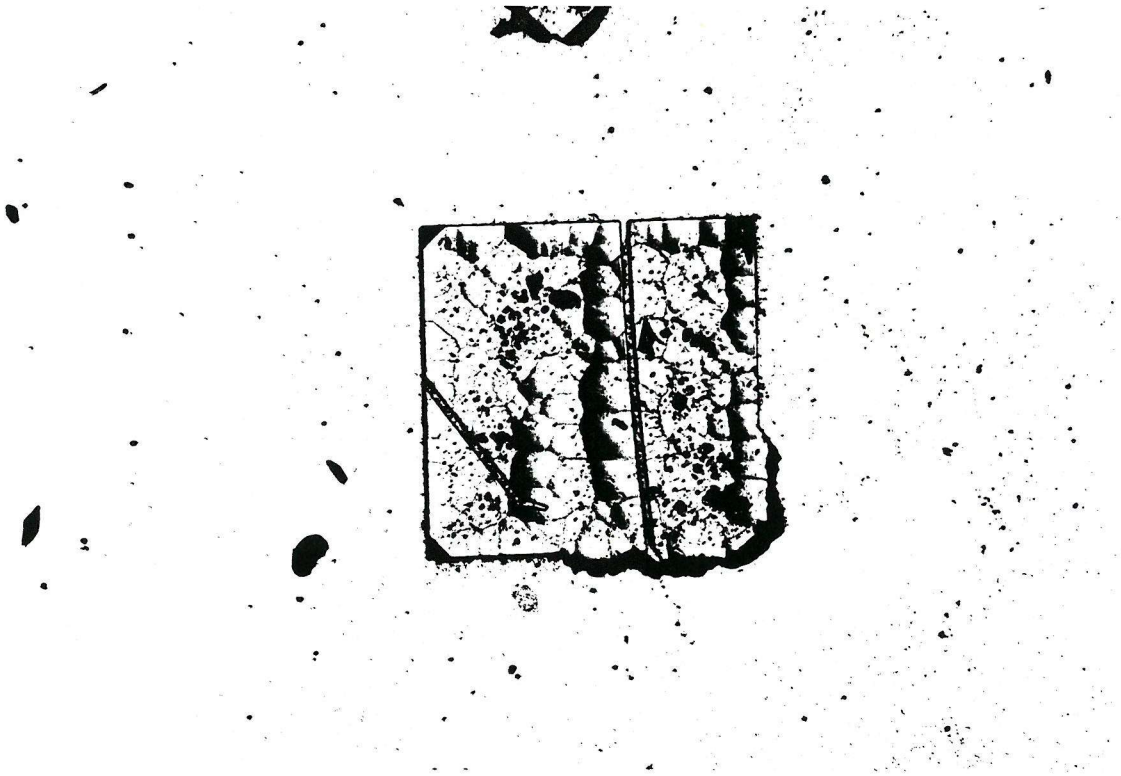

Appendix C - Publication

Sensors and Actuators A, 25–27 (1991) 209–212

An All-optical Single-fibre Micromachined Silicon Resonant Sensor: Towards a Commercial Device

D. R. VINCENT

Penny and Giles Sensors and Systems Ltd., Christchurch, Dorset BH23 3TS (U.K.)

J. N. ROSS

Department of Electronics and Computer Science, University of Southampton, Southampton SO9 5NH (U.K.)

Abstract

A new technique for the actuation and detection of resonant sensor oscillations is presented. Time multiplexing is used to actuate and detect vibrations using a single fibre. The scheme could be extended to permit multiplexing of several sensors onto a single fibre.

The pressure and temperature characteristics of the resonance frequency of a device have been measured. The temperature coefficient is found to be negative.

The efficiency of actuation is calculated to be roughly 0.02%.

Introduction

The aim of this project is to produce a working, bench-top version of an optically excited and interrogated silicon resonant microbridge pressure sensor [1–6]. Based on existing published work [1], a silicon microbridge was designed and manufactured at Southampton. The resonant beam is large enough for the optical system to be aligned with simple optics. A single-mode fibre interferometer was chosen for vibration detection and the same optical source is used for excitation of resonance (see Fig. 1). This avoids the duplication of expensive optical components and alignment. It also means that separation of the modulation required for actuation and the response of the interferometer to vibration is done electronically. The method chosen was to time the multiplex use of the fibre between detection and actuation. A tone burst modulates the laser source to excite the sensor, followed by a constant level to detect vibrations (see Fig. 2).

Up to this time, only two workers have used a single fibre and optical source for actuation and detection [2, 5]. The first method used a pulsed system, detection occurring on the low-power low-coherence part of the laser diode output. This relied on a high-power laser and a large resonator, and used frequency spectrum analysis to detect the resonance. In the second method, the optical cavity formed between the fibre end and resonator was modulated sufficiently by the movement of the resonator that the light

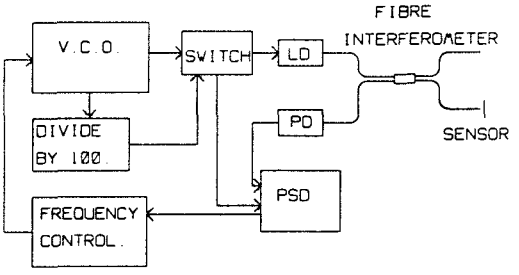

Fig. 1. Schematic of the single-fibre micromachined silicon resonant sensor system.

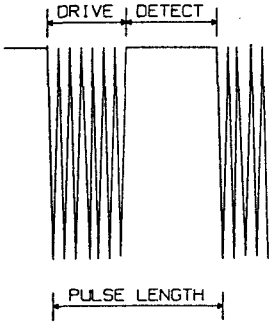

Fig. 2. Output waveform of laser diode.

0924-4247/91/$3.50

intensity change was enough to send the system into oscillation. A problem with this is maintaining a suitable cavity size throughout a wide temperature range. Other systems have used two [1, 3, 4, 6] optical sources and complex but standard optical techniques for detection of vibration (optical heterodyning) [1]. The system described in this paper uses a simple electronic and optical closed-loop system, which can track frequency and provide a single constant square wave for accurate frequency measurement. As it is a tuned system, it would be possible to multiplex sensors while using a single fibre.

Having taken measurements of the dependence of the frequency on pressure and temperature and of the Q of the device (see Results), some calculations were made of the efficiency of actuation as compared with an ideal heat engine with the same temperature changes. This is a start to building a theoretical picture of the process of actuation. Improved efficiency will increase the length of fibre that can be used, with the aim of producing a large network of optical fibres returning highly accurate pressure and temperature information from an intrinsically safe system.

Experimental System and Results

The sensor used in these experiments is of dimensions ($600 \times 4 \times 12$) μm etched into the middle of a ($10 \times 10 \times 0.5$) mm silicon chip with a layer of aluminium 0.5 μm thick. No success was achieved with a bare silicon sensor and chromium-coated sensors are yet to be tested fully.

The 10 mm square silicon chip is sealed into the chip holder (for evacuation and application of pressure to the back face) by using flat polished metal surfaces and silicone vacuum grease. This system works well and is convenient, as it only takes a short time to change devices and no permanent fixing of a device to the system is necessary.

The laser diode is cooled with a Peltier thermoelectric cooler to improve stability. The 780 nm laser light is visible, which simplifies alignment of the optical system. The power output of the laser is 3 mW (peak), with an actuating power at the fibre end of 0.15 mW.

The original system used to test the mechanical and optical design of the sensor used two signal generators for laser modulation and an oscilloscope to detect resonance. Using this system, it was found that a broad range of pulse lengths could be used, ranging from two to more than 100 cycles of the resonance frequency. A brief study showed that a sharper response was found for longer tone bursts. With shorter tone bursts a larger amplitude response was found when the sensor frequency was an even multiple of the burst repetition frequency. From these studies, a burst length of approximately 1 ms was chosen.

The maximum peak-to-peak deflection of the resonator achieved was found to be approximately 50 nm.

The Q of the sensor was measured from the decay of the signal and was found to be between 100 and 150 in air. This rose to 250 in low vacuum. The low Q (compared with other silicon resonators) is probably due to the rather thick layer of aluminium used.

The frequency versus pressure and temperature results are shown in Figs. 3 and 4. The temperature dependence of the device is of opposite sign to the results reported in ref. 6.

The rather bulky system used to make these measurements (using signal generators and an oscilloscope) is easily transferable to a more

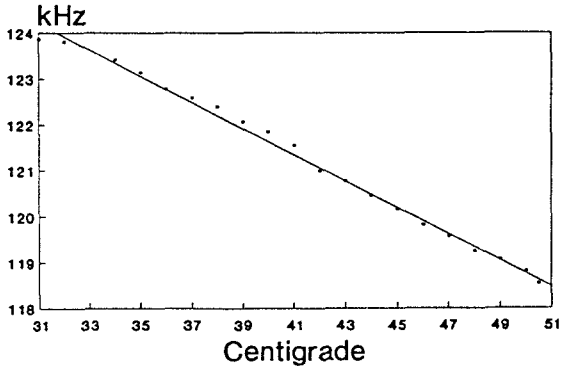

Fig. 3. Temperature vs. frequency results.

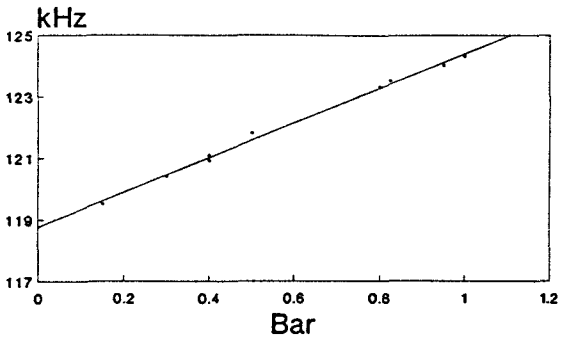

Fig. 4. Pressure vs. frequency results.

integrated system. A voltage-controlled oscillator at the resonance frequency is divided by 100 to control an analog switch to produce tone bursts which keep in step with the resonator. The base frequency is also fed as a reference signal into the phase-sensitive detector, which is switched on during the detection cycles of the circuit. This produces an error signal which is used to track the sensor frequency. The loop can then be closed using either a microprocessor (which could also measure the frequency) or an analog technique. Initial frequency locking is achieved by sweeping up until a response is found. The system is shown in Fig. 1.

Discussion

The maximum efficiency of this device cannot exceed that for an ideal heat engine (as described by the Carnot cycle). A rough estimate of the temperature change achieved is obtained from the temperature rise necessary to conduct the energy away to the bulk material; this rise was found to be 0.5 K, giving a maximum efficiency of 0.2%.

A second way to calculate the efficiency is to find the power necessary to maintain oscillation and the actual energy put into the system. Using standard results [7] for the vibrational energy of a rectangular bar (fixed at both ends), the stored energy of the oscillator was found to be 300 pJ, which for the mechanical Q, frequency and reflectivity of this device gives an experimental efficiency of around 0.02%.

So far, a time-multiplexed single-fibre system for sensor communications has been demonstrated. It is expected that the sensor will have a response time of 100 ms, which is sufficient for most applications. This is a low-cost solution to the problem of an all-optical interface to this type of sensor and has the advantage over other single-fibre systems of being closed loop, the pulsed nature of actuation and detection being disguised by an integration period greater than the pulse frequency. It still suffers from the problem of a simple interferometer, which is that of a null sensitivity point.

The contrast between the frequency versus temperature results presented here and in ref. 6 is interesting because it suggests that considerable mechanical temperature compensation could take place. The difference between the physical clamping of the silicon devices is that the system used in ref. 6 had the silicon permanently bonded to a capillary tube, whereas in this project the temperature coefficient of the frequency is due only to the silicon/aluminium structure. Obviously any sensor development must include a full study of the packaging.

The variation of frequency with pressure shows a useful value of 10% over 1 bar. This could easily be changed by altering the dimensions of the chip which forms the sensor diaphragm.

Conclusions

A new system for the actuation and detection of silicon microbridge sensor resonance has been demonstrated and sets of measurements of the pressure and temperature characteristics of an unclamped sensor have been taken. These results show that mechanical compensation should be possible. The actuation and detection system is resonant and since the high Q (for a filter) gives the sensor a narrow bandwidth requirement, it would be possible to multiplex sensors with different resonance frequencies onto a single fibre.

Acknowledgements

The authors would like to thank the Directors of Penny and Giles Sensors and Systems Ltd., for financial support and permission to publish this paper. We would also like to thank the University of Southampton for the facilities provided for this work and for manufacturing the devices used.

References

1 S. Venkatesh and B. Culshaw, Optically actuated vibrations in a micromachined silica structure, *Electron. Lett.*, *21* (1985) 315–317.

2 L. M. Zhang, D. Uttamchandani and B. Culshaw, Excitation of silicon micro resonators using short optical pulses, *Sensors and Actuators*, *A21–A23* (1990) 391–393.

3 M. V. Andres, K. W. H. Foulds and M. J. Tudor, Optical activation of a silicon vibrating sensor, *Electron. Lett.*, *22* (1986) 1097–1099.

4 S. Venkatesh and S. Novak, Micromechanical resonators in fibre-optic systems, *Optics Lett. 12* (1987) 129–131.

5 N. A. D. Stokes, R. M. A. Fatah and S. Venkatesh, Self excitation in fibre-optic microresonator sensors, *Sensors and Actuators*, *A21–A23* (1990) 369–372.

6 D. Uttamchandani, K. E. B. Thornton and B. Culshaw, Optically excited resonant beam pressure sensor, *Electron. Lett.*, *23* (1987) 1333–1334.

7 L. E. Kinsler, A. R. Frey, A. B. Coppens and J. V. Sanders, *Fundamentals of Acoustics*, Wiley, New York, 3rd edn., 1982, Ch. 3.

References

1 R M Tennent, Ed, Science Data Book, pub Oliver and Boyd, 1971 pp 56-61

2 Kurt E. Petersen Silicon as a Mechanical Material Proc. of the IEEE, Vol. 70, No. 5, May 1982

3 Research Triangle Institute, Physical and Electrical Properties of Silicon, Integrated Device Technology, Vol.5 Ad 605-556 under contract AF33(657)-10390, July 1984, pp98-106

4 R. G. Stearns and G. S. Kino Effect of electronic strain on photoacoustic generation in silicon. Appl. Phys. Lett. 47 (10), 15th Nov. 1985

5 Oxford English Dictionary, 2nd Edition, Ed R.W.Burchfield, Pub Clarendon Press, 1989

6 S. Middlehoek and D. J. W. Noorlag Silicon micro-transducers J Phys E:Sci Instrum, Vol. 14, 1981

7 G Blasquez, P Pons, A Boukabache, Capabilities and Limits of Silicon Pressure Sensors, Sensors and Actuators, 17(1989), pp387-403

8 Solartron Ltd. 7880-Y Series Pressure Transducer Product Data Sheet

9 K T V Grattan, A W Palmer, D P S Saine, Optical Vibrating Quartz Crystal Pressure Sensor Using Frustrated Total Internal Reflection Readout, IEEE J Lightwave Technology, LT5(1987) 972.

10 R W Bogue, Semiconductor sensors: a challenge to Europe, J. Phys E: Sci. Instrum. 20 1987 pp 1059 - 1060

11 S Middlehoek, S A Auder, Silicon sensors: full of promises and pitfalls, Phys. E: Sci. Instrum., 20 1987 No9 pp 1080 - 1086

12 M M Farooqui and A G R Evans, Polysilicon pressure sensors, IEEE coloquium on Silicon Sensors, 1987.

13 M. V. Andres, K. W. H. Foulds, M. J. Tudor Optical Activation of a Silicon Vibrating Sensor. Electronics Letters 9th Oct. 1986 Vol. 22 No. 21

14 D. Uttamchandani, K. E. B. Thornton, B. Culshaw Optically excited resonant beam pressure sensor. Electronics Letters 3rd Dec. 1987 Vol. 23 No. 25

15 M. J. Tudor, M. V. Andres, K. W. H. Foulds, J. M. Naden, Silicon resonator sensors: interrogation techniques and characteristics. IEE Proceedings, Vol. 135, Pt.D, No. 5, Sept. 1988

16 D. Uttamchandani, K. E. B. Thornton, B. Culshaw Optically excited resonant beam pressure sensor. Electronics Letters 3rd Dec. 1987 Vol. 23 No. 25

17 D. Uttamchandani, K. E. B. Thornton, J. Nixon, B. Culshaw Optically excited resonant diaphragm pressure sensor. Electronics Letters 12th Feb. 1987 Vol. 23 No. 4

18 S. Venkatesh, B. Culshaw Optically activated vibrations in a micromachined silica structure. Electronics Letters 11th April 1985 Vol. 21 No. 8

19 B. Culshaw, J. Nixon, K. Thornton, D. Uttam, A. Wright Optically Excited Resonant Sensors. IEEE Colloquium on Micromachinig, 1987

20 K E B Thornton, A Sensitive Optically Excited Silicon Beam Mechanical Resonator, Electronics Letters, vol 23, No 14

21 M. B. Othman, A. Brunnschweiler Electrothermally Excited Silicon Beam Mechanical Resonators Electronics Lets. 2nd July 1987 Vol. 23 No. 14

22 J C Greenwood Etched silicon vibrating sensor J.Phys.E:Sci.Instrum.Vol.17, 1984

23 J C Greenwood, D D Satchell, Miniature Silicon Resonant Pressure Sensor, IEE Proc D, 135 (1988)369-3725

24 R. A. Buser and N. F. DeRooij Very High Q-Factor Resonators in Monocrystalline Silicon Sensors and Actuators, A21-A23 (1990) 323-327

25 Harrie A. C. Tilmans, Miko Elwenspoek and Jan H. J. Fluitman Micro resonant force gauges, Sensors and Actuators A, 30 (1992) 35-53

26 Erik Stemme, G oran Stemme A capacitively excited and detected resonant pressure sensor with temperature compensation. Sensors and Actuators A.32 (1992) 639-647

27 Theodor Gast Sensors with oscillating elements. J. Phys. E:Sci.Instrum., Vol. 18 1985 Invited Keynote Paper

28 R M Langdon, Resonator Sensors: A Review, J.Phys. E: Sci Instrum, Vol. 18, pp103-115

29 L. M. Zhang, D. Uttamchandani and B. Culshaw Excitation of Silicon Microresonators using short optical pulses Sensors and Actuators, A21-A23 (1990) 391-393.

30 N A D Stokes, R M A Fatah, S Venkatesh, Study of Optical Self-Oscillation in Micromachined Resonator Sensors, Electron Lett, 24 (1988) 777-778

31 L M Zhang, D Uttamchandani, B Culshaw, Stabilisation of Optically Excited SElf Oscillation, Elec Lett, Vol 25, No 18, pp1235-1236

32 B E Jones,New transducers using microcomputers fibre optics and thin films, Phys. Technol., vol 14, 1983

33 J E Brignell, Sensors within systems, J. Phys E: Sci. Instrum., vol 17, 1984 pp 759 - 765

34 J E Brignell, Interfacing solid state sensors with digital systemsJ. Phys. E: Sci.Instrum., vol 18, 1985 pp559 - 565

35 A T Bradshaw, Smart pressure transmitters,Measurement and control, vol 17, October 1984 pp 353 - 357

36 J C Legras, M Privel and C Ranson,Application of multiple regression methods and automatic testing equipment to

characterization of `smart' sensors Sensors and actuators, 12 1987 pp 235 - 243

37 J E Brignell and A P Dorey, Sensors for microprocessor based applications,J Phys. E. Sci: Instrum., vol 16, 1983 pp 952 - 958

38 J E Brignell, Digital compensation of sensors,Journal of Phys. E: Sci. Instrum., vol 20 No9, September 1987 pp 1097 - 1102

39 J M Favennec, Smart sensors in industry,J. Phys. E: Sci, Instrum., 20 1987

40 C M Davis,Fibre-optic sensors: an overview, Optical engineering March/April 1985, vol 24 No2 pp 347 - 352

41 Kexing Liu, B E Jones, Pressure Sensors and Actuators Incorporating Optical Fibre LinksSensors and Actuators, 17(1989) pp 501 - 507.

42 A Cheshmehdoost, R C Spooncer B E Jones,High Integrity Bus Structure For Optical Fibre Sensors Sensors and Actuators, 17(1989) pp 173 - 179.

43 A J Rogers, Distributed optical fibre sensors, J.Phys. D 19 (1986) 2237-2255.

44 OSCA, Report on First Year's Work on Phase III, Safety of Optical Systems in Flammable Atmospheres, Doc. No., 89/67, May 1989

45 H Reichl, Packaging and Interconnection of Sensors, Sens+Act A, 25-27 (1991) pp 63-71

46 Leland J Spangler, Kensall D Wise, A Technology for High Performance Single Crystal Silicon-on-Insulator Transistors, IEEE Electron Device Letters 4, April 1987

47 G Wallis, D I Pomerantz, Field Assisted Glass-Metal Sealing, J.Appl.Phys, Vol 10 pp 3940, Sept 1969.

48 B C James,The Welding Institute, Contract Progress Report WGTAT(87) 4, November 1987.

49 C Harendt, B Höfflinger, H Graf, E Penteker, Silicon Direct Bonding for Sensor Applications: Characterisation of the Bond Quality, Sens+Act A, 25-27 (1991) pp 87-92.

50 Y. Lee, F. Sequeda and J. Salem Field-assisted bonding below 200oC using metal and glass thin-film interlayers. Appl. Phys. Lett. Vol.50, No. 9, 2nd March 1987.

51 W Schäfer Temperature sensors: New technologies on their way to Industrial Application, Sensors and Actuators, 17(1989) 27-37.

52 See Radio Spares Catalogue, section on sensors.

53 J N Ross, Optically Powered Sensor Interface, Proceedings USITT Coloquium, Advances in Digital Interfacing of Transducers 19th April 1991.

54 A Hartog, A Distributed Temperature Sensor Based on Liquid-Core Optical Fibres, J Lightwave Technol, LT1 (1983) pp 498

55 Terje Kvisterøy, Ole Henrik Gusland, Birger Stark, Hilde Nakstad, Morten Eriksrud, Bjørn Bjørnstad, Optically Excited Silicon Sensor for Permanently Installed Downhole Pressure Monitoring Applications.

56 B S Douma, P Eigenraam, P Hatlem, Modelling the Pressure and Temperature Sensitivity of an Optically Excited Micromachined Silicon Sensor for Permanently Installed Downhole Monitoring Systems. Sens+Act A31(1992) 215-219.

57 Druck Pressure Calibrator DPI 103, released late 1992

58 for example the Mansor Quartz Manometer

59 T Rogers, Formerly of Fulmer Research, Private Communication, 1992.

60 K. T. V. Grattan and A. W. Palmer Optical-fibre sensor technology: a challenge to microelectronic sensors? Sensors and Actuators A,30 (1992) 129-137

61 Y. N. Ning, K. T. V. Grattan, W. M. Wang and A. W. Palmer A systematic classification and identification of optical fibre sensors. Sensors and Actuators A, 29 (1991) 21-36

62 W J Bock, GaAs-Based Fibre-Optic Pressure Sensor, IEEE Trans. on Instrumentation and Measurement, Vol 41, No 1, Feb 1992

63 M Rapp, D Binz, I Kabbe, M Von Schickfus, S Hinklinger, H Fuchs, W Schrepp, B Fleischmann, A New High Frequency High Sensitivity SAW Device for NO^2 Gas Detection in the Sub-ppm Range, Sens+Act B, 4(1991) pp103-108.

64 Y. J. Rao and B. Culshaw Comparison between optically excited vibrations of silicon cantilever and bridge microresonators. Sensors and Actuators A, 30 (1992) 203-208.

65 D. Walsh and B. Culshaw Optically activated Silicon Microresonator Transducers - An Assessment of Material Properties, Sens+Act A25-27 (1991) 711-716

66 Y. J. Rao, D. Walsh, D. Uttamchandani and B. Culshaw. Temperature characteristics of an all-fibre optically addressed silicon microresonator sensor. Sensors and Actuators A32 (1992) 706-709.

67 R J Pitcher and K W H Foulds, Optothermal Drive of Silicon Resonators: The influence of surface Coatings, Sens+Act, A21-A23(1990) 387-390.

68 M J Tudor, M V Andres, K W H Foulds and J M Naden Silicon Resonator Sensors:interrogation Techniques and Characteristics, IEE Proc., Vol 135, Pt D, No5, Sept. 1988.

69 M V Andrews, M J Tudor, H W H Foulds, Analysis of an interferometric optical fibre detection technique applied to silicon vibrating sensors, Electronics Letters, 16th January 1987, vol 23 No15 pp 774 - 775

70 S Venkatesh, S Novak, Micromechanical Resonators in Fibre-Optic Systems, Opt Lett, 12 (1987) 129-131

71 M V Andres, K W H Foulds, M J Tudor, Nonlinear Vibrations and Hysteresis of Micromachined Silicon Resonators Designed as Frequency out Sensors, Elec.Lett, 1987, 23 (18) ppp 952-954

72 H Wolfelschneider, R Kist, G Knoll, S Ramakrishnan, H Hofflin, W Benecke, L Cspregi, A Heubereger, H Seidel, Optically Excited and Interrogated Micromechanical Silicon Cantilever Structure, SPIE Vol 798, Fiber Optic Sensors II (1987), 61

73 J Smith, University of Southampton, Private Communication 1988

73 T Rogers, Fulmer Research, Private Communication 1992

74 Gilles Delapierre, Micromachining: A Survey of the Most Commonly Used Processes. Sens+Act, 17(1989) pp 123-138.

75 Y N Ning, K T V Grattan, A W Palmer, Fibre Optic Systems Using Low -Coherence light sources,Sens+Act 130(1992) 181-192

76 W.T.Thompson, Theory of Vibration With Applications, 3rd Edition pub. Unwin Hyman, 1988

77 S P Timoshenko, S Woinowsky-Kreiger, Theory of Plates and Shells, pub McGraw-Hill, 1970,

78 R M White,Generation of Elastic Waves by Transient Surface Heating, P. Appl.Phys., vol 34 (1962) No12 pp 3559 - 3567

79 G S Kino and R G Stearns, Acoustic Wave Generation by Thermal Excitation of Small Regions, Appl. Phys. Letters 47 (9), 1985 pp 926 - 928

80 W Arnold, B Betz, B Hoffmann, Efficient generation of surface acoustic waves by thermoelasticity, Appl. Phys. Letters 47 (7), 1985 pp 672 -674

81 Reif, Statistical Physics

85 E Hecht, A Zajac, Optics, pub Addison-Wesly, 1974.

82 S M Sze, Physics of Samiconductor Devices, 2nd Ed,pub Wiley&Sons, 1981.

83 Horowitz and Hill, The Art of Electronics,

84 Penny and Giles Instrumentation Ltd, TP range of transducers.

86 E Boas, Mathematics for the Physical Sciences,

87 Sharp Electronics Corporation, Leaser Diode User Manual